TECHNISCHE UNIVERSITÄT MÜNCHEN

Lehrstuhl für Anorganische Chemie

Synthesis, characterisation and application of cyclometalated gold(III) complexes as anticancer drugs

Sophie Jürgens, M. Sc.

Vollständiger Abdruck der von der Fakultät für Chemie der Technischen Universität München zur Erlangung des akademischen Grades eines

Doktors der Naturwissenschaften (Dr. rer. nat.)

genehmigten Dissertation.

Vorsitzender:	Prof. Dr. Klaus Köhler
Prüfer der Dissertation:	1. Prof. Dr. Fritz E. Kühn
	2. Prof. Dr. Angela Casini

Die Dissertation wurde am 20.12.2016 bei der Technischen Universität München eingereicht und durch die Fakultät für Chemie am 19.01.2017 angenommen.

Die vorliegende Arbeit entstand in der Zeit vom Februar 2013 bis Dezember 2016 unter der Anleitung von Herrn Univ.-Prof. Dr. Fritz E. Kühn, Lehrstuhl für Anorganische Chemie der Technischen Universität München, und Frau Univ.-Prof. Dr. Angela Casini, Chair of Medicinal and Bioinorganic Chemistry, der University Cardiff.

Mein besonderer Dank gilt meinem Doktorvater

Herrn Univ.-Prof. Dr. Fritz E. Kühn

für die Aufnahme in seinen Arbeitskreis, das mir entgegengebrachte Vertrauen und die vielzähligen Forschungsmöglichkeiten

Ebenso geht mein innigster Dank an

Frau Univ.-Prof. Dr. Angela Casini

für ihre stetige fachliche Unterstützung, ihre vielen Anregungen und ihre generelle Hilfe in sämtlichen Belangen

Danksagung

Herrn **Prof. Dr. Fritz Kühn** danke ich für die Aufnahme in seine Arbeitsgruppe, die menschliche und fachliche Unterstützung und das entgegengebrachte Vertrauen innerhalb der letzten vier Jahre.

Frau **Prof. Dr. Angela Casini** danke ich für die stetige Unterstützung während der Promotion und ganz besonders für die Ermöglichung von spannenden Forschungsaufenthalten an der Rijksuniversiteit Groningen und der University of Cardiff.

Für die Übernahme des Vorsitzes der Prüfung bedanke ich mich bei Herrn **Prof. Klaus Köhler**.

Für finanzielle Unterstützung und die Forschungsmöglichkeiten bedanke ich mich bei der **University of Cardiff**, der **Rijksuniversiteit Groningen** und der **TUM graduate school**.

Für ihren stetigen Einsatz für die Doktoranden danke ich ganz herzlich allen Technikern der TU München. **Ulrike Ammari**, **Petra Ankenbauer** und **Bircan Dilki** der Elementaranlytik, sowie **Jürgen Kudermann** und **Maria Weindl** für das Messen von Kryo- und Langzeit-NMRs und ihre ständige Bereitschaft zu diskutieren. Herrn Kudermann dabei insbesondere ein großes Dankeschön für das Aufsetzen der ^{199}Hg NMR Methode. **Martin Schellerer** danke ich ganz herzlich für das Liefern von Chemikalien und Hilfe bei der Versendung von Proben. Ebenso geht mein herzlichster Dank an **Thomas Williams** der Universität Cardiff für die vielen ESI-MS Messungen und **Rodica Dumitrescu** für FAB- und MALDI-MS Messungen. Für das Messen von Kristallen danke ich ganz herzlichst **Christian Jandl**. Ich danke **Natalia Estrada-Ortiz** und **Jurriaan Brouwer** für das Durchführen biologischer Studien. Weiterer herzlicher Dank an die Damen des Sekretariats, Frau **Ulla Hifinger** und Frau **Irmgard Grötzsch,** für ihre Hilfe bei vielen organisatorischen Angelegenheiten.

Meinen Kolleginnen aus der medizinischen Chemie Subgruppe **Andrea Schmidt, Eva Hahn** und **Özden Karaca** in München danke ich für die gute Zusammenarbeit und gemeinsames Meistern diverser Konferenzen und Präsentationen. Ebenso danke ich meinen Kollegen in Cardiff und in Groningen **Andreia de Almeida**, **Margot Wenzel**, **Benjamin Woods**, **Darren Wragg, Samuel Meier, Brech Aikman** und **Valeria Ugone** für die gute Zusammenarbeit und lustige Pub Abende.

Meinen weiteren Laborkollegen über die gesamte Zeit **Robert Reich**, **Teresa Meister**, **Esther Bayon, Manuela Hollering** und insbesondere **Florian Groche** danke ich für eine gute Zusammenarbeit und ein entspanntes Arbeitsklima. Danke an **Caro Obermayer** und **Lilli Bauer** für die kurzfristige Laboraufnahme zum Ende meiner Doktorarbeit und für die tolle Atmosphäre. Ebenso danke ich allen weiteren Doktoranden des Lehrstuhls Anorganische Chemie für die gute Zusammenarbeit über die Jahre und die netten Pausen im Kaffeeraum.

Ich danke meinen Studenten **Irene**, **Rachel**, **Shi Rui, Federica, Beth** und **Maximilian** für ihre tatkräftige Mitarbeit im Labor.

Ich danke herzlichst meinen Freunden, die mich immer aufgemuntert haben, wenn es nötig war. Es sind leider zu viele, um sie alle namentlich zu nennen, aber dabei besonderer Dank an **Andi**, **JJ**, **Lana**, **Chris**, **Edith, Aldo, Jerome** und **Max**.

Ich danke **Jonas**, der mir den nötigen Ausgleich außerhalb der Chemie gegeben hat, wenn mal wieder alles ein bisschen viel war.

Mein größter Dank gilt meiner Familie. Meinen Großeltern **Ingrid** und **Peter Jürgens** und **Erika** und **Richard Krüger**, dass sie sich immer für mein Fortkommen im Studium und der Promotion interessiert und mich unterstützt haben. Ein großes Dankeschön auch an meine kleine Schwester **Christine**, mit der auch graue Tage gleich ein bisschen heller sind.

Für die andauernde Unterstützung während der Schulzeit, des Studiums und in der Promotion bin ich meinen Eltern, **Dr. Birgit Jürgens** und **Dr. Dirk Jürgens**, unendlich dankbar. Ohne euch wäre mir mein Weg so nur schwer möglich gewesen. Dafür möchte ich mich von Herzen bei euch bedanken.

“Ein Gelehrter in seinem Laboratorium ist nicht nur ein Techniker, er steht auch vor den Naturgesetzen wie ein Kind vor der Märchenwelt.“

Marie Curie

Meinen Eltern gewidmet

Zusammenfassung

Organogoldverbindungen bieten eine differenziertere Alternative zu traditionell angewandten Pt(II) Chemotherapeutika, wobei cyclometallierte Au(III) Komplexe von besonderem Interesse sind, da sie nicht nur die Stabilisierung des ansonsten leicht reduzierten Au(III) Kerns ermöglichen, sondern auch die Einführung funktioneller Gruppen.

In der vorliegenden Arbeit wurden cyclometallierte Au(III) Komplexe unter Verwendung eines C^N^C (= 2,6-diphenylpyridin), C^N(R)^C (= 2,4,6-triaryl-pyridin) oder eines C^N (= 2-benzylpyridin) Gerüsts synthetisiert. Alle Au(III)[C^N^C] und Au(III)[C^N(R)^C] Komplexe wurden durch Transmetallierung ihrer zuvor synthetisierten jeweiligen Hg(II) Vorstufe erhalten.

Der Einfluss des adhäsiv gebundenen Liganden L auf das Au(III) C^N^C System wurde durch Ersetzen des Chloridoliganden des ursprünglichen Komplexes [Au(C^N^C)Cl] mit einer PTA (1,3,5-triaza-7-Phosphaadamantan) bzw. einer GluSH (thio-β-D-Glucosetetraacetat) Gruppe untersucht. Alle Komplexe bewiesen gute zytotoxische Aktivität gegen Eierstockkrebszellen. Erste mechanistische Studien zeigen, dass die Komplexe potente Inhibitoren des Selenoenzyms Thioredoxin-Reduktase sind. Das Thioglucose Derivat induziert zudem Veränderungen des gesamten intrazellulären Redoxzustands, was auf zusätzliche Wechselwirkungen mit thiolhaltigen Biomolekülen hindeutet.

Innerhalb des Au(III) C^N(R)^C Systems wurde der Einfluss des para-Substituenten R der 6-Phenyl-Position untersucht (R = OH, F, Br, NO_2). Für das Ligandensystem allein wurde die höchste zytotoxische Aktivität gegen A549 und SKOV-3-Krebszellen für R= OH gefunden, während R = NO_2 gar keine zytotoxische Aktivität aufwies. Die erhaltenen Goldkomplexe wiesen Löslichkeitsprobleme im Zellkultur Milieu auf.

Schlussendlich wurde ein Ligand auf Cumarin-Basis an einen Au (III) C^N Komplex gekoppelt und auf seine photochemischen Eigenschaften untersucht. Obwohl die erhaltenen Quantenausbeuten sehr niedrig waren, besitzt dieser charakteristische UV-Vis Merkmale und wird für weitere biologische Tests empfohlen.

Abstract

Organogold compounds display a more sophisticated alternative to traditional applied Pt(II) chemotherapeutics with cyclometalated Au(III) complexes being of special interest, since they not only allow for the stabilization of the otherwise easily reduced Au(III) centre, but also for the introduction of functional groups.

In this work, cyclometalated Au(III) complexes were synthesized, utilizing a C^N^C (= 2,6-diphenylpyridine), a C^N(R)^C (= 2,4,6-triaryl-pyridine) or a C^N(= 2-benzylpyridine) scaffold. All Au(III)[C^N^C] and Au(III)[C^N(R)^C] complexes were obtained *via* transmetalation of their previously synthesized respective Hg(II) precursor.

The influence of the ancillary ligand L was investigated for the Au(III) C^N^C system by replacing the chlorido ligand of the original [Au(C^N^C)Cl] complex with a PTA (1,3,5-triaza-7-phosphaadamantane) and a GluSH (thio-β-D-glucose tetraacetate) moiety, respectively. All complexes showed good cytotoxic activity against ovarian cancer cells. Initial mechanistic studies demonstrate that the compounds are potent inhibitor of the seleno-enzyme thioredoxin reductase. The thioglucose derivative also induces alterations of the overall intracellular redox state, which may be due to additional interactions with thiol-containing biomolecules.

Within the Au(III) C^N(R)^C system, the influence of the *para* substituent R of the 6-phenyl position was investigated (R = OH, F, Br, NO_2). For the sole ligand system the highest cytotoxic activity against A549 and SKOV-3 cancer cells was found for R= OH, whereas R = NO_2 did not display any cytotoxic activity at all. The obtained gold complexes displayed solubility issues within the cell culture medium.

Finally, a coumarin based ligand was coupled to an Au(III)C^N complex and investigated for its photochemical properties. Although the displayed quantum yields were very low, characteristic UV-Vis features were displayed and the complex recommended for further biological testing.

Content

Zusammenfassung 1

Abstract 2

List of abbreviations 5

List of figures 8

List of tables 10

I Introduction and motivation 11

1.1 Cancer - background and statistics 11

1.2 Organometallic anticancer agents 18

1.3 Cyclometalation 25

1.3.1 Cyclometalated Au(III) compounds as anticancer agents 26

1.3.1.1 Au(III) C^N complexes 27

1.3.1.2 Au(III) C^N^N complexes 29

1.3.1.3 Au(III) C^N^C complexes 31

1.3.1.4 Au(III) C^N^S complexes 34

1.4 Coumarin based ligand systems 35

1.5 Objective 39

II Results and Discussion 40

2.1 Au(III)[C^N^C] system 40

2.1.1 Synthesis and structural characterization of Au(III)[C^N^C] complexes .. 40

2.1.2 Biological evaluation of Au(III)[C^N^C] complexes 47

2.1.2.1 Antiproliferative activity 48

2.1.2.2 Thioredoxin reductase inhibition 48

2.1.2.3 Effects on the cellular redox state 50

2.2 Au(III)[C^N(R)^C] system 52

2.2.1 Optimization of C^N(R)^C ligand synthesis 52

2.2.2 Synthesis and structural characterization of Au[C^N(R)^C] complexes .. 56

2.2.3 Biological evaluation of Au(III)[C^N(R)^C] complexes 63
2.3 Au(C^N) coumarin system 65
2.3.1 Synthesis of the Au(C^N) coumarin system 65
2.3.2 Investigation of photochemical properties 68
2.4 Conclusion and outlook 71
III Experimental 74
4 Synthesis of [Au(III)(C^N^C] complexes 81
4.1 Hg(II) precursor synthesis 81
4.2 Synthesis of [Au(III)(C^N^C] complexes 83
5 Synthesis of Au(III)[C^N(R)^C] complexes 86
5.1 Synthesis of [C^N(R)^C] ligand system 86
5.2 Synthesis of [Hg(II)[C^N(R)^C]Cl] complexes 92
5.3 Synthesis of [Au(III)[C^N(R)^C]Cl] complexes 96
6 Synthesis of C^N Au(III) complexes 100
Appendix 105
Crystalstructur report for [Au(C^N^C)(PTA)][PF_6] 105
Bibliography 112
Curriculum Vitae 120
Publikationsliste 121

List of abbreviations

AQP	aquaporine
ASR	age-standardized cancer incidence and mortality rates
BSA	bovine serum albumin
Bz	benzyl
$CDCl_3$	d-Chloroform
CI	chemical ionization
CLL	chromatic lymphocytic leukemia
Cp	cyclopentadiene
ct	calf-thymus
cyc	cyclic
damp	2[dimethylamino)methyl]-phenyl
DAPTA	(3,7-diacetyl-1,3,7-triaza-5-phosphabicyclo[3.3.1]nonane)
DCM	dichloromethane
DDR	DNA damage response
DLC	delocalized lipophilic cations
DMDT	dimethyldithiocarbamate
DMSO	dimethylsulfoxide
DNA	deoxyribonucleic acid
dpdtc	dipeptidedithiocarbamate
dppe	bis(diphenylphosphino)ethane
dppp	bis(diphenylphosphino)propane
DSB	double strand breaks
ER	endoplasmic reticulum
ESI-MS	Electrospray ionization-mass spectrometry
eq	equivalent
FAB	fast atom bombardment
g	gram
GluSH	thio-β-D-Glucosetetraacetat
GLUT	glucose transporter
GPx	glutathione peroxidase

GR	glutathione reductase
GSH	glutathione
G4	G-quadruplex
h	hour
HPV	Human papilloma virus
HTS	5-(hydroxymethyl)-8-methyl-3-thiol-7-azacoumarin
Hz	Hertz
IC_{50}	half maximal inhibitory concentration
L	ligand
M	metal
MALDI	Matrix-assisted laser desorption/ionization
MAOS	microwave-assisted organic synthesis
MeCN	acetonitrile
mim	1-methylimidazole
MRSA	Methicillin-resistant Staphylococcus aureus
mTOR	mammalian target of rapamycin
MTT	3-(4,5-dimethylthiazol-2-yl)-2,5-diphenyltetrazolium bromide
NAMI-A	imidazolium-trans-tetrachloro(dimethyl-sulfoxide)imidazole-ruthenium(III)
NHC	*N*-heterocyclic carbene
NHEJ	Non-homologous end joining
NMR	nuclear magnetic resonance
OLED	organic light-emitting diodes
OTf	triflate
PAGE	polyacrylamide gel electrophoresis
PARP	poly(-adenosine diphosphate (ADP)-ribose) polymerase
PBS	Phosphate-buffered saline
PLL	prolymphocytic lymphoma
PPh_3	triphenylphosphine
ppm	parts per million
PTA	1,3,5-triaza-7-phosphaadamantane
pydoxmetsc	pyridoxal methylthiosemicarbazone

ROS	reactive oxygen species
RT	room temperature
SEM	scanning electron microscopy
SLL	small lymphocytic lymphoma
^{t}Bu	tert-butyl
TEM	transmission electron microscopy
TOF	turnover frequency
TrxR	thioredoxin reductase
UV-Vis	Ultraviolet-Visible
W	Watt
WHO	World Health Organization
XRD	X-ray diffraction
ZF	zinc finger
°C	degree Celsius
δ	chemical shift (delta)
4-dpt	2,4-diamino-6-(4 pyridyl)-1,3,5-triazine

List of figures

Figure 1. DNA mutations and their respective repair mechanisms. 12
Figure 2. Cancer ASR per 100.000 worldwide. 13
Figure 3. Prominent anticancer Pt(II) and Au(I)/Au(III) complexes. 15
Figure 4. Organometallic complexes with medicinal properties. 19
Figure 5. General representation of cyclometalated complexes. 25
Figure 6. Au(III) C^N complexes with cytotoxic properties. 28
Figure 7. Mononuclear and dinuclear Au(III) C^N^N complexes. 30
Figure 8. Au(III) C^N^C complexes synthesized by Che *et al.* 33
Figure 9. General complex formation of Au(III) C^N^C complexes 34
Figure 10. Au(III) pseudo-pincer and Au(III) S^N^S complexes. 35
Figure 11. Coumarin based systems with medicinal properties. 37
Figure 12. Synthesis of complexes 1 and 2. 40
Figure 13. Ligand exchange reactions as performed for complex 3 and 4. 41
Figure 14. ^{1}H NMR of complex 2 and 3. 42
Figure 15. ^{1}H NMR complex 4 43
Figure 16. ESI-MS spectrum of complex 3. 44
Figure 17. Theoretically calculated ESI-MS spectrum of complex 3. 45
Figure 18. ESI-MS spectrum of complex 4. 45
Figure 19. ESI-MS spectrum of complex 2. 46
Figure 20. Two perspectives of the molecular structure of complex 3 in the solid state. 47
Figure 21. Thioredoxin reductase (A) and glutathione reductase (B) activities in 2008 ovarian cancer cells 50
Figure 22. Total thiols (A) and glutathione (B) in ovarian cancer cells after the treatment with complexes 2 - 4. 51
Figure 23. $Bi(OTf)_3$ catalyzed C^N(R)^C ligand synthesis. 52
Figure 24. Microwave irradiated synthesis of C^N(R)^C ligands. 53
Figure 25. Obtained crude microwave products. 56
Figure 26. Synthesis of Au[C^N(R)^C] complexes. 57
Figure 27. ^{1}H NMR of ligand 6, reacted to complex 10 with $Hg(OAc)_2$. 58

Figure 28. ^{199}Hg NMR of monomercurated and bismercurated complex 9. 58
Figure 29. ^{13}C NMR spectra of complex 13 - 16..... 59
Figure 30. ESI-MS spectrum of complex 13..... 60
Figure 31. ESI-MS spectrum of complex 14..... 60
Figure 32. Theoretically calculated ESI-MS spectrum of complex 14. 61
Figure 33. ESI-MS spectrum of complex 15..... 61
Figure 34. ESI-MS spectrum of complex 16..... 62
Figure 35. Synthesis of complex 17 and 20. 65
Figure 36. ^{1}H NMR of complex 20. 67
Figure 37. ^{1}H NMRs of complex 17, ligand 18 and complex 20 68
Figure 38. UV-VIS spectra of ligand 18 and complex 20. 69
Figure 39. Normalized fluorescence spectrum of complex 20. 70
Figure 40. Redox western blot of Trx1 (A) and Trx2 (B) in 2008 cells after incubation with complex 2 and 4 79
Figure 41. CEM Focused Microwave and Biotage Initiator Robot as applied in the thesis. 80
Figure 42 . Complete crystal structure with Ortep drawings complex 3..... 107

List of tables

Table 1. IC_{50} values of the inhibition of TrxR1, TrxR2 and GR 48
Table 2. Yield determination for variation of the irradiation power P [W]. 54
Table 3. Yield determination for variation of the irradiation temperature T [°C]. 54
Table 4. Yield determination for variation of the irradiation time t [min]. 55
Table 5. IC_{50} values of compounds 5-8 and cisplatin against A549 and SKOV-3. 63
Table 6. Varied reaction conditions for complex 19. 102
Table 7. Physical data collection details for complex 3. 105
Table 8. Sample and crystal data for complex 3. 106
Table 9. Data collection and structure refinement for complex 3. 106
Table 10. Bond lengths(Å) of complex 3. 108
Table 11. Bond angles(°) for complex 3. 109
Table 12. Torsion angles (°) for complex 3. 110

I Introduction and motivation

1.1 Cancer - background and statistics

Cancer is a broad term describing the abnormal growth of cells to malignant tumors, possibly leading to metastasis. This uncontrolled proliferation of cells can theoretically occur in any tissue of the body. Therefore cancer cannot be regarded as a single disease, since the term describes more than 100 different and distinctive diseases.

According to the World Cancer Report 2014 of the World Health Organisation (WHO), 8.2 million cancer related deaths were reported in 2012[1], making cancer one of the leading causes of morbidity and mortality worldwide. The number of new reported cases increased with 14.1 million significantly in comparison to 12.4 million in 2008 and is expected to rise up to 22 million by 2022[1]. Major risk factors for cancer are obesity, ionizing and non-ionizing radiation (e.g. ultraviolet radiation), virus infections (e.g. HPV, hepatitis B and C), malnutrition, lack of physical activity and misuse of alcohol and tobacco. Only 5-10 % of cancer cases can thereby be related to a genetic predisposition[2]. Tobacco use is the leading risk factor, causing approximately 20% of all cancer deaths and 70% of lung cancer deaths globally[3]. Factors that lead to cancer are called carcinogens, causing changes in the DNA (deoxyribonucleic acid) sequence and are therefore also mutagens. UV radiation for example can cause up to 10^5 DNA lesions per cell/day[4]. Various repair mechanisms involving different proteins are utilized, collectively forming the DNA damage response (DDR). However, if DNA breaks are left unrepaired or get mismatched, these breaks can induce mutations from normal cells to malignant neoplasms (oncogenesis). Figure 1 illustrates possible DNA damages and the respective proteins involved in their repair, such as the zinc finger (ZF) enzyme poly(-adenosine diphosphate (ADP)-ribose) polymerase 1 (PARP-1) in the base excision repair (BER) [5].

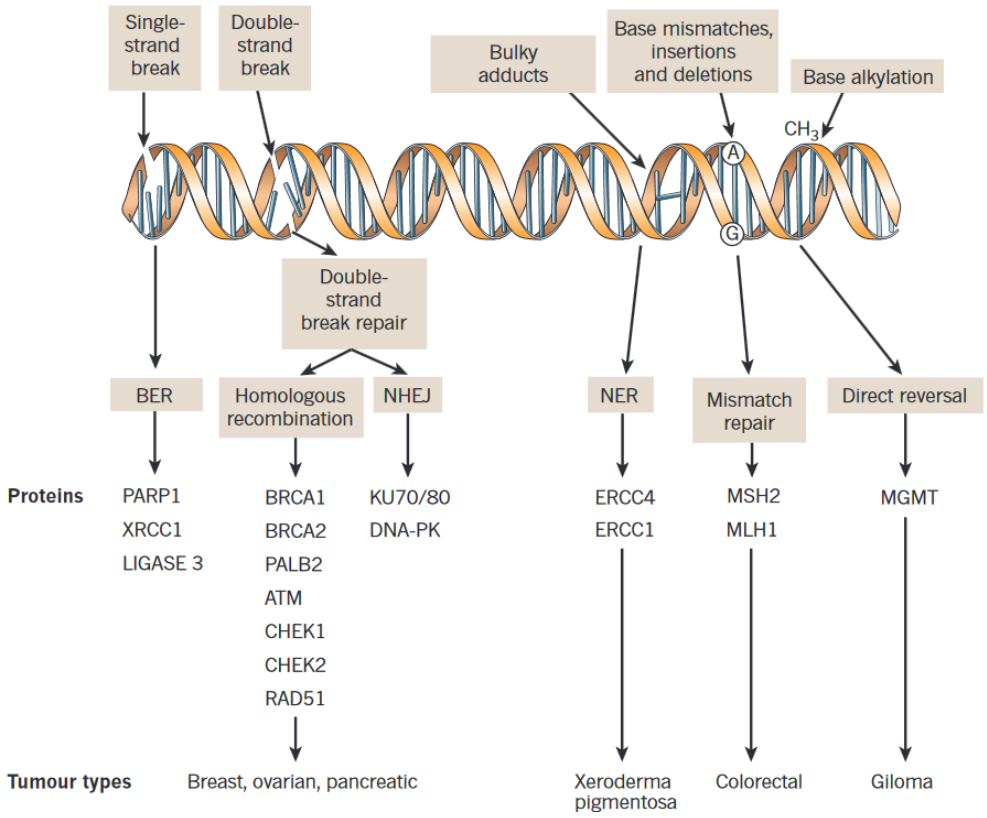

Figure 1. DNA mutations and their respective repair mechanisms. Reprinted with permission from Nature Publishing Group: Nature 2012, *481*, 287-294[5].

Double strand breaks (DSB) in the DNA for example are repaired by homologous recombination or non-homologous end joining (NHEJ). Homologous recombination is a process that occurs mainly in the S and G2 phases of the cell cycle, in which DNA around the DSB is partly removed (resection) and a homologous sister chromatid DNA template is used for synthesizing new nucleobases at the DSB site. Non-homologous end joining (NHEJ) is the alternative repair mechanism within the cell cycle, in which a DBS is directly repaired by simply ligating the lesioned ends together. These processes, especially the mechanistically less elaborate NHEJ, can easily lead to mismatches and have been demonstrated to be the main mutagen reason for breast, ovarian and pancreatic cancer[6].

The frequency of a particular cancer is thereby gender dependent. Figure 2 gives an overview of the age-standardized cancer incidence and mortality rates (ASR) per 100.000 worldwide.

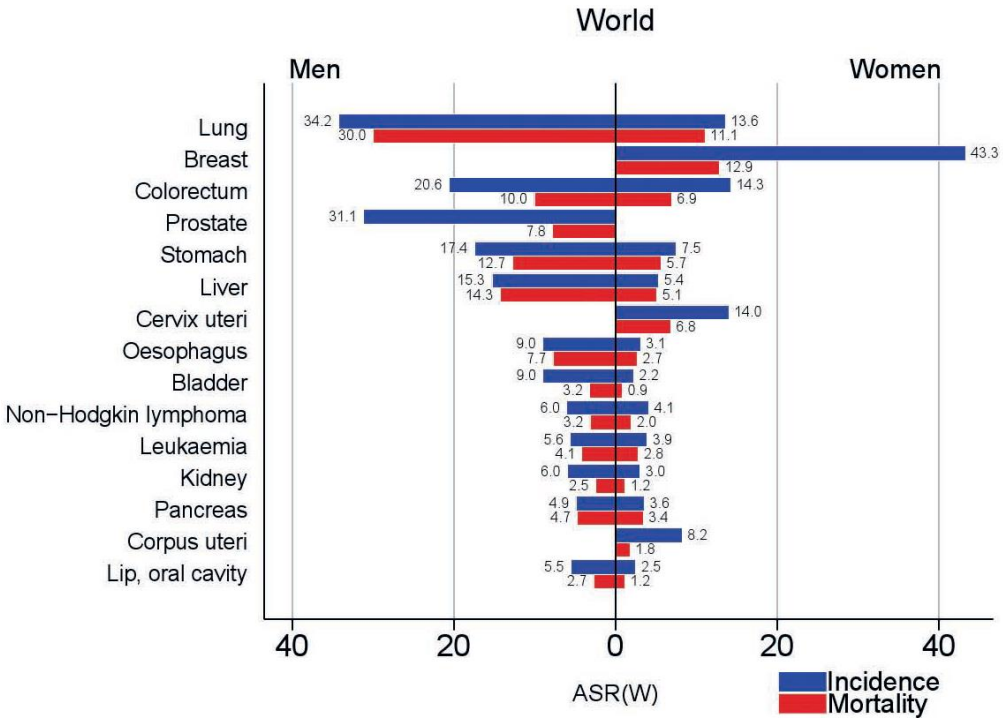

Figure 2. Cancer ASR per 100.000 worldwide. Reprinted with permission from ©International Agency for Research on Cancer Publications: World Cancer report 2014[1].

Among men, the most common sites of cancer diagnosed in 2012 globally were lung, prostate, colorectum, stomach, and liver cancer. Among women the most common sites of cancer diagnosed were breast, colorectum, lung, cervix, and stomach cancer[1].

It can be seen that the cancer frequency does not equate the cancer mortality. Whereas breast cancer is the leading cancer incidence for women and prostate cancer the number two cancer incidence for men, these cancer types have a comparably low mortality rate, since they are often operable[7]. Opposite to that is lung cancer as one of the most aggressive human cancer types, with the incidence rate close to the mortality rate for both genders and a 5-year overall survival chance of only 10–15%[8].

The three major approaches for the treatment of cancer are surgery, radiation and chemotherapy (or combination treatment of two or all three). Chemotherapy is thereby the treatment of diseases with chemical drugs and was pioneered by Paul Ehrlich who synthesized the first chemotherapeutic agent “Salvarsan” (an organoarsenic compound) to treat syphilis.

The first chemotherapeutic drug with anticancer properties was discovered accidentally by Rosenberg and co-workers in 1965. The observable cytostatic effect of *cis*-diamminedichloridoplatinum(II) (cisplatin, **1.1a**) on *E. coli* paved the way for the application of platinum based drugs in cancer therapy[9]. Since the clinical approval of cisplatin in the USA in 1978 (and one year later in several European countries), another 25 cisplatin analogues have been approved for clinical trials. However, only carboplatin (**1.1b**) and oxaliplatin (**1.1c**) display pharmacological advantages compared to cisplatin and have been marketed worldwide since their discovery. The established mechanism of action for this family of chemotherapeutic agents involves their binding to nucleic acids after exchange of the chloride ligands with water molecules (or OH^- ligands), followed by direct coordination to DNA nucleobases. This reactivity with DNA leads to a stop of the transcription and translation of the cell DNA which results in cell death by apoptosis. Three other Pt(II) drugs have been additionally approved for single markets, namely nedaplatin in Japan, lobaplatin in China and heptaplatin in Korea[10]. Despite their clinical success, traditional Pt(II) based drugs for cancer therapy present major drawbacks, such as resistance, limited spectrum of action and severe side effects in patients, in part due to their non-selective binding to other intracellular components[11]. Thus, research has been focused on developing new inorganic drugs to circumvent these limitations and enable a more sophisticated, targeted approach towards cancer cells.

In this context, gold complexes have been present in therapy for quite a while now, however their exploration as anticancer agents is more recent and has strongly increased throughout the last decade[12]. In fact, gold(I) and gold(III) complexes are an emerging class of metal complexes with potential antitumor properties alternative to cisplatin. This is mainly due to their outstanding cytotoxic properties exhibited through different antitumor mechanisms, specifically the selective inhibition of target proteins and enzymes.

As an example, auranofin (**1.1d**) (Ridaura®) is a relatively simple Au(I) thiolate complex which is presently used in clinics to treat severe rheumatoid arthritis[13]. Initially approved as an antirheumatic agent in 1982 for worldwide clinical use, it recently passed phase II of clinical trials for the treatment of chromatic lymphocytic leukemia (CLL), Small Lymphocytic Lymphoma (SLL) and Prolymphocytic

Lymphoma (PLL)[12b]. Early studies on the anticancer activity of auranofin revealed activity levels similar to cisplatin *in vitro*, which subsequently led to a large number of Au(I) complexes being evaluated for their antiproliferative activity[12b].

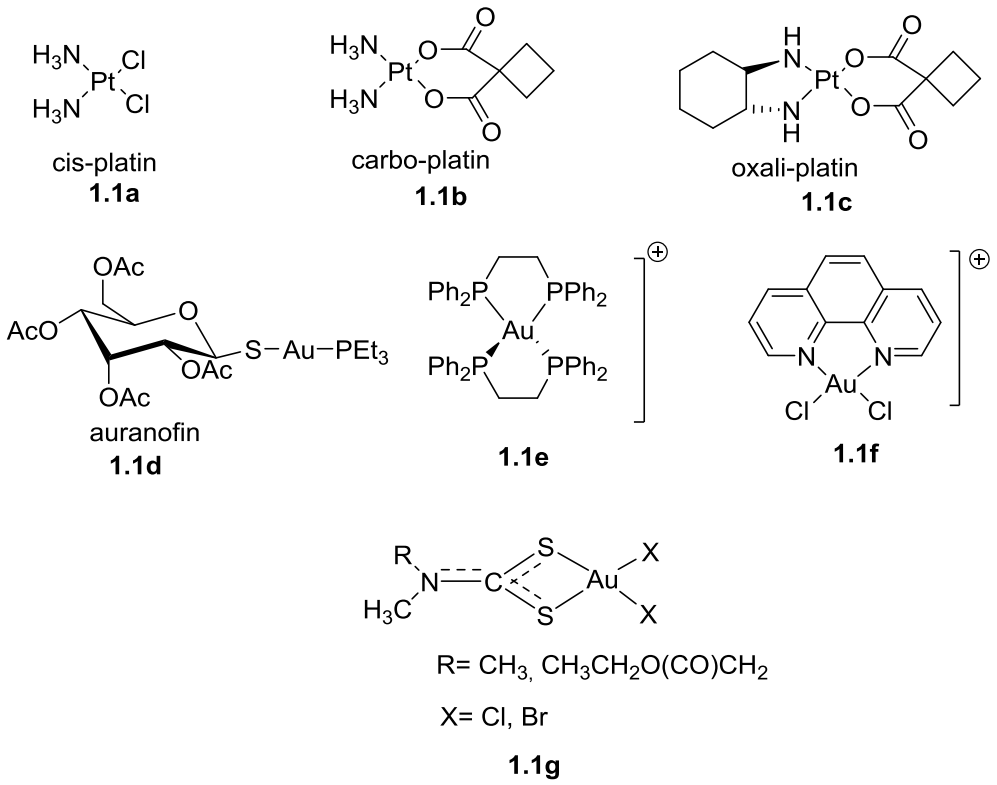

Figure 3. Prominent anticancer Pt(II) complexes and experimental cytotoxic Au(I) and Au(III) complexes.

Following the clinical success of auranofin, other Au(I) complexes featuring auxiliary phosphine ligands were synthesized by Berners-Price *et al.*[14], such as the bis[1,2-bis(diphenylphosphino)ethane]Au(I) chloride ([Au(dppe)$_2$]Cl) with chelating diphosphine ligands (**1.1e**). Notably, **1.1e** is more stable with respect to ligand exchange reactions than the linear complexes and less reactive towards thiols. [Au(dppe)$_2$]Cl has shown reproducible and significant *in vivo* antitumor activity in a range of murine models. However, due to severe hepatoxicity of the compound, the studies were not continued[15].

The modes of action of cytotoxic gold(I) compounds are still a matter of intense

debate. However, there is now quite a wide consensus on the concept that their behaviour diverges profoundly from that of cisplatin and analogues, mainly grounded on a documented poor reactivity with double-helix DNA. On the other hand, there is good evidence that they often produce severe mitochondrial damage[12a]. In this context, among the most studied and recognized targets for gold compounds, the seleno-enzyme thioredoxin reductase (TrxR) has been widely investigated[16]. Human TrxR contains a cysteine-selenocysteine redox pair at the C-terminal active site and the solvent-accessible selenolate group constitutes a likely target for soft metal ions such as gold.

A broad number of Au(III) complex families have been synthesized and their anticancer activity has been evaluated against numerous cancer cell lines *in vitro*. In most cases, the donor atoms stabilizing the Au(III) centre are either Cl, Br, S or P atoms[17]. As an example, the complex [Au(phen)Cl_2]Cl (**1.1f**) contains a 1,10-phenanthroline as a chelating N-donor moiety and two stabilizing chlorido ligands. Although displaying lower stabilities compared to other ligands, the phenanthroline chelated complex shows higher cytotoxicity towards various cancer cell lines[18]. Recently it was demonstrated that **1.1f** is a functional selective inhibitor of the human water and glycerol channel aquaglyceroporin-3 (AQP3), possessing inhibitory effects on the proliferation of cells over-expressing this isoform[19]. Hence, **1.1f** may produce a targeted therapeutic effect on carcinomas with enhanced AQP3 expression[20].

Pursuing the search of novel protein targets for anticancer gold compounds, some groups reported on the inhibitory effects of different cytotoxic gold-based complexes with phosphine or bipyridyl ligands, towards the zinc finger enzyme PARP-1[21]. Interestingly, Au(III) coordination complexes were one of the most efficient compounds, inhibiting PARP-1 at the nM level, followed by Au(I) compounds. Among the most recent reports, a new gold(III) complex bearing a 2-((2,2'-bipyridine)-5-yl)-1*H*benzimidazol-4-carboxamide ligand has been synthesized and characterized for its biological properties *in vitro*[22]. In addition to showing promising antiproliferative effects against human cancer cells, the compound potently and selectively inhibits the zinc finger protein PARP-1, with respect to the seleno-enzyme TrxR. The results hold promise for the design of novel gold-based

anticancer agents disrupting PARP-1 function and are to be used in combination therapies with DNA alkylating agents.

Furthermore, dithiocarbamate ligands were also described as efficient coordinating ligands for Au(III) ions[23]. Thus, Fregona *et al*. reported on the design of targeted Au(III) dithiocarbamate complexes with peptide-based ligands for carrier-mediated delivery of the compounds in cancer cells via peptide transporters[24]. Compounds of the type [Au(dpdtc) Cl_2] (dpdtc = dipeptidedithiocarbamate) (**1.1g**) lead to reduced toxic and nephrotoxic side-effects in comparison to their analogues without the peptide moiety, while displaying increased tumor selectivity. Notably, several of these compounds resulted to be potent proteasome inhibitors.

Unfortunately, the majority of the cytotoxic Au(I)/Au(III) coordination compounds show limitations concerning stability in aqueous solution, and especially Au(III) complexes are easily reduced to Au(I) or Au(0), resulting in loss of activity and possible side effects. Therefore, research is nowadays dedicated to a larger extent to the design and synthesis of more stable derivatives, including organometallic compounds.

1.2 Organometallic anticancer agents

In recent years, organometallic compounds have become more popular and are now quite widespread as experimental anticancer agents. In fact, they combine the advantages of a classical inorganic system with the higher stability of an organic scaffold[25]. The organic ligands allow for the introduction of stereospecifity which gives access to an even higher amount of structural possibilities. Furthermore, "fine tuning" possibilities within the organic moiety regarding functional groups etc. is given, determining the physiochemical properties of the respective metal compound[26]. In fact, in organometallic complexes it is the metal–carbon (M–C) bond that endows these coordination compounds with peculiar features. On the one hand, M–C bonds have high *trans* effects and *trans* influences, which affects the lability of bonds to other ligands (M–L) in the complex. On the other hand, π-bonded aromatic arene and cyclopentadienyl ligands can act both as electron donors and π-acceptors. These ligands can therefore modify the donor/acceptor behaviour (and reactivity) of other ligands in the complex. Finally, by choosing specific targeting moieties, either incorporated into the ligand or attached to the metal centre, targeting at specific cancer cells' receptors can be achieved.

Typical classes of organometallics include metallocenes, metallo-arenes, metallo-carbonyls, metallo-carbenes (e.g. *N*-heterocyclic carbenes) and alkynyl complexes, respectively[27]. Classically, these complex classes have been widely applied in catalysis[28]. However, their medicinal use has been recently demonstrated. The utilized complexes show thereby a great variety, as not only mononuclear compounds, but also multinuclear compounds have been synthesized and investigated. In this respect one has to distinguish between homonuclear and heteronuclear compounds. In Figure 4 an overview of some of the most representative structures of medicinally relevant organometallic complexes is provided.

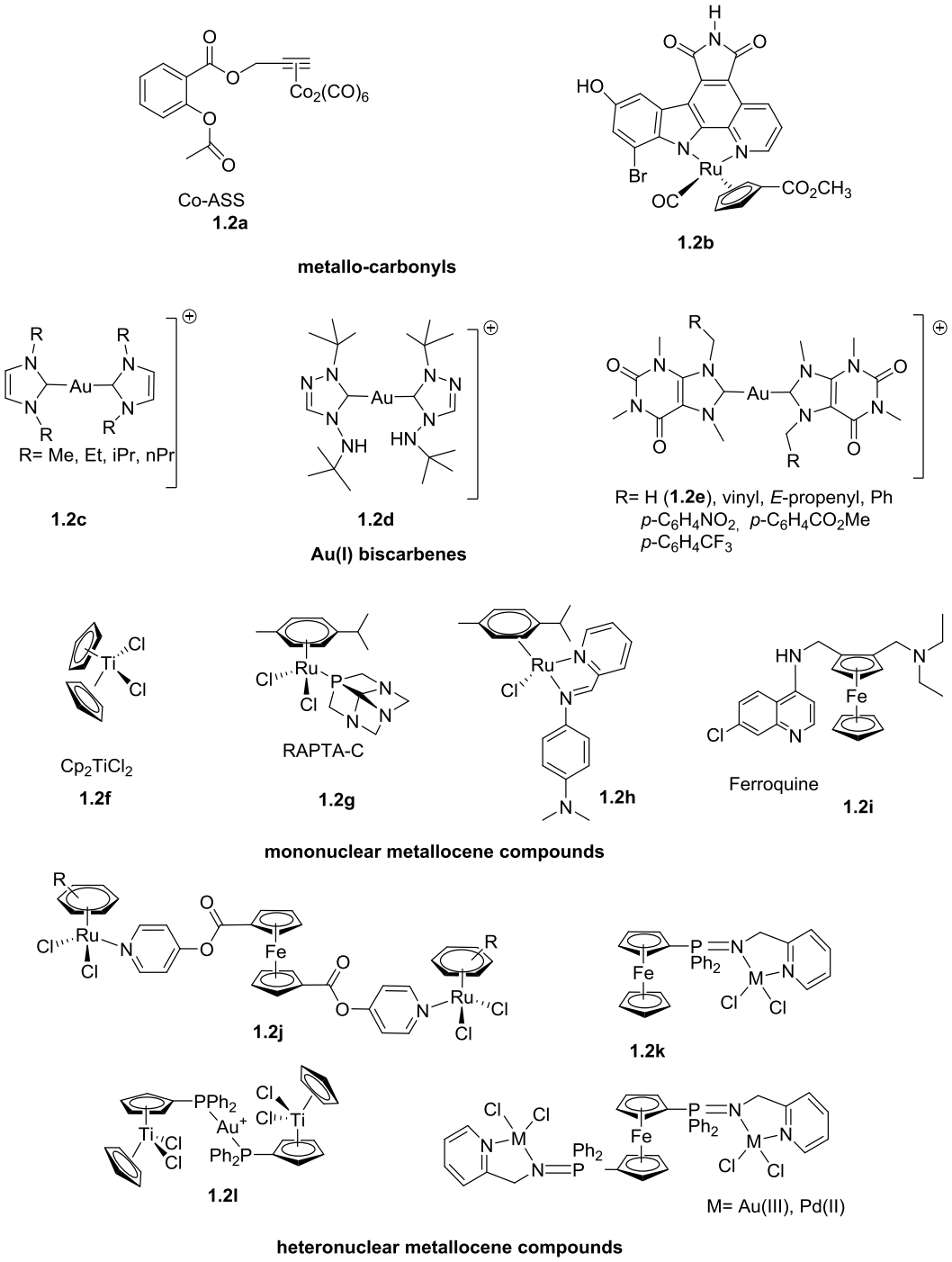

Figure 4. Organometallic complexes with medicinal properties.

To begin with, the biological properties of metallo-carbonyls have been studied for a number of metals, such as iron[29], ruthenium[30] and manganese[31]. Carbonyl complexes offer the benefit of displaying high lipophilicity, leading to increased cellular uptake levels, which could be demonstrated in several studies[32]. Among the various examples present in literature, the alkyne hexacarbonyldicobalt $Co_2(CO)_6$

species Co-ASS (**1.2a**) contains an acetylsalicylic acid (aspirin) moiety. Aspirin has been shown to reduce the recidivism risks in cancer patients, therefore making it valuable as a ligand in a combination therapy approach. Indeed, **1.2a** was found to display good stabilities under physiological conditions, to strongly inhibit both the COX-1 and COX-2 enzymes and to induce of apoptosis[32]. Further recent studies with zebra fish embryos also indicate that **1.2a** has anti-angiogenic properties, a trait which is not present with aspirin[33].

In contrast to modifying somewhat remote groups of organic inhibitors, in 2009 Meggers *et al.* have taken the concept of using metal fragments to occupy defined regions of 3D-space in enzyme active sites one step further, and synthesized a number of Ru(II) compounds as protein kinase inhibitors[34]. The high selectivity displayed by these compounds is believed to be achieved by the rigid scaffold, leaving the metal as a pure structural motif. Complex **1.2b** has therein shown promising activities against several cancer cell lines and in a melanoma spheroid model[35]. Furthermore, the CO ligands apparently play a significant role in the molecular interaction with biological targets, although the interactions need further systematic investigations[27, 36].

Organometallic compounds displaying *N*-heterocyclic carbene (NHC) ligands have also been investigated closely throughout the last decades, since they offer benefits such as easy accessibility from imidazolium salts, non-toxicity of the ligands and high complex stability[37]. Steric and electronic effects contribute to the bonding of metals to NHC ligands. Whereas NHC complexes were initially considered as pure σ-donors, it is now commonly established that besides the NHC-to-metal σ → d donation also metal-to-NHC d → π* and NHC-to-metal π → d donations contribute to the bonding. Moreover, saturation or aromaticity of the NHC ligand and the volume of attached side chains influence the stability and reactivity of the complexes. The first reports on biological activity of metal NHC compounds were published between 1996 and 1999 by Cetinkaya *et al.*, who described the antibacterial properties of ruthenium(II) and rhodium(I) NHC complexes[38].

Berners-Price *et al*. pioneered this field by synthesizing a series of linear, cationic Au(I) NHC complexes (**1.2c**) with remarkable anticancer properties *in vitro* and inducing mitochondrial damage. By varying the substituents at the N,N

positions of the imidazolium precursor, the lipophilic properties could be finely tuned[39]. Moreover, these compounds allow selective targeting of mitochondrial selenoproteins, such as TrxR. The antimitochondrial activity of cationic gold(I) NHC complexes could be related to their cationic and lipophilic character, linking to properties that are known from the class of delocalized lipophilic cations (DLCs). Notably, DLCs can selectively accumulate in the mitochondria of cancer cells driven by their enlarged mitochondrial membrane potential.

The effects of gold(I) NHC complexes on cell metabolism and their interference with pathways relevant for cancer cell proliferation have been studied for many derivatives[40]. In this area, Ott *et al.* reported on the synthesis of an Au(I) N-heterocyclic carbene **1.2d**, utilizing an aminotriazole NHC carbene ligand[41], that displayed good activity against various cancer cell lines and good to moderate inhibitory activity of TrxR. As 1,2,4-triazoles possess different electronic properties than the classical imidazolium salts, these complexes may show a different behaviour concerning donor abilities and physiochemical properties[42].

A further interesting linear, cationic Au(I) NHC complex series was reported by Casini, Picquet *et al.* in 2014[43] featuring xanthine ligands, including caffeine, which naturally possesses an imidazole ring and has recently been reported for its anticancer properties[44]. Within this series, the bis-carbene complex [Au(9-methylcaffein-8-ylidene)$_2$]$^+$ **1.2e** showed selectivity *in vitro* against various cancer cell lines, with respect to non-tumorigenic ones, and most importantly was also demonstrated to be a selective G-quadruplex stabilizing agent. X-ray structural studies showed that the three molecules of compounds are bound to a G-quadruplex structure[45]. G-quadruplexes (also known as G4) are nucleic acid sequences, rich in guanines, capable of forming a characteristic four-stranded fold. Remarkably, formation of quadruplexes causes a net decrease in the activity of the enzyme telomerase, which is responsible for maintaining the length of telomeres. Therefore, molecules that template the formation or stabilize the structure of G-quadruplex DNA might lead to development of new effective anticancer drugs based on selective telomerase inhibition[46].

Within the NHC family, also Pt(II) complexes have been described, including [(1,3-dibenzyl)imidazol-2-yl]platinum(II) carbene complexes with different spectator

ligands (Cl^-, DMSO, PPh_3)[47]. Some of these compounds were shown to bind DNA predominantly by initiating its aggregation and precipitation to the effect of a G1 phase cell cycle arrest in melanoma cells.

Metallocene compounds, homonuclear as well as heteronuclear, have gained considerable interest in anticancer research throughout the last years. For example, titanocene dichloride (Cp_2TiCl_2) (**1.2f**), was one of the early non-platinum based anticancer complexes that reached phase II of clinical trials[48]. However, the clinical response was not significant enough to pursue it, especially since Cp_2TiCl_2 displays rather poor solubility and stability in water, leading to problems in drug formulation [49]. Furthermore, the exact mode of action could not be elucidated so far[50]. Addressing the solubility and stability properties, various titanocene analogues have been synthesized. McGowan *et al.*[51] demonstrated that by introducing amino groups to the bent metallocenes, improved hydrolytic stability could be achieved[52].

The organometallic arene complexes termed "RAPTAs" are among the most investigated examples of Ru(II) half-sandwich complexes with antimetastatic and antiangiogenic properties[53]. Consisting of a monodentate 1,3,5-triaza-7-phosphaadamantane (pta) ligand and a facial η^6-arene ligand coordinated to Ru(II) in a so-called "piano-stool" conformation, RAPTA complexes display good stabilities under physiological conditions. Concerning the mode of action, aquation of the chloride ligands appears a prospective intracellular drug activation process[54]. Although the exact target identification is still elusive, RAPTA compounds have been found to alter the expression, and thereby the activity, of key proteins involved in the regulation of the cell cycle and apoptosis[55]. RAPTA-C (arene=cymene) (**1.2g**) is the most representative example of this series[56]. Similar to titanocene dichloride, a number of derivatives have been synthesized in order to stepwise alter the physicochemical properties[57].

Metal complexes can interfere with the cellular redox chemistry in several ways: directly through metal or ligand redox centres or indirectly by binding to biomolecules involved in cellular redox pathways. Within the metallocene family, Sadler *et al.* illustrated that organometallic ruthenium(II) and osmium(II) arene complexes and iridium(III) cyclopentadienyl complexes of the type $[(arene/Cp^{xPh})M(N,N)Cl/I]^{n+}$ can achieve nanomolar potency toward cancer cells in

combination with the redox modulator L-buthionine sulfoximine[53b, 58]. A representative member of this series, the chlorido(iminopyridine)arene- ruthenium(II) complex [Ru(η^6-*p*-cym)(*p*-Impy-NMe_2)Cl]$^+$ (**1.2h**), is reported in Figure 4. Thus, these complexes were proposed for possible use in combination therapy with redox modulators to increase their anticancer effects. The results highlight the importance of determining not only the distribution of metal anticancer complexes in cells but also their speciation, the chemical form of the metal complex, including the oxidation state of the metal, the fate of the ligands, and dynamic processes such as efflux.

Ferrocene, a compact metallocene possessing stability in non-oxidating media, low toxicity, and reversible redox behaviour, has recently played an important role in bioorganometallics, as an antiparasitic or an antibacterial[59], and indeed as an antitumoral agent[60]. Examples of the vast and regularly increasing number of biologically active ferrocene compounds with antitumoral potential are presented in a recent review by Jaouen, Vessieres *et al.* and will not be treated in details here[61]. Overall, they illustrate the richness of the activity in this field, the variety of the structures brought into play and the diversity of possible mechanisms of activity.
A remarkable complex in that matter is the ferrocene containing complex ferroquine (**1.2i**) which is structurally close to the antimalarial drug chloroquine[62]. It shows similar activity compared to chloroquine but most importantly it is also active against chloroquine resistant malaria parasites[63]. Since malaria resistance has become a critical issue in malaria-endemic countries, development of new organometallic analogues is crucial. Ferroquine has completed phase IIb of clinical trials and is about to enter phase III[64].

Recently, there has been a strongly growing interest in the utilization of heteronuclear compounds as anticancer agents[65]. This is due to the hypothesis that different metals within the same compound can either react in different pathways towards the targeting of cancer cells or improve the chemicophysical properties of the overall scaffold. A greater challenge in this concept of *multinuclearity* is displayed by the combination of two (or more) different metal containing moieties, requiring a design of suitable ligands to coordinate selectively both metal cores. A number of successful compounds have been described in the literature, including

ferrocene-based complexes. In 2008 for example, Dyson *et al.* reported on the synthesis of a ferrocenoyl pyridine arene ruthenium complex (**1.2j**). This complex proved to be twice as active towards cancer cells, as their monomeric analogue[66]. Contel *et al.* demonstrated the cytotoxic propertied of a heterometallic complex series containing both a gold(III) and a palladium(II) metal centre with iminophosphorane ligands (**1.2k**), derived from ferrocenylphosphane[67]. Especially the trimetallic derivatives have shown significant higher anticancer properties with respect to their corresponding monomeric analogues.

Stepping away from iron based multinuclear complexes, Casini *et al.* reported in 2011 on the synthesis of the titanocene-gold trimetallic complex (**1.2l**) showing 10-fold higher activity against cancer cells than the monomeric titanocene-phosphine and enhanced stability in aqueous solution[68]. Captivatingly, this complex also exhibits luminescent photophysical properties, originating from the bent metallocenes, making it suitable for distinctive uptake studies. The same group also reported on a series of bimetallic Ti-Ru complexes based on a titanocene-phosphine backbone anchored to a Ru(II)-arene scaffold, which showed improved antiproliferative effects on cancer cells in comparison to their mononuclear Ti and Ru organometallic precursors[69].

Notably, the synthesis, characterization and stability studies of new titanocene complexes containing a methyl group and a carboxylate ligand (mba = S–C_6H_4–COO) bound to gold(I)-phosphane fragments through a thiolate group [(η-$C_5H_5)_2$TiMe(μ-mba)Au(PR_3)] were recently reported[70]. Two compounds were selected for further *in vivo* studies on mice based on their selectivity *in vitro* against renal cancer cell lines when compared to non-tumorigenic human kidney cell lines (HEK-293T and RPTC) and the favourable preliminary toxicity profile in C57BL/6 mice. Evaluation of Caki-1 xenografts in NOD.CB17-Prkdc SCID/J mice showed an impressive tumor reduction (67%) after treatment for 28 days (3 mg per kg per every other day) with heterometallic compound [(η-$C_5H_5)_2$Ti(CH_3)[OC(O)C_6H_4SAu(PPh_3)]].

1.3 Cyclometalation

Cyclometalation is a convenient method of stabilizing metals in different oxidation states. This is particularly useful in the case of Au(III) compounds which are otherwise prone to be reduced to their respective Au(I) species, as well as to colloidal Au(0) gold. In general, cyclometalation is defined as the metal mediated C-R bond activation of a cyclic organic ligand system. The chelating ring consists of a strong, covalent C-M σ bond and a coordination D-M bond. These ligands incorporate one or more donor atoms (such as O-, N-, P-, S- or Se). Figure 5 illustrates a general representation of the different classes of cyclometalated compounds.

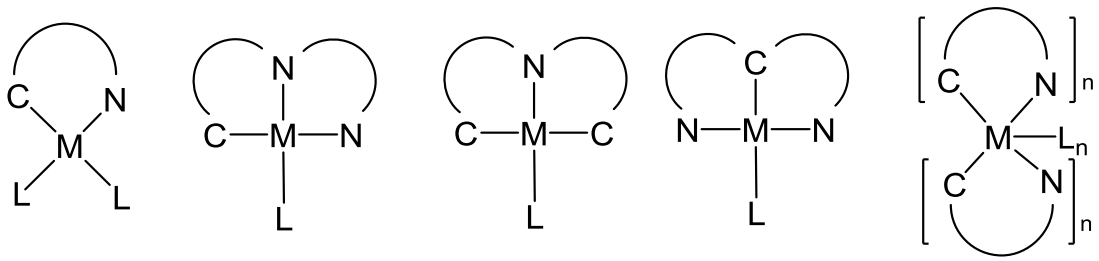

M = metal L =ancillary ligand

Figure 5. General representation of cyclometalated complexes.

Cyclometalation reactions proceed especially easy and with high regioselectivities for the formation of five-membered ring products, due to their higher stability in comparison to their corresponding four- or six-membered ring products. Their synthesis is generally found to proceed with high yields and selectivities due to the five-membered ring chelate effect[71]. The first intramolecular five-membered ring complex incorporating a main group element was already reported back in 1955 by Bäller and Müller, when they introduced a cyclometalated organoaluminum complex[72]. Since the 1970s, a vast number of cyclometalated organotransition metal compounds have been reported for metals such as Pt, Pd, Rh, Ir, Ru, Os and Au[73]. As they are not only easy accessible but also demonstrate high turnover frequencies (TOF), they were traditionally applied in dehydrogenation and metal-

catalyzed cross-coupling reactions[73].

More recently, cyclometalated organotransition metal compounds have also been investigated as anticancer compounds, as the metal centre gets stabilized conveniently, and especially five-membered ring products are relatively easy obtained. Therein, a variety of substrates has been reported, such as amines, imines, 2-phenylpyridines, benzo[*h*]quinones and other compounds incorporating nitrogen-, oxygen, phosphorus- or sulphur donor atoms. Thus, a consistent number of reports include these families of complexes.

In the following, the main results obtained on the synthesis and biological activities of cyclometalated Au(III) compounds are summarized. Numerous ligand systems utilizing different donor atoms have been reported[27]. As they offer the highest stabilizing properties, most cyclometalated systems incorporate one or more nitrogen atoms as the electron donating component. The best stabilities in physiological environment, as well as suitable chemicophysical properties for therapeutic applications, are therein displayed by C^N, C^N^C, C^N^N and C^N^S Au(III) pincer complexes and shall therefore be discussed in the following chapters. Furthermore, a number of studies report on the compounds promising biological effects and constitute the basis for future drug design.

1.3.1 Cyclometalated Au(III) compounds as anticancer agents

Au(III) compounds as anticancer agents appeared to be a logical step forward from Pt(II) based compounds, since Au(III) is isoelectronic (d^8) and isostructural to Pt(II), featuring the same square-planar geometry. However, at variance with Pt(II) complexes, numerous studies have shown that anticancer gold compounds aim at other biomolecules and biological pathways as possible targets[74]. As Au(III) is labile to the reduction to its more stable Au(I)/Au(0) forms, Au(III) complexes are generally strongly oxidizing agents. Reductions can easily be driven by thiols groups of biological systems, making Au(III) potentially toxic[75]. Therefore, Au(III) complexes were long believed not to be suitable for medicinal applications[76]. As a consequence, Pt(II) cyclometalated complexes for the treatment of cancer cells are

(yet) more numerous. Cyclometalation, however, offers a convenient way for the stabilization of the Au(III) centre and “fine tuning” of the physiochemical properties within the cyclometalated moiety.

1.3.1.1 Au(III) C^N complexes

Representative members of this family are reported in Figure 6 below. The class of Au(III) C^N complexes with cytotoxic properties was first introduced by Parish, Buckley *et al.* in 1996[77]. They synthesized a series of Au(III) complexes of the structure [(damp)AuX_2] with a 2[dimethylamino)methyl]-phenyl (damp) backbone (**1.3a**). The compounds displayed cytotoxic activities comparable to cisplatin against various cancer cell lines, such as bladder (HT1376) and ovarian (CH1) cancer cells, with the malonato and acetato substituted complex being the most selective and active of the series *in vitro* and showing moderate anticancer effects *in vivo*. Although the structure appears to be very similar to cisplatin, an alkaline elution study showed that the series does not cause interstrand DNA cross-links. Instead, both complexes lead to submicromolar inhibition of cysteine protease cathepsin B[78] and inhibition of TrxR[79].

Messori *et al.* reported on the synthesis of complex **1.3b** enabling a dimethybenzyl-pyridine backbone in 2005[80]. This complex proved to be stable under cellular reducing conditions and although its cytotoxic activity against ovarian cancer cell line A2780 is comparable to cisplatin, complex **1.3b** displays significant cross-resistance, suggesting a different mechanism of action. It was demonstrated that **1.3b** selectively inhibits TrxR activity, which is presumed to be caused by progressive oxidative damage of (seleno)cysteine residues of the active site of TrxR[17a]. Other studies showed that the hydrolysis product of **1.3b** is able to disrupt mitochondrial function and alter the glycolytic pathway in A2780 cancer cells, leading to apoptosis[81].

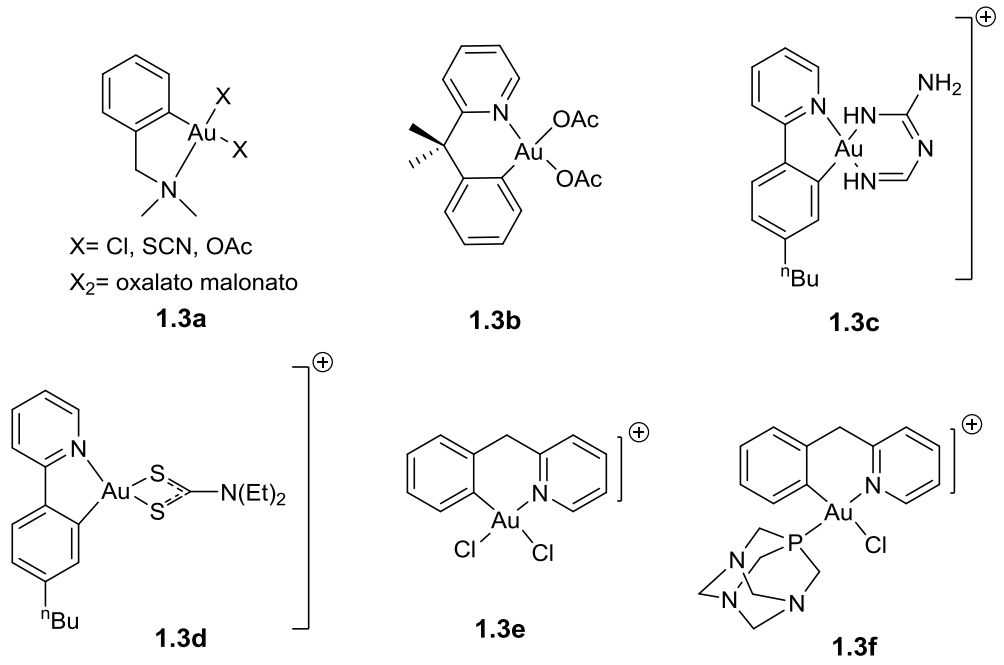

Figure 6. Au(III) C^N complexes with cytotoxic properties.

The cationic complex **1.3c**, bearing a biguanide moiety, was synthesized by Che *et al.* in 2012[82]. By introducing the polar biguanide ligand, a water-soluble complex was obtained that is able to form an Au(III)-GSH complex and is detectable by ESI-MS. The complex displays higher toxicity than cisplatin against several cancer cell lines, such as cervical cancer (HeLa) cells. The toxicity of complex **1.3c** is believed to be caused by swelling of the endoplasmic reticulum (ER), being supported by oligonucleotide microarray analysis and western blotting assays cells. Irreversible ER stress triggers apoptosis, with the activation of the canonical mitochondrial cell death pathway playing an essential role[83]. A structural analogue (**1.3d**) was reported by the same group, also utilizing a dimethybenzyl-pyridine C^N backbone and a dithiocarbamate ligand[84]. This complex selectively inhibits breast cancer cells (MCF-7) but is less toxic to non-tumorigenic immortalized liver cells (MIHA). Complex **1.3d** was demonstrated to form adducts with cysteine-containing peptides and proteins (e.g. deubiquitinases) by ESI-MS experiments. Notably, Au(III) C^N complexes bearing a dithiocarbamate ligand had been previously proven by Contel *et al.* to cause mitochondria dysfunction induced by reactive oxygen species (ROS) and Bax/Bak activation[85].

Synthesis of the 2-benzylpyridine derivative **1.3e** was reported by Cinellu *et al.*[86]

already in 1996 by reacting $NaHAuCl_4$ with 2-benzylpyridine in refluxing $MeCN/H_20$ overnight. In 2015 Casini, Cinellu *et al.* synthesized the structural analogue by replacing one chlorido ligand in the presence of excess KPF_6 with 1,3,5-triaza-7-phosphaadamantane (PTA)[87]. PTA offers multiple benefits as a ligand, since it is non-toxic and increases the water solubility of the resulting complexes. The cytotoxic properties of complex **1.3e** and **1.3f** against various cancer cell lines such as ovarian adenocarcinoma (A2780), mammary carcinoma (MCF-7) and lung carcinoma (A549) were explored. Both complexes demonstrate good cytotoxic activity, with complex **1.3f** displaying higher cytotoxic activity than **1.3e**, which can probably be contributed to the increased water solubility induced by the PTA moiety. Among the possible mechanism of actions, potent inhibition of the zinc-finger protein PARP-1 is reported, which has been already demonstrated for several coordination gold(III) complexes with N-donor ligands[88]. Of note, organic compounds as PARP inhibitors are currently in clinical trials for their selective cytotoxic properties, as well as their DNA damage repair inhibiting abilities[89] [5].

1.3.1.2 Au(III) C^N^N complexes

In 2003, Cinellu and co-workers reported on the synthesis of the Au(III) complex **1.3g** with a dimethylbenzyl-bipyridine C^N^N backbone (Figure 7)[90]. By choosing a OH^- ligand in ancillary position to the Au(III) centre, good solubility of the complex under physiological conditions was obtained. Upon reaction with bovine serum albumin (BSA), tight metal–protein adducts were formed. It is believed that binding of complex **1.3g** to BSA is achieved *via* histidine moieties on the protein surface. Interaction studies of organometallic complexes with serum albumin have attracted considerable interest during the last years[91]. Serum albumin is the most abundant plasma protein and serves many physiological functions, such as maintaining both the colloid osmotic blood pressure and – together with other compounds - the blood pH value. Furthermore, it is suspected that serum albumin protects cells against oxidative stress[92]. Complex **1.3g** shows higher cytotoxic activity and selectivity against a series of 12 human tumor cell lines than cisplatin. Inhibition of

biomolecular systems, such as mammalian target of rapamycin/rapamycin-analouges (mTOR), have been suggested as possible mechanism of action[93].

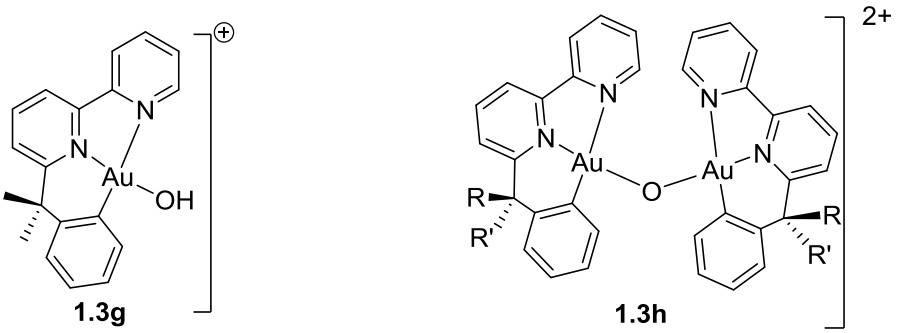

Figure 7. Mononuclear and dinuclear Au(III) C^N^N complexes.

The same group reported on the dinuclear, oxo-bridged complex variants of general formula $[(N^N^C)_2Au_2(\mu\text{-}O)][PF_6]_2$ (**1.3h**) (Figure 7) and their cytotoxic properties in 2011[90]. Coordination oxo-bridged Au(III) N^N complexes had been reported before[94] (named "Auoxo" compounds), showing antiproliferative effects towards various human cancer cell lines. However, the latter compounds displayed stability issue of the Au(III) centre in the reducing intercellular milieu, which were overcome introducing the strong Au-C bond in the organometallic analogues. Notably, these compounds reveal remarkable redox stability even in the presence of effective biological reductants such as ascorbic acid and glutathione. In comparison to complex **1.3g**, complexes **1.3h (a)** and **(b)** showed in general rather moderate cytotoxic activity against the series of 12 human tumor cell lines. However, **1.3h (a)** proved to be particularly active against human breast cancer cells (401NL), while **1.3h (b)** displayed only scarcely selective cytotoxic activity. Mass spectrometry studies with model proteins (hen egg white lysozyme and horse cytochrome c) indicate that upon reaction with proteins, complexes **1.3h (a)** and **(b)** form monometallic adducts, preserving the Au(III) centre and retaining the multidentate ligand. This also indicates that the complex-protein interaction facilitates the cleavage of the oxo-bridge and the conversion into the more active monometallic species.

1.3.1.3 Au(III) C^N^C complexes

The field of Au(III) C^N^C complexes with anticancer properties has been closely examined by Che and co-workers (Figure 8). As C^N^C pincer ligands allow the highest stabilization of the Au(III) centre among the herewith presented ligands, it is not surprising that this family, at variance with the case of Pt(II) complexes, makes up for the majority of the reported cyclometalated Au(III) compounds.

The Au(III) complex class utilizing the 2,6-diphenylpyridine as a C^N^C ligand was reported by Che *et al.* already in 1998[95] via reaction of $K[AuCl_4]$ and [Hg(C^N^CH)Cl] under reflux in acetonitrile. Substitution of the chlorido ligand of complex **1.3i** leads to a number of cationic Au(III)C^N^C complexes with different ancillary ligands (**1.3j**-**1.3l**). Complex **1.3j** (mim = 1-methylimidazole) and **1.3k**, containing non-toxic N-donor ligands, display cytotoxic activities similar to cisplatin against various cancer cell lines, such as HeLa cancer cells[96]. However, they do not show cross-resistance with cisplatin against nasopharyngeal (NPC) cancer cells. Gel-mobility shift assays and viscosity analysis show that **1.3j** intercalates with DNA, causing DNA elongation. It has been reported that DNA intercalators enhance the assembly of G-quadruplexes. Consequently, native polyacrylamide gel electrophoresis (PAGE) was employed to examine the ability of **1.3j** to intercalate with DNA and induce the formation of intramolecular G-quadruplexes from a model oligonucleotide[96]. This indicates that **1.3j** may be regarded as the classical metallointercalator $[Pt(terpy)Cl]^+$ from the perspective of DNA intercalation and potential telomerase inhibition. In addition, by flow cytometry analysis in SUNE1 cells, it was demonstrated that **1.3j** and **1.3k** target cellular DNA *via* S-phase cell arrest, leading to apoptosis.

As reviewed by Sadler and Berners-Price already in 1987, phosphine containing compounds exhibit phosphine ligand-mediated cytotoxicity[97]. However, due to their poor stability under physiological conditions and non-specific binding affinities towards various biomolecules, the application of these compounds as anticancer compounds is hindered. By introducing the C^N^C scaffold, significantly higher complex stabilities were obtained. For example, complex **1.3l** and its

dinuclear analogue **1.3m** are soluble and stable in aqueous media[96]. These compounds neither change the melting temperature of calf-thymus DNA (ctDNA) significantly, nor cause S-phase cell arrest, suggesting a different mode of action with respect to cisplatin. The dinuclear complexes of type **1.3m** show higher cytotoxic activity against various cancer cell lines than their mononuclear counterparts. The highest cytotoxicities were displayed for n = 3, relating to the cytotoxicity of the free 1,2-bis(diphenylphosphino)propane (dppp) ligand. *In vivo* studies in rats with liver cancer (HCC) orthografts showed that the dppp derivative is a nanomolar inhibitor of TrxR1 and induces ER stress[98].

By replacing the PPh_3 moiety with a NHC ligand complex **1.3n** and complex **1.3o** - as the respective dinuclear compound – can be obtained[99]. This results in a reduction of the cytotoxic activity and selectivity of the compounds, supporting the fact that indeed phosphine ligand-mediated cytotoxicity is crucial for complexes **1.3l** and **1.3m**. In this case, the mononuclear complex **1.3n** displays higher cytotoxic activity than its dinuclear analogue **1.3o**, being 167-fold more cytotoxic to non-small lung carcinoma cells (NCI-H460) than to normal lung fibroblast cells (CCD-19Lu). By DNA interaction studies with ctDNA it was demonstrated that complex **1.3n** induces DNA strand breaks and subsequent cell death through the stabilization of TopoI-linked DNA[100].

A recent development in the field of Au(III) C^N^C complexes is the discovery of supramolecular polymers, self-assembled from cyclometalated Au(III) C^N^C complexes. In this framework, the mononuclear complex $[Au(C,N,C)(4\text{-dpt})]^+$ (4-dpt = 2,4-diamino-6-(4-pyridyl)-1,3,5-triazine) **1.3p** was chosen by Che *et al.* due to the ability of the antiangiogenic 4-dpt ligand to form intramolecular hydrogen bonds and to establish π-π interactions[101]. These factors proved to be essential for supramolecular complex formation by self-assembly in acetonitrile at ambient temperature. The stability of **1.3p** in phosphate-buffered saline in the absence and presence of the biological reductant glutathione (GSH) was examined. UV-Vis absorption spectrophotometry demonstrated that upon reaction with GSH, **1.3p** shows an increased absorbance between approximately 260 nm and 380 nm. For incubation periods over 24 hours the 4-dpt ligand is released into the solution, and both [Au(C^N^C)Cl] and 4-dpt contribute to precipitation, as was demonstrated by

ESI-MS and ^{1}H NMR. These results suggest that the 4-dpt ligand of complex **1.3p** can be replaced by chloride ions in PBS, with formation of [Au(C^N^C)Cl] and release of 4-dpt. The log–log plot of the concentration-dependent specific viscosity of **1.3p** in CH_3CN measured at 294±1 K shows a significant increase in viscosity at concentrations above 6.3 g L^{-1}, relating to typical characteristics of supramolecular polymer solutions. Via transmission electron (TEM) and scanning electron microscopy (SEM), partially aligned nanofibers with diameters and lengths of about 50 nm could be demonstrated for **1.3p.** The significant viscosity at high concentration of **1.3p** (20 mM) is contributed to the partial entanglement of these nanofibers. Complex **1.3p** displays high cytotoxic activity towards the murine cancer cell line B16 and non-tumorigenic lung fibroblast cells (CCD-19Lu). It was suggested that the sustained release of free 4-dpt ligand and simultaneous formation of Au(III)-glutathione adducts account for the observed cytotoxicity. GSH adduct formation was assessed via ESI-MS and UV-VIS for **1.3p** in phosphate-buffered saline containing GSH (2 mM), showing significant cluster peaks for $[(C^N^C)Au(GSH)]^{+}$ and the dimeric species $[(C^N^C)_2Au_2(GSH)_2]^{2+}$.

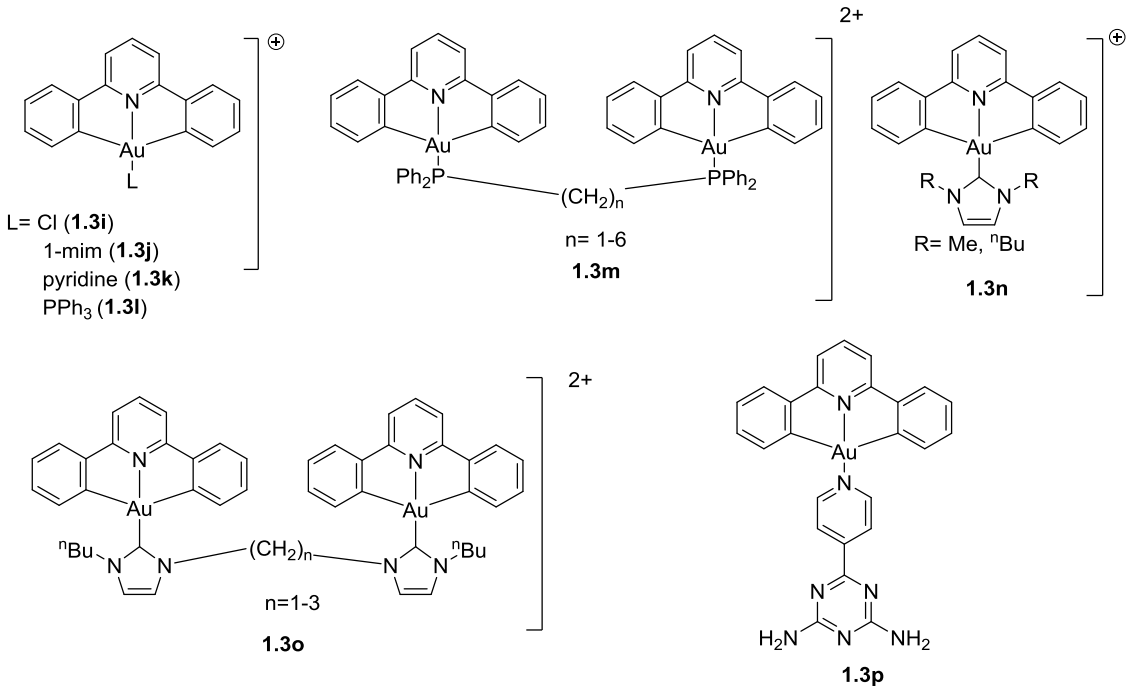

Figure 8. Au(III) C^N^C complexes synthesized by Che *et al.*

Furthermore, the nanofiber network of the polymer could be used to encapsulate

other cytotoxic agents, thus enabling a localized drug delivery while reducing side toxicity.

All Au(III) C^N^C complexes follow a general synthesis route as depicted in Figure 9. A direct C-H activation of the respective C^N^C ligand in the presence of an Au(III) precursor (usually $KAuCl_4$) is theoretically possible, but requires high temperatures, which can also result into decomposition of the ligand. As an alternative, a transmetalation pathway using organomercury(II) reagents is the most common synthesis strategy nowadays, as it allows milder reaction conditions and less formation of by-products occurs[102]. In a first reaction step, the 2,6-diphenylpyridine derivative is reacted with mercury(II) acetate, followed by metathesis with LiCl, yielding an organomercury(II) species. Subsequent transmetalation is achieved by reacting the organomercury(II) complex with $KAuCl_4$ in acetonitrile under reflux.

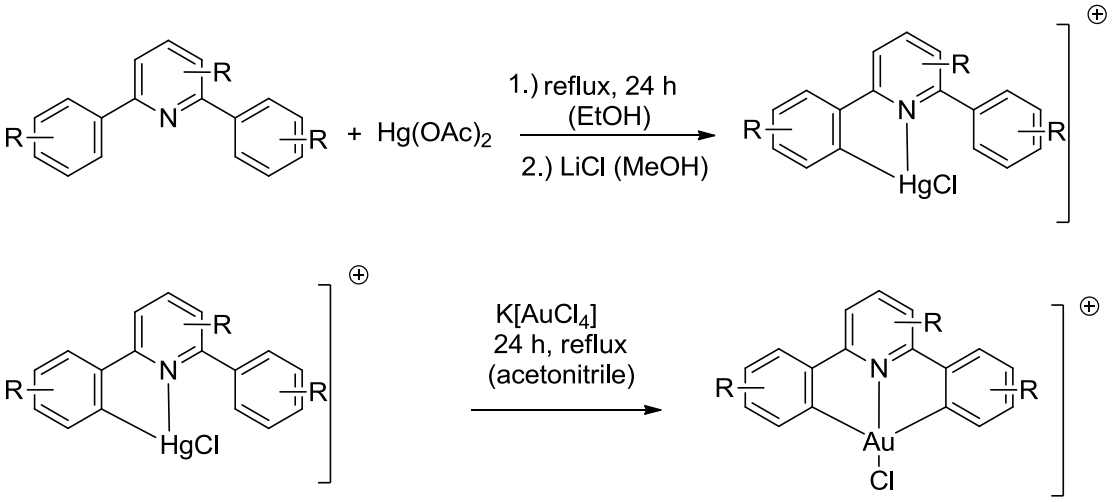

Figure 9. General complex formation of Au(III) C^N^C complexes via transmetalation.

1.3.1.4 Au(III) C^N^S complexes

Bidentate 2-pyridyl carboxylate[103] and 2-pyridyl amidate complexes[104] of Au(III) have been reported to show both catalytic and biological activity. Tridentate analogues of bis(amidate), bis(carboxylate), and bis(iminothiolate) ligands as a C^N^S or S^C^S moiety, have been reported for stabilizing other transition metals, mainly Pd(II)[105] and Ru(II)[106]. Surprisingly, these ligand classes have not been

extended to Au(III) and there are practically no reports of Au(III) C^N^S complexes with anticancer properties. Some related “pseudo-pincer” compounds have been reported though (Figure 10).

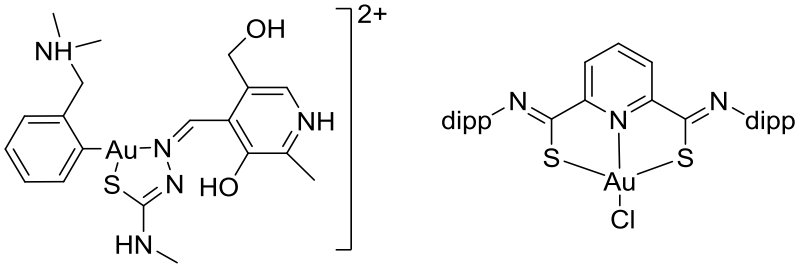

1.3q **1.3r**

Figure 10. Au(III) pseudo-pincer and Au(III) S^N^S complexes.

For example, Sommer *et al.* synthesized the Au(III) complex **1.3q** with a tridentate thiosemicarbazone ligand of the formula [Au(Hdamp-*C*^{1})Cl(H_2pydoxmetsc)]Cl_2 (pydoxmetsc = pyridoxal methylthiosemicarbazone) in 1999[107]. This complex is involved in extended hydrogen bonding networks with counter ions and solvent molecules. The antiproliferative effect of **1.3q** was tested on breast cancer cells (MCF-7) in vitro with promising cytotoxic results. In 2014, Bergman, Toste *et al.* reported on the Au(III) S^C^S complex **1.3r** with bis(iminothiolate) ligands, which displays high stability in reducing environments and was recommended for further testing in various fields of application, including as anticancer agent[108].

1.4 Coumarin based ligand systems

As mentioned before, coupling of specific ligands to the metal centre allows for the introduction of various physicochemical characteristics. Coumarin ligands display in this matter a highly interesting ligand class.

Coumarins are naturally occurring compounds and have therefore been known for decades[109]. One characteristic trait of coumarin itself (**1.4a**, Figure 11),

and most coumarin derivatives, are the highly luminescent properties. Coumarin dyes (as well as rhodamines) are therefore nowadays mainly used as gain media in blue-green tuneable organic dye lasers[110]. The luminescence of coumarin systems could also be highly relevant for medicinal application as it would allow for sophisticated cell-uptake studies.

Since many coumarin based systems display furthermore distinct medicinal properties, they have been in the focus of research by several working groups[111]. The aminocoumarin **1.4b**, commercialized under the tradename Novobiocin™, was already clinically approved in 1960 for its antibiotic properties[112]. In 1990, novobiocin attracted further interest since it was demonstrated to be an efficient antistaphylococcal agent against the (especially in hospitals problematic) Methicillin-resistant Staphylococcus aureus (MRSA) bacterium in combination therapy[113].
Coumarin derivatives have since successfully been used in the treatment of a range of diseases such as diabetes mellitus[114] or bacterial and microbial infections[115] and their role in the treatment of neurodegenerative diseases, such as Huntington's disease, is being investigated[116]. Furthermore, they have also been shown to possess cytotoxic activity against various cancer cell lines, including malignant melanoma or renal cell carcinomas[111b, 117].

The discovery that organometallic complexes enabling coumarin based ligands are more effective than the sole coumarins ligands shifted the research focus to the respective complexes. This can be attributed to the synergistic effect between the coumarin based ligands and the respective metal ions as the change in structure due to coordination results into alteration of solubility, lipophilicity, conductivity, dipole momentum and cell permeability[118]. Thus, different metal systems like Cu, Pt and Pd have been thoroughly investigated for coumarin complex formation and their resulting cytotoxic properties[111a].

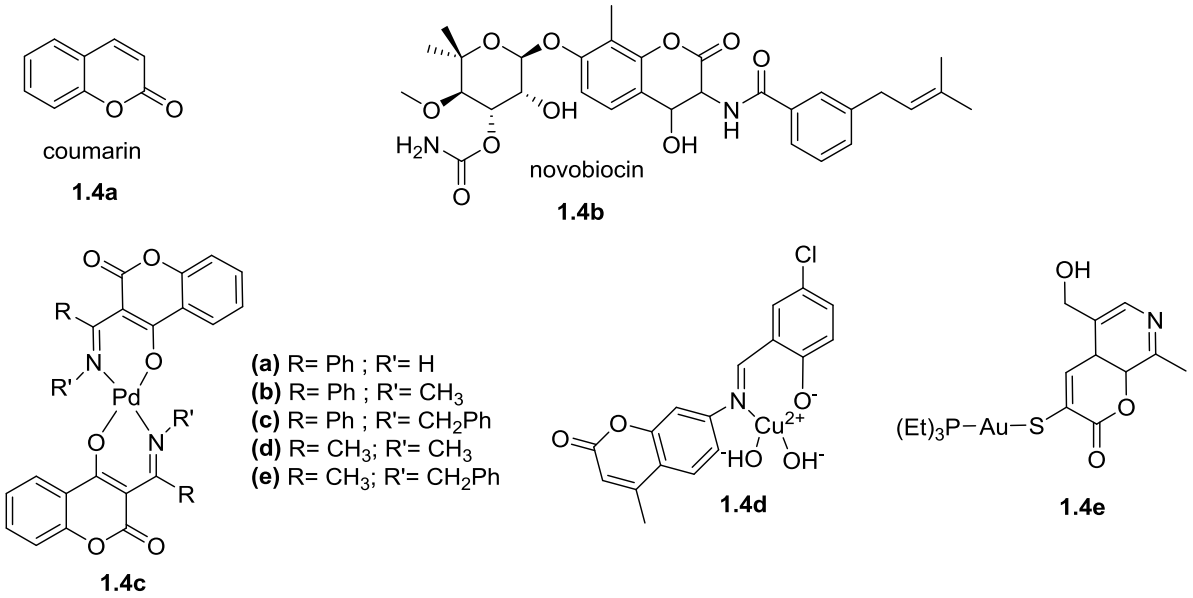

Figure 11. Coumarin based systems with medicinal properties.

Nawrot *et al.* synthesized a series of palladium(II) complexes with unsubstituted coumarin or N-alkylated derivatives (**1.4c(a) – (e)**)[119] in 2008. The series was obtained by reaction of 2-phenyl-4-oxo-4-H-chromone-3-carboxylic acid ethylester with 2-methyl-4-oxo-4-H-chromone-3-carboxylic acid methylester and amines. It could be demonstrated that the cytotoxic activity of the series' complexes depends strongly on the structure of the substituents at the nitrogen atom. Complex **1.4c(a)** presented the highest cytotoxic activity in the series against NALM-6 (human peripheral blood, leukemia, pre-B cell) and HL-60 (human promyelocytic leukemia) cancer cells with IC_{50} values comparable to carboplatin. Furthermore, **1.4c(a)** possesses high cytotoxic activity against the K562 (human erythroleukemia) cancer cell line with an IC_{50} value of 0.0078 µmol. The high cytotoxicity correlates with the low stability of complex **1.4c(a)**, which exists in two tautomeric forms.

In 2010, Walsh *et al.* reported on a series of Cu(II) complexes of Schiff base-derived coumarin ligands that showed not only antibacterial properties but also promising cytotoxic activity against human colon cancer (HT29) and human breast cancer cells (MCF-7)[115]. The Cu(II) complexes were obtained via reaction of the respective secondary amines with $Cu(OAc)_2$ in refluxing ethanol overnight. The best results were obtained for complex **1.4d**, with IC_{50} values comparable to the commercially available Mitoxantrone™, a drug to which HT29 cells are sensitive to.

So far, to the best of my knowledge, there have been no publications on Au(III) coumarin systems with anticancer properties. However, Taboada *et al.* reported on the synthesis of the Au(I) 7-azacoumarin complex **1.4e** with interesting luminescent properties[120]. The synthesis of this complex is a convenient one-pot synthesis: pyridoxalrhodanine, triethylphosphinegold(I) chloride and sodium methoxide in equimolar amounts react in methanol to afforded the azacoumarin complex [Au(TS)(PEt_3)] (HTS = 5-(hydroxymethyl)-8-methyl-3-thiol-7-azacoumarin). This reaction is noteworthy since both, the ligand and the complex, are formed in this one-pot reaction and the synthesis of azacoumarins is in general not trivial[121]. **1.4e** is only weakly luminescent in the solid state but exhibits strong luminescence in solution, making it suitable for sophisticated cell-uptake studies. Concerning cytotoxic activity, **1.4e** displayed higher cytotoxic activity against A2780 cells than cis-platin and proved also cytotoxic activity in the micromolar range against the cisplatin-resistant cancer cell line A2780cis.

1.5 Objective

Traditional Pt(II) chemotherapeutic agents display several disadvantages, such as resistance, limited spectrum of action and severe side effects in patients. This can mainly be contributed to their non-specific binding to intercellular components. Au(I) and Au(III) complexes exhibit therein a more sophisticated approach, as they are able to selectively inhibit target proteins and enzymes. In this respect, as an example, Au(III) coordination compounds have been shown to be efficient inhibitors of the zinc finger protein PARP-1, via displacement of Zn^{2+} ions and formation of the so-called "gold finger" domain. However, a major disadvantage of Au(III) coordination compounds is their limited stability in aqueous solution. Therefore, more stable Au(III) derivatives are in the focus of current research, such as organometallic compounds.

The prime objective of this PhD project is the stabilization of the Au(III) core in metal complexes and their biological evaluation, mainly as anticancer agents. For this aim, two cyclometalated systems based on 2,6-diphenylpyridine are chosen: the C^N^C system utilizing the sole 2,6-dipheylpyridine ligand and the C^N(R)^C system using 2,4,6-triaryl pyridines with different *para* substituents in the 6-aryl position. For the synthesis of the C^N(R)^C ligands a microwave procedure is evaluated and optimized. A transmetalation route *via* the respective Hg(II) precursor is applied and optimized for the synthesis of all Au(III) complexes. For the Au(III)[C^N^C] system, exchange of the ancillary ligand L against a PTA (1,3,5-triaza-7-phosphaadamantane) and a GluSH (thio-β-D-glucose tetraacetate) ligand is evaluated concerning solution behaviour and altered cytotoxic activity. The antiproliferative activity of the obtained Au(III) compounds is examined against the human cancer cell lines A549, SKOV-3 and 2008.

A further objective of this work is the coupling of a coumarin based ligand, N-(4-ethynylphenyl)-2-oxo-2H-chromene-3-carboxamide, to an Au(III) centre. For the stabilization of the Au(III) core, a bisdentate C^N (py^b-H = C^N cyclometalated 2-benzylpyridine) ligand is chosen. Coumarin ligands display interesting properties in the sense of medicinal and possible fluorescent properties. The obtained Au(III) C^N complex is therefore studied with UV-Vis and fluorescence spectroscopy.

II Results and Discussion

2.1 Au(III)[C^N^C] system

2.1.1 Synthesis and structural characterization of Au(III)[C^N^C] complexes

The C^N^C ligand (C^N^C = 2,6-diphenylpyridine) is a convenient choice for the cyclometalated precursor as it is moderately cheap and commercially available (purchased from Sigma Aldrich (CAS 3558-69-8)).

Synthesis of cyclometalated Au(III) complexes can generally be achieved *via* two routes: a) direct cycloauration or b) transmetalation of the respective Hg(II) precursor. Direct C-H activation of cyclometalated precursors by $[AuCl_4]^-$ is rather unfavourable, as it has to be executed at very high temperatures and long reaction times, raising the chances of product decomposition or by-product formation[122]. Transmetalation *via* the respective Hg(II) precursor is mostly preferred, as this allows for reactions under ambient temperatures, significantly shorter reaction times and normally leads to cleaner products at higher yields.

In a first reaction step, the Hg(II)[C^N^C]Cl precursor **1** is obtained in an adapted synthesis route according to Leese *et al.* from 1987[123] by refluxing equimolar amounts of 2,6-diphenylpyridine and mercury(II) acetate in ethanol under argon for 24 hours (Figure 12). Subsequent salt metathesis with LiCl affords complex **1** as a white solid.

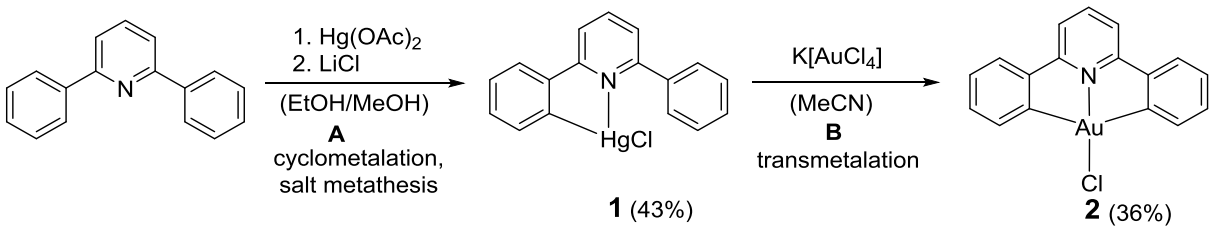

Figure 12. Synthesis of complexes 1 and 2.

It was found that the reaction occurs under air as well; however the obtained yields were significantly higher when using Schlenck techniques. This can possibly be explained by the relatively low bond strength of M–N bonds, with respect to that of M–P, M-O or M–S bonds for example[124] and therefore a facilitated bond formation in the absence of oxygen. The monomercurated Hg(II)[C^N^C]Cl complex **1** was separated from the bismercurated species by means of hot methanolic extraction, utilizing the better solubility of the monomercurated complex in comparison to the bismercurated one. ^{1}H-, ^{13}C-, ^{199}Hg- NMR and elemental analysis verify that the monomercurated species, rather than the bismercurated one, was synthesized. In the second reaction step, complex **2** is obtained in an adapted synthesis route according to Che *et al.*[95] by refluxing equimolar amounts of complex **1** and K[AuCl$_4$] in acetonitrile at 80°C under argon for 24 hours overnight.

Although complex **2** has been known for almost 20 years[95], it has not been fully characterized and was not evaluated for its biological properties so far. Complex **3**, [Au(C^N^C)(PTA)][PF$_6$], and complex **4**, [Au(C^N^C)(GluS)], have not been described in the literature so far. Both complexes were obtained in good yields by ligand exchange reactions of the chlorido ligand of complex **2** as shown in Figure 13.

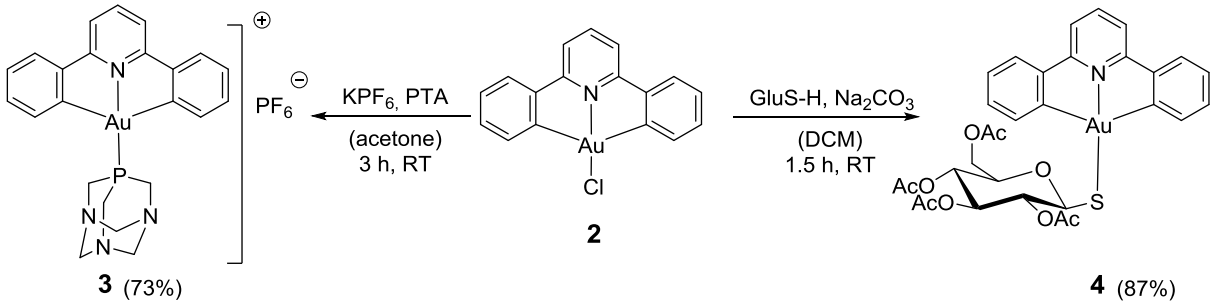

Figure 13. Ligand exchange reactions as performed for complex 3 and 4.

Complex **3** contains the water-soluble, cage-like aminophosphine ligand 1,3,5-triazaphosphaadamantane (PTA), which improves the overall water solubility of the

complex, while being non-toxic itself at the same time. This ligand was chosen with the intension of facilitated cell uptake due to the higher complex solubility in aqueous media such as PBS. As has been reported before, replacement of a *trans* bound chlorido ligand by a tertiary phosphine at an Au(III) centre can be achieved by reacting the respective precursor with one equivalent of the tertiary phosphine in the presence of excess KPF_6 or $NaBF_4$.[87, 125] By reacting complex **2** with one equivalent of PTA in the presence of KPF_6 in acetone for 3 hours at room temperature, complex **3** was obtained in good yields.

Complex **2** was also treated with one equivalent of thio-β-D-glucose tetraacetate (GluSH) and sodium carbonate in DCM for 1.5 hours at room temperature to obtain compound **4** in good yields. The $GluS^-$ ligand was chosen for two reasons: 1) facilitated cellular uptake into cancer cells by modulating the lipophilic/hydrophilic character of complex **2** and 2) possible interaction of the $GluS^-$ ligand with GLUT1 transporters, which are overexpressed in various cancer cell lines.

Figure 14 shows the ^1H NMR spectra of complex **2** and **3**.

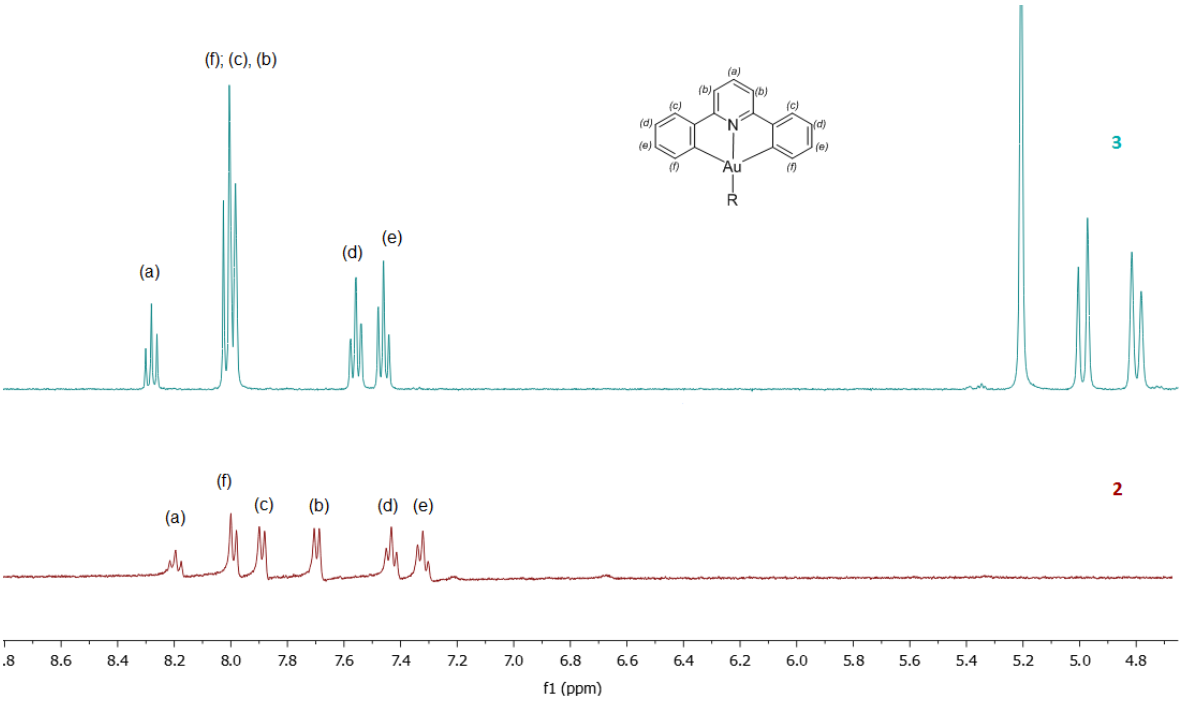

Figure 14. ^1H NMR of complex 2 and 3.

Complex **3** displays the distinctive signals of the PTA ligand between 4.6 and 5.3 ppm. Exchanging the chlorido ligand of complex **2** for the PTA ligand of complex **3**

results into a slight downfield shift of the C^N^C signals, which can be attributed to the PTA resonance. When comparing the free 2,6-diphenylpyridine ligand to the obtained complexes **2**-**4**, a significant shift in the ^{1}H NMR spectrum for the gold neighbouring proton can be observed in general, resulting from the strong deshielding caused by the –I effect of the electron-accepting Au-Cl moiety (Δδ = 0.48 ppm for complex **2**).

As complex **4** has a ligand that is optically active, the ^{1}H NMR presents itself with less sharp signals than the spectrum for complex **3,** as can be seen in Figure 15.

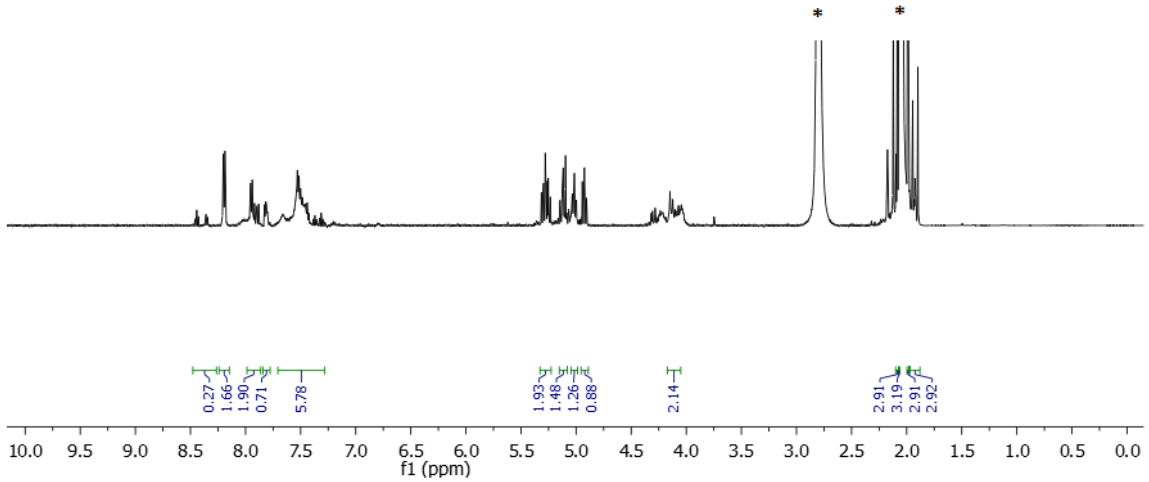

Figure 15. ^{1}H NMR complex 4 (* = d-acetone signals at 2.05 and 2.806 ppm).

The proton count however fits the structure of **4** perfectly and the signal of the thiolate proton at 2.20 ppm is not present in the product NMR, confirming the bond formation between gold and sulphur, while the four acetate groups of the thio-β-D-glucose appear as sharp singlet signals between 1.77 and 1.96 ppm. Moreover, all protons of the thio-β-D-glucose group are shifted downfield as well, resulting from the strong deshielding caused by the –I effect of the electron-accepting Au(III) centre.

The structures of complexes **2**, **3** and **4** were further assessed by ESI-MS measurements and their characteristic isotopic patterns compared to the theoretically calculated ones. Figure 16 displays the obtained ESI-MS spectrum for complex **3**, while Figure 17 shows exemplarily the theoretically calculated ESI-MS spectrum for complex **3**. The main m/z signal at 583.1330 is in perfect accordance with the calculated spectrum and can be attributed to the [Au(C^N^C)(PTA)]$^{+}$

cationic complex after loss of the PF_6^- counterion. The ESI-MS spectrum of complex **4** is depicted in Figure 18. The highest signal for m/z at 790.1442 is also in perfect accordance with the theoretically calculated isotopic pattern for the [M+H$^+$] peak of complex **4**. The signal for m/z at 616.1652 can be attributed to a partial decomposition of the ancillary GluS$^-$ ligand.

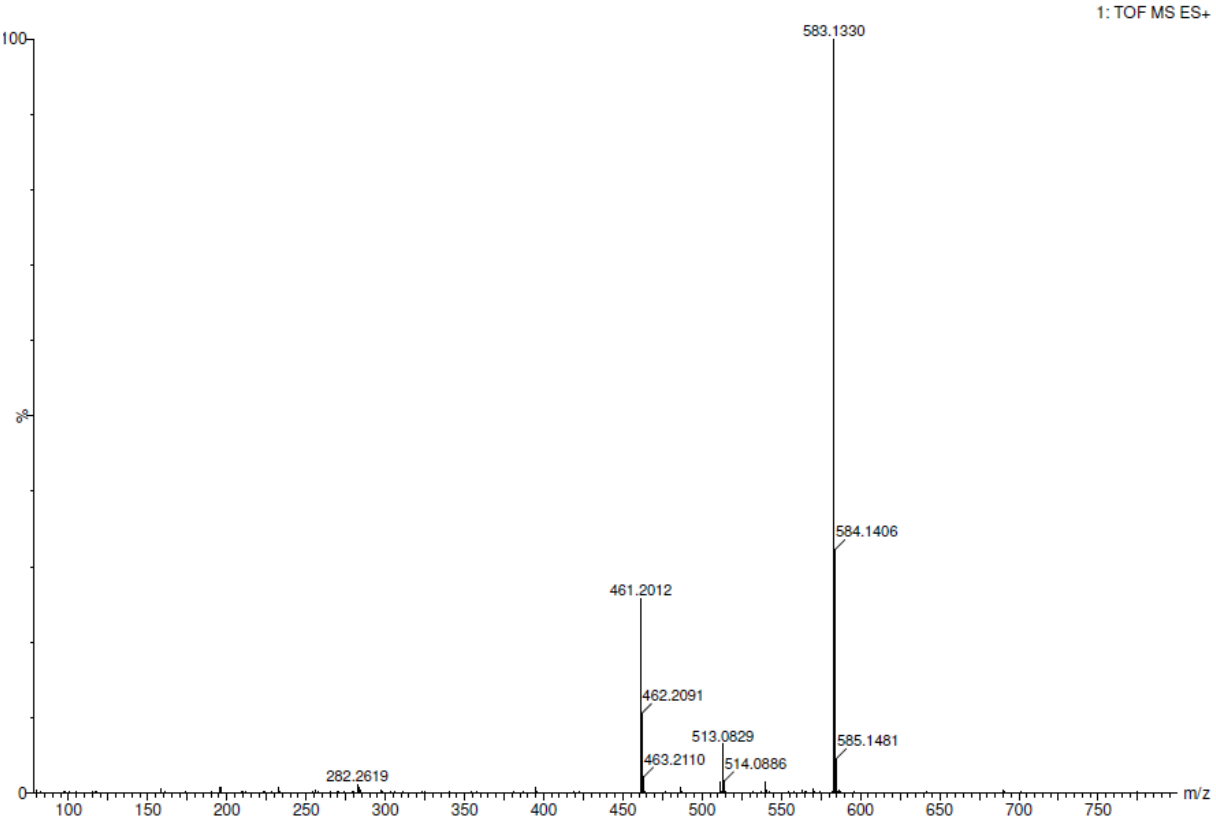

Figure 16. ESI-MS spectrum of complex 3.

C: 0-23 H: 0-23 N: 0-4 P: 0-1 197Au: 0-1

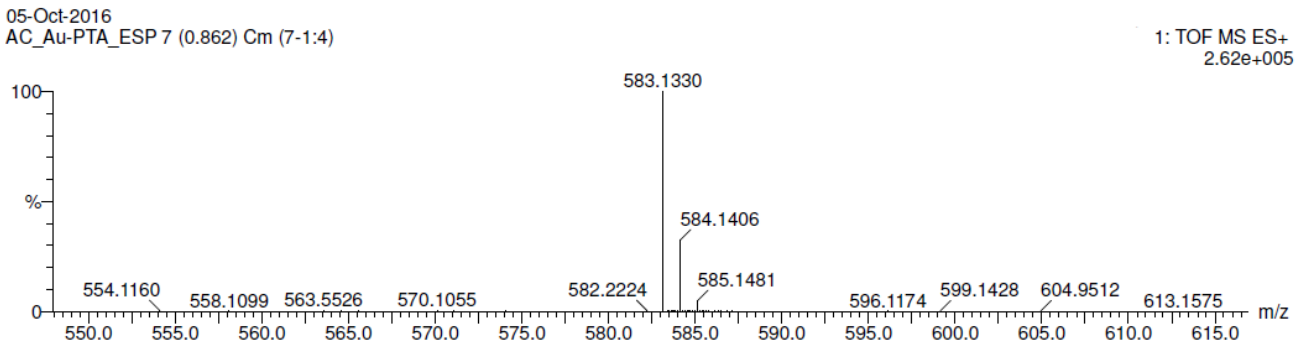

Minimum:				-1.5			
Maximum:		5.0	5.0	50.0			
Mass	Calc. Mass	mDa	PPM	DBE	i-FIT	i-FIT (Norm)	Formula
583.1330	583.1326	0.4	0.7	15.5	411.7	0.0	C23 H23 N4 P 197Au

Figure 17. Theoretically calculated ESI-MS spectrum of complex 3.

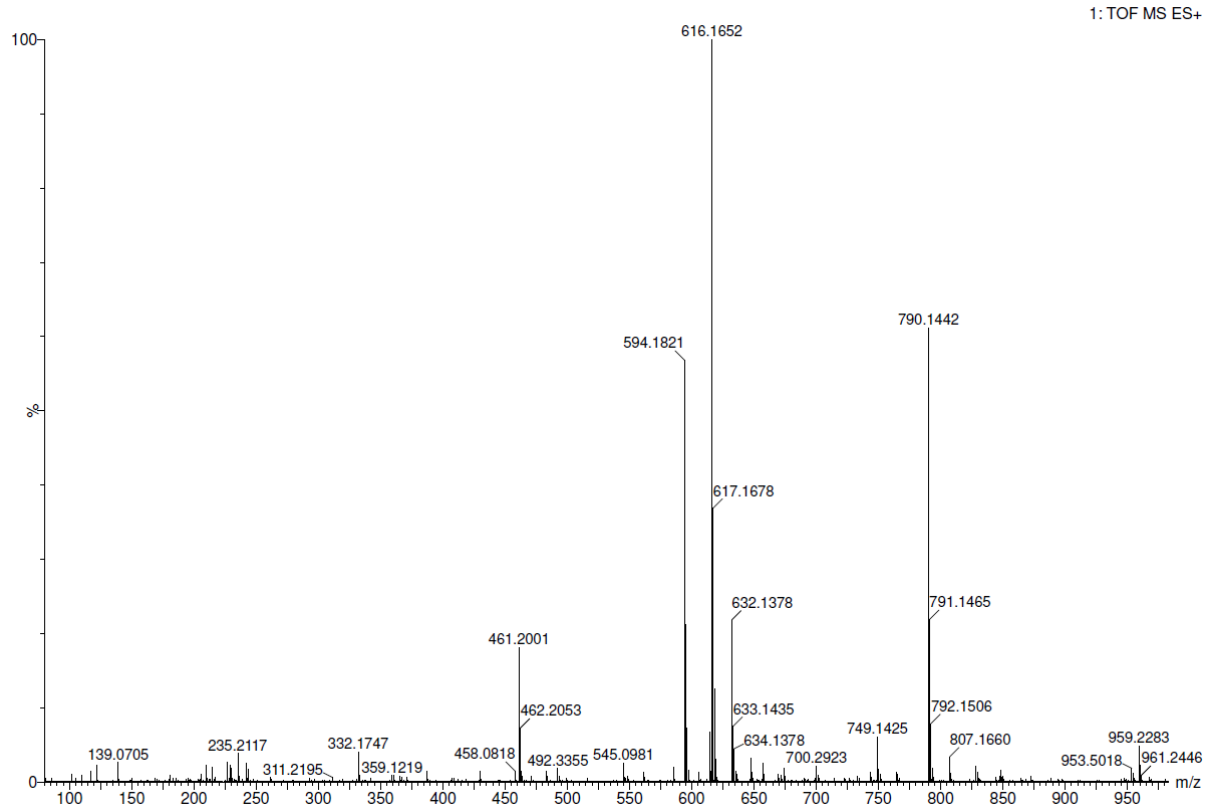

Figure 18. ESI-MS spectrum of complex 4.

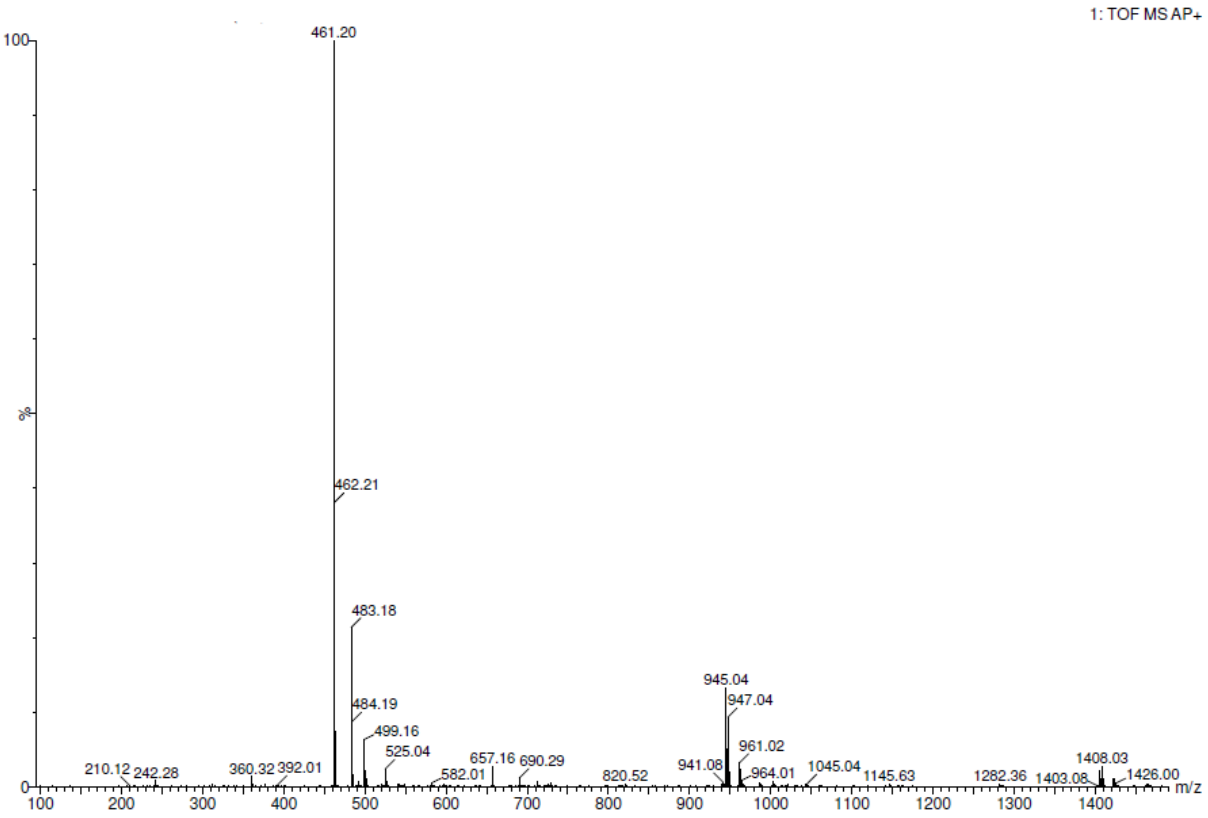

Figure 19. ESI-MS spectrum of complex 2.

Both, complex **3** and **4**, show signals for m/z at 461.20, signalling the total loss of the respective ancillary ligand and therefore correspond to the ESI-MS spectrum of complex **2** (Figure 19). Further structural conformation for complexes **3** and **4** was given by elemental analysis, with the difference of the measured CHN values to the calculated ones being less than 0.5% in general.

For complex **3**, single X-ray-quality crystals suitable for X-ray diffraction could be obtained by slow diffusion of pentane into an acetone solution of complex **3**. The crystallographic results confirm the expected structure of complex **3**, which is depicted in Figure 20. All hydrogen atoms, the hexafluorophosphate counterion and one co-crystallized water molecule are faded out for clarity. The Au(III) centre is coordinated in a slightly distorted square planar fashion by the C^N^C pincer ligand and PTA with bond lengths of Au1—C1 = 2.106(3) Å, Au1—N1 = 2.025(2) Å, Au1—C17 = 2.091(3) Å and Au1—P1 = 2.2707(7) Å which are comparable to literature-reported values for the Au(III)-C^N^C[126] scaffold and an Au(III) centre binding to PTA[87, 127].

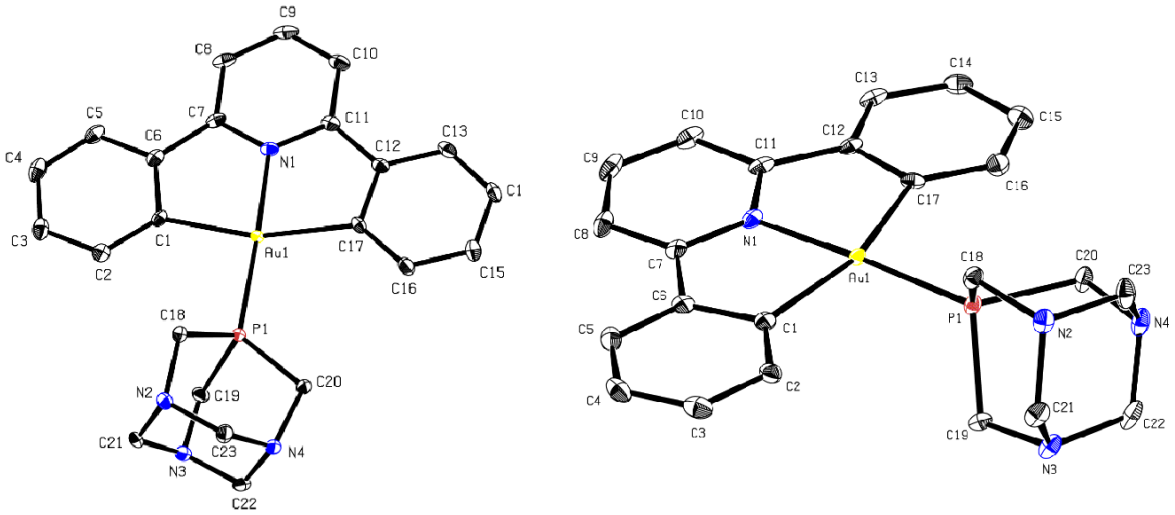

Figure 20. Two perspectives of the molecular structure of complex 3 in the solid state with ellipsoids at the 50% probability level. Selected bond lengths (Å) and angels (°): Au1—C1 2.106(3), Au1—N1 2.025(2), Au1—C17 2.091(3), Au1—P1 2.2707(7), P1—Au1—C1 97.13(7), P1—Au1—C17 102.10(7), N1—Au1—C1 80.32(9), N1—Au1—C17 80.44(9).

While there is no significant out-of-plane distortion of the square planar arrangement, the geometry of the pincer ligand causes an in-plane distortion illustrated by the C1—Au1—C17 angle of 160.8(1)°. The pincer ligand itself is close to perfect planarity, with only the phenyl-sidearm that contains C17 slightly being bent out of plane and the C1-C6 phenyl ring being bent even more slightly in the antipodal direction. A full overview of bond lengths, angles and torsion angles is given in the appendix.

2.1.2 Biological evaluation of Au(III)[C^N^C] complexes

Biological evaluation was performed at the Department of Biomedical Sciences, University of Padova, and the Department of Pharmacokinetics, Toxicology and Targeting, University of Groningen.

2.1.2.1 Antiproliferative activity

Complexes **2** – **4** were tested against human cancer cell lines A549 (lung adenocarcinoma), SKOV-3 (ovarian adenocarcinoma) and 2008 (human ovarian cancer), in comparison to their ligands, using a classical MTT assay as reported in the experimental section. Overall, the compounds showed modest activity in both A549 and SKOV-3 cell lines, with IC_{50} values above 50 µM. As predicted, the presence of respectively the PTA and $GlutS^-$ ligand improved the compounds' solubility in comparison to their Au(III) precursor complex **2**, with IC_{50} values in the range of 60-70 µM vs and IC_{50} value of 110 µM for complex **2**. The highest antiproliferative effects were detected for complexes **2** and **4** in 2008 cells, with IC_{50} values of 29.09 µM ± 2.51 and 6.64 µM ± 1.23 respectively.

2.1.2.2 Thioredoxin reductase inhibition

Since TrxR is also a potential target for Au(III) complexes, *in vitro* inhibition of purified rat TrxR by compounds **2** - **4** was studied using established protocols as described in the experimental section. The results are summarized in Table 1. All compounds are inhibitors of cytosolic thioredoxin reductases TrxR1 in the same range as auranofin, with complex **4** being the most potent. Further studies demonstrated that complex **3** is also able to inhibit the TrxR closely related, but selenium-free, enzyme glutathione reductase (GR) with an IC_{50} value of 180 nM, about 60-fold less efficiently than in the case of TrxR (Table 1).

Table 1. IC_{50} values of the inhibition of TrxR1, TrxR2 and GR on the isolated enzymes.

	IC_{50} (nM)*

complex	TrxR1	TrxR2	GR
auranofin	0.9 ± 0.25	3.2 ± 0.5	>10 000
2	10.01 ± 1.32	59.01 ± 5.32	219.4 ± 18.34
3	9.84 ± 1.25	213.41± 20.35	439.3 ± 6.82
4	3.00 ± 0.85	60 ± 3.72	180.1 ± 22.35

(*TrxR1 (70 nM) or TrxR2 (70 nM) in 0.2 M NaKPi buffer (pH 7.4), 5 mM EDTA, and 0.25 mM NADPH were tested in the presence of different concentrations of the various compounds.)

Afterwards, the effect of complexes **2** – **4** on TrxR and GR activities was evaluated in cell lysates. For this purpose, 2008 cells, where the three compounds showed markedly different cytotoxic effects, were pre-treated for 48 h with complexes **2** – **4** at different concentrations (Figure 21 [A]). In addition, GR activity was also determined and, as reported in Figure 21 [B], the enzyme did not show any inhibition even at 50 µM compounds' concentration.

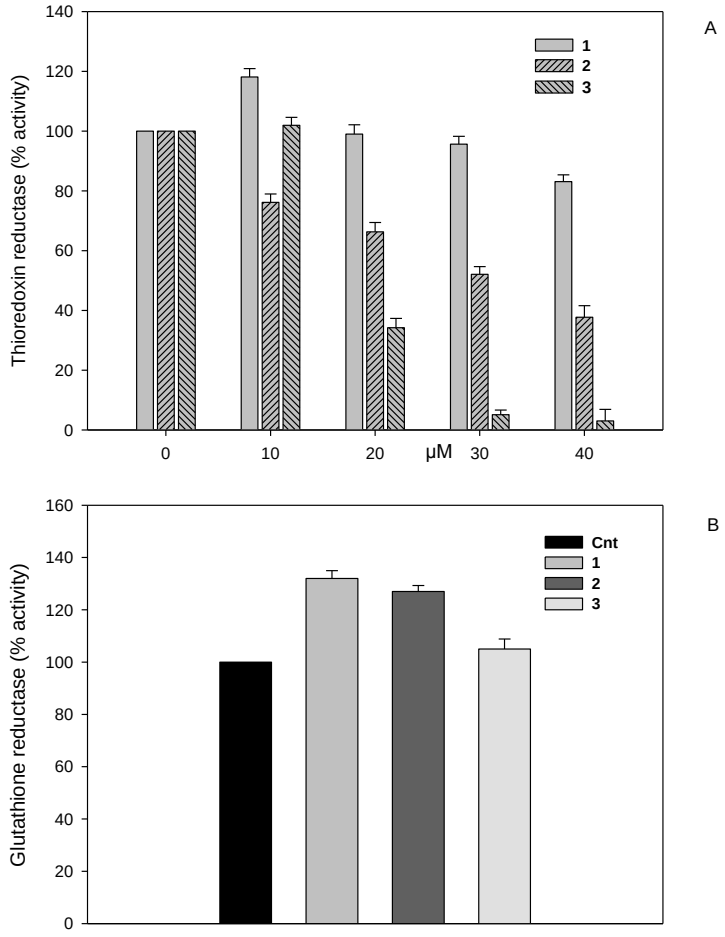

Figure 21. Thioredoxin reductase (A) and glutathione reductase (B) activities in 2008 ovarian cancer cells after the treatment with complexes 2 - 4. For TrxR activity determinations, cells (1x 10^6) were treated with the compounds at the indicated concentrations between 0-40 μM. Glutathione reductase activity was evaluated after the treatment with 50 μM of the three compounds.

2.1.2.3 Effects on the cellular redox state

The cellular redox state was evaluated after the incubation of 2008 cells with complexes **2** – **4.** For the determination of the total thiols present in cell lysates, an assay was conducted according to the protocol described in the experimental section. The results presented in Figure 22 show that the total amount of thiols is unaltered upon treatment with complexes **2** and **3**, indicating that these complexes

have no effect on the redox state of the intracellular sulfhydryl groups, while at 50 µM, complex **4** shows a decrease of about 40% of the total thiols. This suggests that complex **4** not only binds selenocysteines, but is also able to interact with thiols inside the cells.

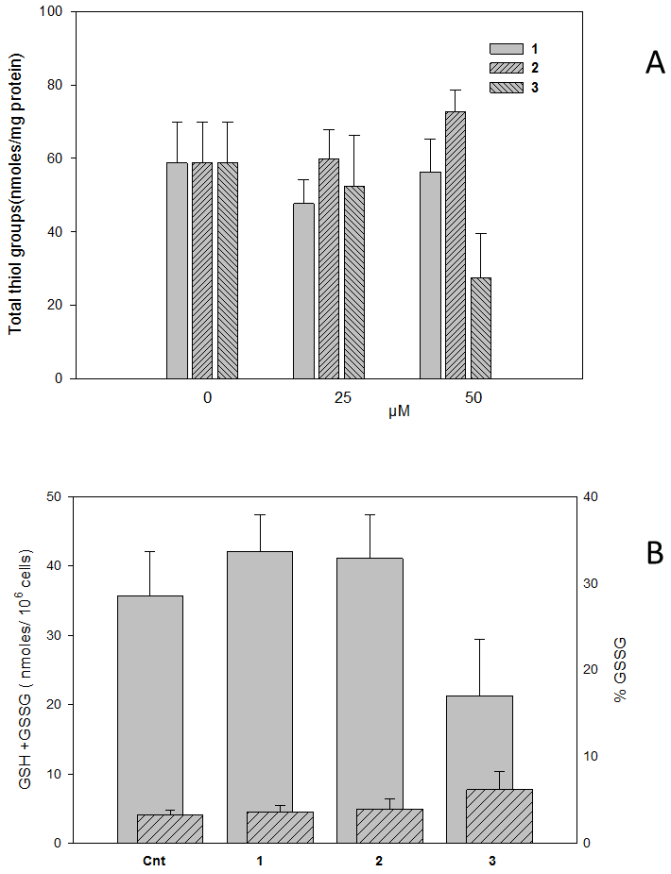

Figure 22. Total thiols (A) and glutathione (B) in ovarian cancer cells after the treatment with complexes 2 - 4. 2008 cells (5x 10^5) were treated with the compounds at the indicated concentrations [A]. In [B], total glutathione and oxidized glutathione after the cell treatment with 50 µM of the three compounds was depicted.

The glutathione redox pair (GSH/GSSG) is another fundamental component of the cell redox regulation. Therefore, the study continued with the analysis of the total glutathione content (reduced + oxidized) and the GSH/GSSG ratio in 2008 cells, after treatment with complexes **2** – **4** for 48 hours. The obtained results are elucidated in Figure 22 [B]. After treatment of 5x10^5 ovarian cancer cells, a slight increase of oxidized glutathione (caused by thiol oxidation), was only observed in the

presence of 50 µM of complex **4**. Therefore, the redox state of Trx1 and Trx2 in the presence of complexes **2** and **4** was studied, to confirm that the inhibition of TrxR leads to an increased oxidation of the principal substrates. Interestingly, complex **4** shows a significant oxidation of Trx1 and Trx2, providing indirect evidence that TrxR is a principal target of complex **4** in cells.

2.2 Au(III)[C^N(R)^C] system

2.2.1 Optimization of C^N(R)^C ligand synthesis

The synthesis of C^N(R)^C (= para substituted 2,4,6-triaryl pyridine ligands) has been described by Shingare *et al.*[128] before. Thus, at first synthesis was carried out accordingly, utilizing $Bi(OTf)_3$ as a catalyst:

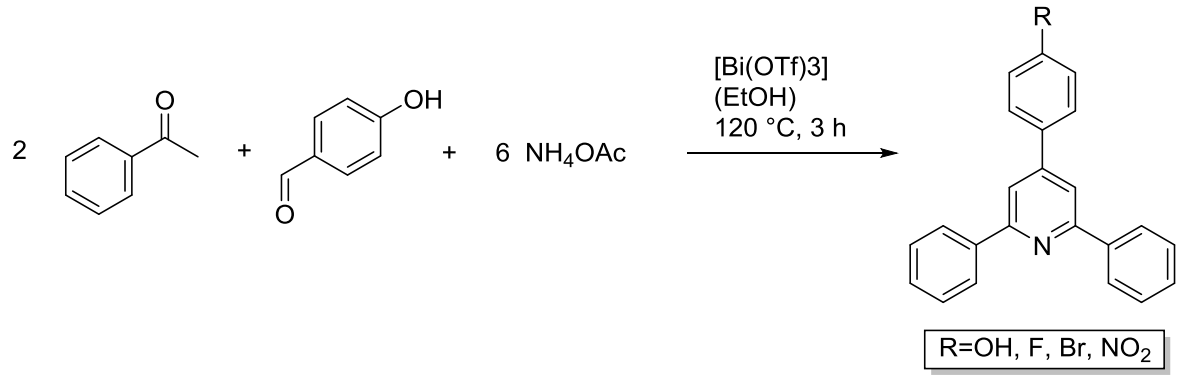

Figure 23. $Bi(OTf)_3$ catalyzed C^N(R)^C ligand synthesis.

However, it was found that yields were quite low (<20 %) for this system and the workup proved to be difficult, as the crude products are obtained rather as oily suspensions than as the described solids.

Therefore a second synthesis approach was conducted, utilizing microwave irradiation as depicted in Figure 24.

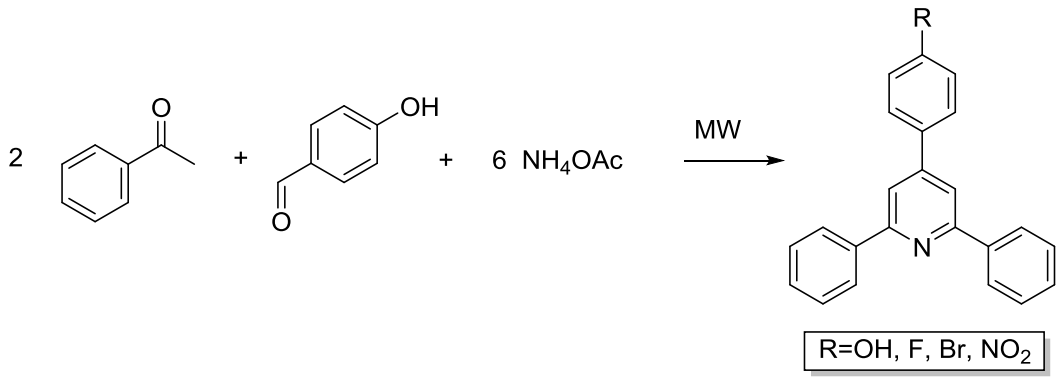

Figure 24. Microwave irradiated synthesis of C^N(R)^C ligands.

Microwave assisted synthesis has become progressively more recognized throughout the last decade, since it has been shown to significantly increase product yields, reduce reaction times and enhance product purities by reducing undesirable side reactions compared to conventional heating methods. It is generally referred to as microwave-assisted organic synthesis (MAOS)[129]. The short reaction times provided by microwave synthesis make it ideal for fast reaction scouting or optimization of reaction conditions.

For the C^N(R)^C ligand synthesis microwave synthesis offers three major advantages, namely: 1) omission of $Bi(OTf)_3$ as a catalyst and therefore metal free ligand synthesis, 2) solvent-free synthesis, since the educt acetophenone is a liquid and provides enough liquidity to the system for microwave synthesis and 3) shorter reaction times and higher throughput potential by using a microwave initiator robot. Previously reported procedures describe reaction conditions of 400 Watt and above[130]. However, when these reaction conditions were applied, major pressure build-up within the system was observed, which forced the synthesis to stop. Therefore, a milder starting reaction condition set of 100 Watt, 30 minutes and 120°C was chosen and optimized for the synthesis of 4-(4'-hydroxyphenyl)-2,6-diphenylpyridine. Each parameter was optimized with the other two respective parameters being fixed at the basic conditions. A pre-stirring period of one minute was applied to every reaction before starting the microwave heating, in order to ensure an optimized distribution of the educts.

Table 2, Table 3 and Table 4 give an overview of the obtained yields for the alteration of the respective parameter.

Table 2. Yield determination for variation of the irradiation power P [W].

Entry	Power [W]	Yield [%]
1	25	4.48%
2	50	5.18%
4	100	16.19%
5	175	30.43%
6	200	19.80%
7	250	9.80%

Table 3. Yield determination for variation of the irradiation temperature T [°C].

Entry	Temperature [°C]	Yield [%]
8	100	19.90%
9	120	18.92%
10	140	18.48%
11	160	24.00%
12	180	27.01%
13	200	22.49%
14	220	13.30%

Table 4. Yield determination for variation of the irradiation time t [min].

Entry	Time [min]	Yield [%]
15	30	16.59%
16	40	20.20%
17	50	31.74%
18	60	34.39%
19	70	35.72%
20	80	35.78%

It can be seen that increasing the temperature and the power enhances the yields significantly, reaching a maximum at 180°C and 175 Watt respectively. Afterwards, decomposition of the product occurs, as was monitored by ^{1}H and ^{13}C NMR. Furthermore, the applied reaction conditions can be visualized quite conveniently as can be seen in Figure 25. The crude product (A) obtained at optimized parameters is an oily suspension, containing 4-(4'-hydroxyphenyl)-2,6-diphenylpyridine as a white solid. If the applied temperature and irradiation power is too low (T below 120°C and P below 100 Watt), no precipitation of the crude product occurs but rather a slurry suspension (B) with very low yields after the work-up. If the microwave energy input is too high (T above 180°C and P above 175 Watt) the decomposition of the product becomes obvious, as the suspension turns brown. For the variation of the reaction time it can be seen that a prolongation of the reaction time affords higher yields as expected, which becomes especially eminent when increasing the reaction time from 40 minutes to 50 minutes. After reaching a plateau after 70-80 minutes a prolongation of the reaction time does not change the yield (significantly) any more, indicating that the reaction has fully occurred at that point of time.

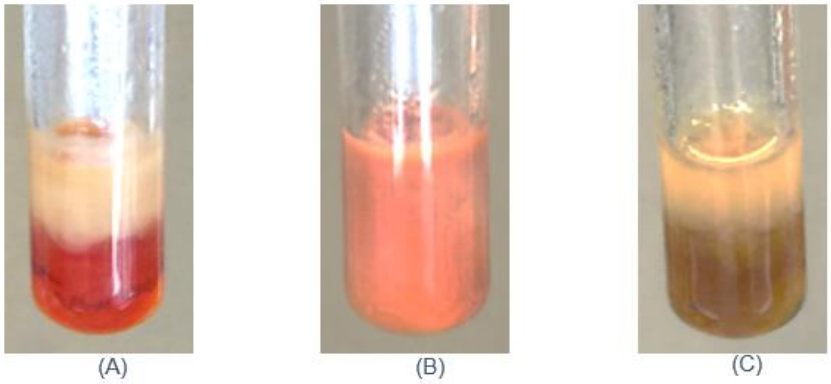

Figure 25. Obtained crude products (A) optimized parameters; (B) P<100 W, T<120°C; (C) P>175 W, T>180°C.

Thus, the optimized microwave settings were found to be at 180 W at 175°C and 80 minutes and were applied for the synthesis of all presented 2,4,6-triaryl pyridine ligands. Purity of the products was verified by ^{1}H, ^{13}C NMR and elemental analysis. Scale up batch reactions were performed in a Biotage microwave initiator robot

2.2.2 Synthesis and structural characterization of Au[C^N(R)^C] complexes

For the Au[C^N(R)^C] class, the influence of the *para* substituent R of the 6-phenyl position of the respective Au(III) complex on the biological properties was investigated.

Analogue to the Au[C^N^C] system, the Au[C^N(R)^C] complexes were obtained *via* transmetalation of the respective Hg(II) precursor as presented in Figure 26.

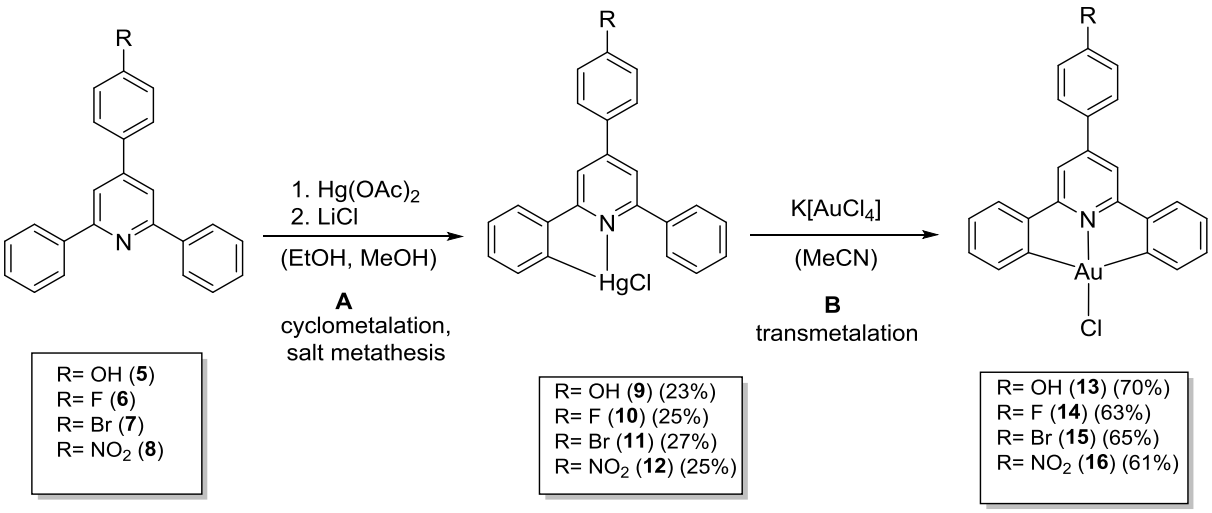

Figure 26. Synthesis of Au[C^N(R)^C] complexes.

Also in accordance to the Au[C^N^C] system, reaction yields were higher when the reactions were performed under argon. Complex **14** has been described before by Che *et al.* in 2013, as a precursor for photoactive functionalized bis-cyclometalated alkynylgold(III) complexes, suitable as phosphorescent organic light-emitting diodes (OLEDs)[131]. However, ^{13}C NMR spectra were not reported and its biological activity was not investigated. Complexes **13**, **15** and **16** have not been reported in literature so far.

The cyclomercuration step can be visualized in the ^{1}H NMR spectra as it is exemplarily shown for ligand **6** and complex **10** in Figure 27. Binding of HgCl to the ligand goes along with a significant downfield shift of the signals, resulting from the strong deshielding effect caused by the –I effect of the electron-accepting Hg-Cl moiety.

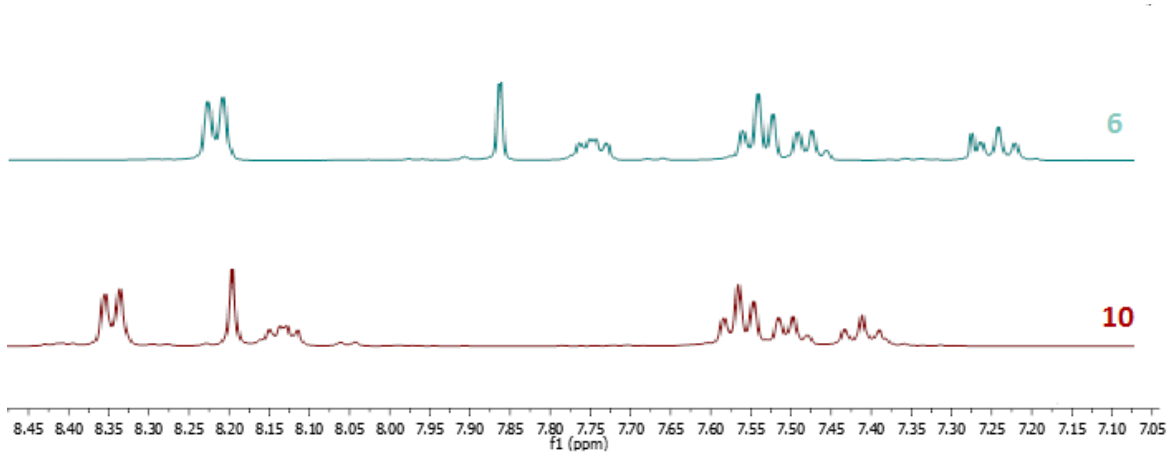

Figure 27. ^{1}H NMR of ligand 6, reacted to complex 10 with $Hg(OAc)_2$.

The monomercurated Hg(II)[C^N(R)^C]Cl complexes **9** – **12** were separated from the bismercurated species by means of hot methanolic extraction, utilizing the better solubility of the monomercurated complex in comparison to the bismercurated one. Figure 28 shows exemplarily the ^{199}Hg-NMR spectrum of the monomercurated and the bismercurated species of complex **9**.

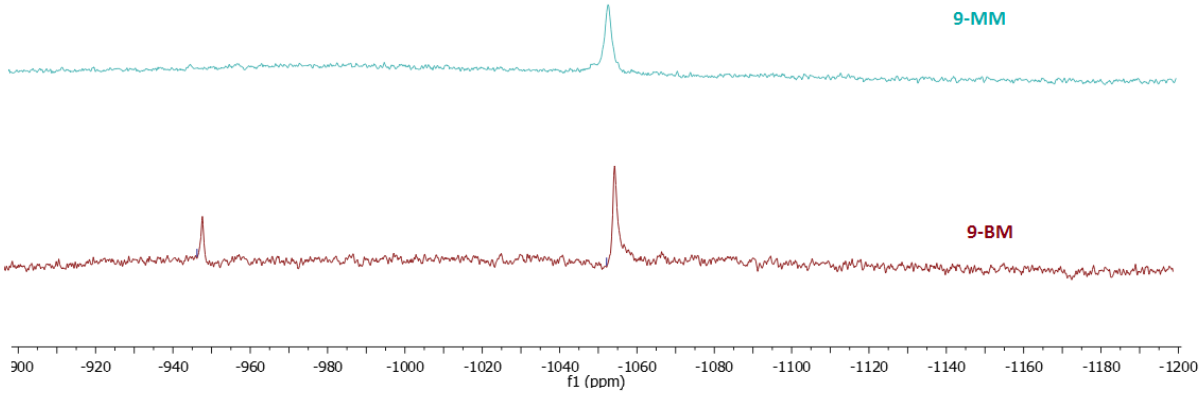

Figure 28. ^{199}Hg NMR of monomercurated (MM) and bismercurated (BM) complex 9.

The signals are not equivalent, making the monomercurated species conveniently distinguishable in the ^{199}Hg NMR spectrum. The non-equivalence of the signals can most likely be attributed to an out-of-plane orientation of the two HgCl groups

respectively to each other, in order to obtain the biggest possible distance to each other, as this is energetically most favorable.

The structure of the Au[C^N(R)^C] complexes **13** - **16** were further verified by means of ^{1}H NMR, ^{13}C NMR and ESI-MS spectroscopy. Especially ^{13}C NMR spectroscopy allows in this respect for a good characterization of the complexes as the C-R bonds of the *para* substituent R of the 6-phenyl position and the C-Au bonds are very characteristic. Figure 29 displays the ^{13}CNMR spectra of complexes **13** – **16**. The typical C-Au bond (A) is displayed around 142 ppm by all complexes. Furthermore the C-R bonds can be seen very well for the respective functional group, being C-OH (B) at 151.21 ppm for complex **13**, C-F (C) at 189.11 ppm for complex **14**, C-Br (D) at 127.44 ppm for complex **15** and C-NO_2 (C) at 148.29 ppm for complex **16**.

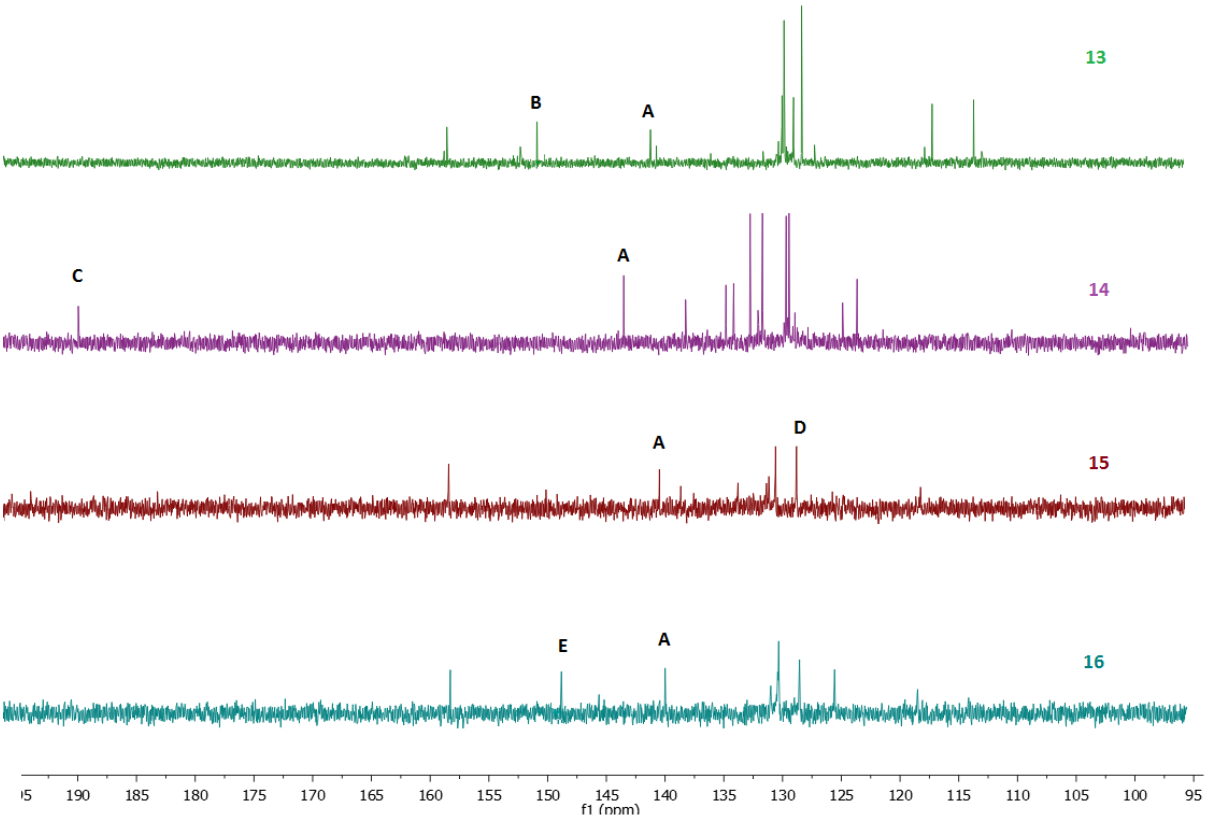

Figure 29. ^{13}C NMR spectra of complex 13 - 16.

The ESI-MS spectra of complexes **13** - **16** are in perfect accordance with the calculated $[M]^+$ spectra and displayed in Figure 30, Figure 31, Figure 33 and Figure 34.

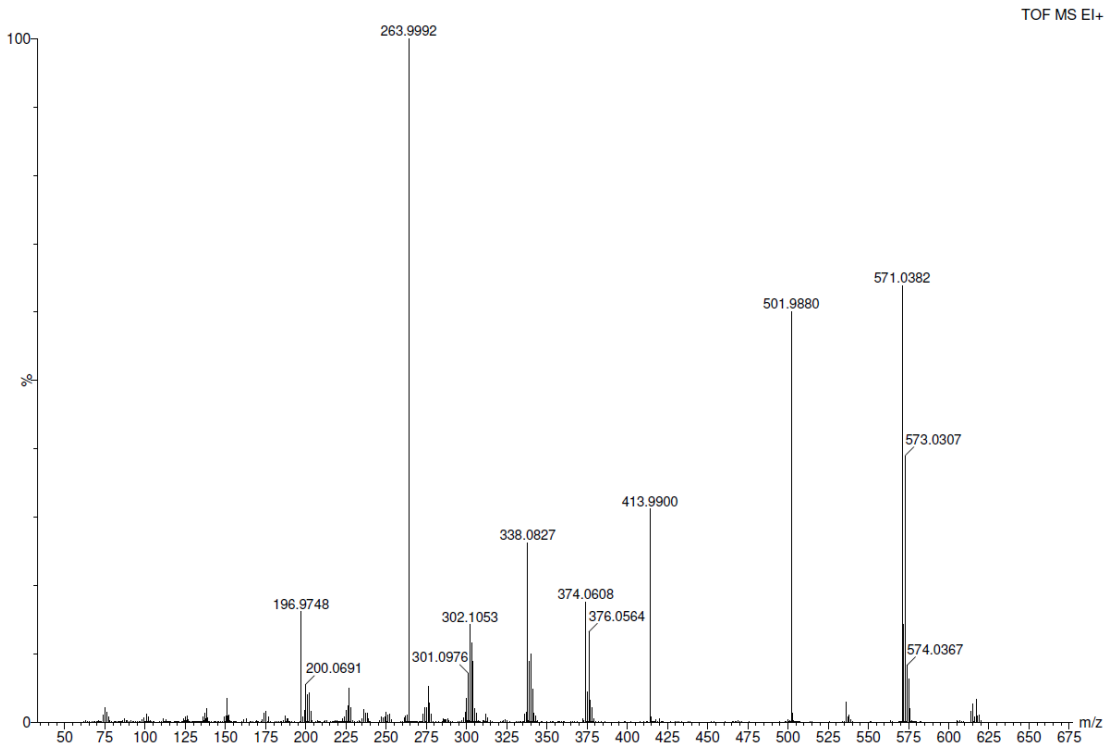

Figure 30. ESI-MS spectrum of complex 13.

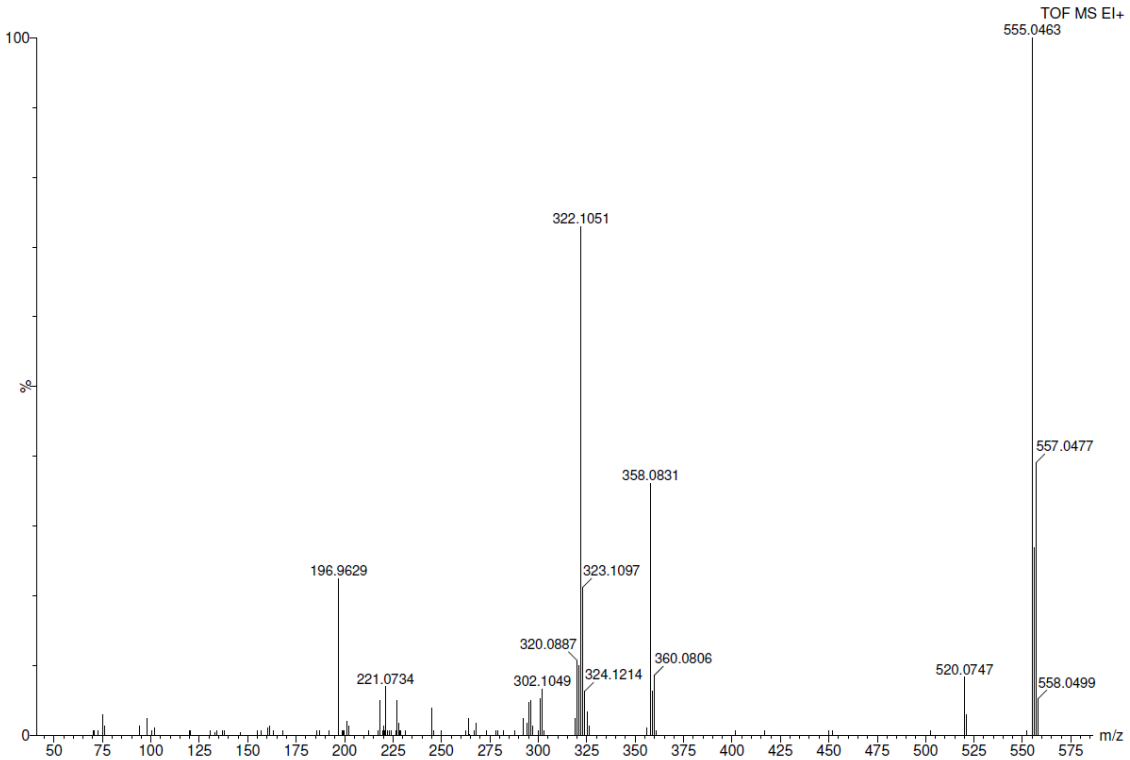

Figure 31. ESI-MS spectrum of complex 14.

Monoisotopic Mass, Odd and Even Electron Ions
12 formula(e) evaluated with 1 results within limits (all results (up to 1000) for each mass)
Elements Used:
C: 0-23 H: 0-14 N: 0-1 Cl: 0-1 F: 0-1 197Au: 0-1

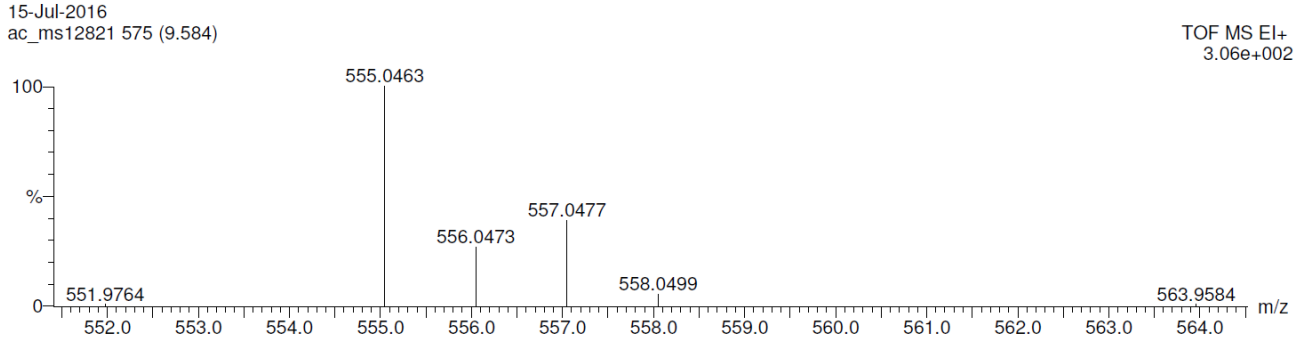

Minimum:				-1.5		
Maximum:		5.0	100.0	50.0		
Mass	Calc. Mass	mDa	PPM	DBE	i-FIT	Formula
555.0463	555.0464	-0.1	-0.2	17.0	0.5	C23 H14 N Cl F 197Au

Figure 32. Theoretically calculated ESI-MS spectrum of complex 14.

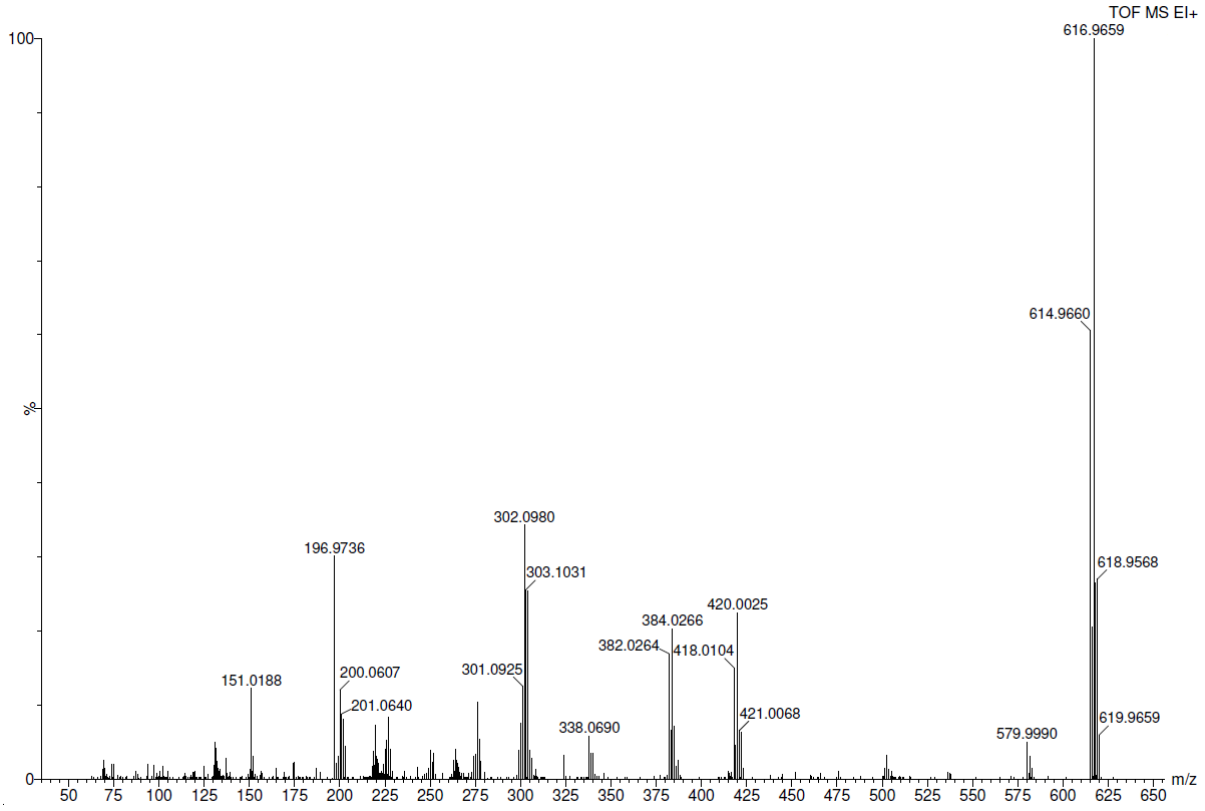

Figure 33. ESI-MS spectrum of complex 15.

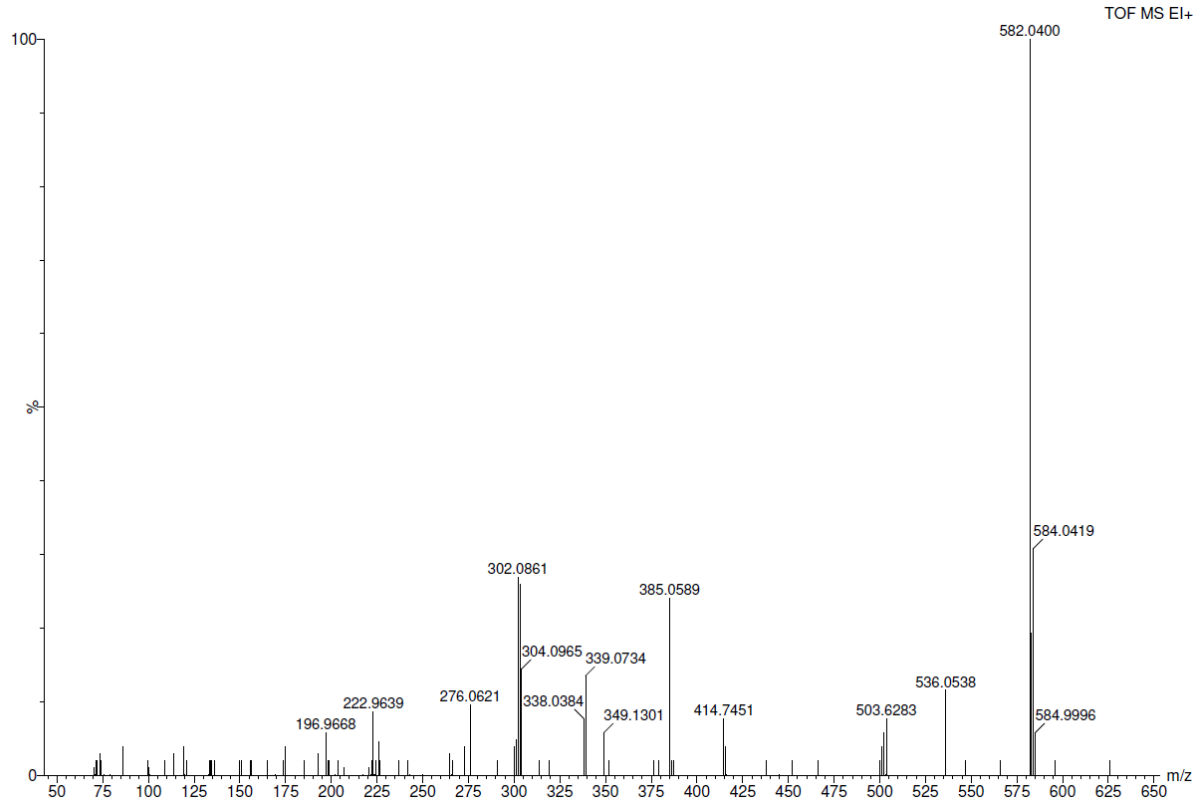

Figure 34. ESI-MS spectrum of complex 16.

For complex **13**, the $[M+H_2O]^+$ signal for m/z at 571.0382 was obtained, as measurements were performed in acetone/water. Figure 32 shows exemplarily the theoretically calculated ESI-MS spectrum for complex **14**, with the main signal for m/z at 555.0463 being in perfect accordance with the measured spectrum.

Further structural verification of complexes **13** – **16** was provided by means of elemental analysis, with the difference of the measured CHN values to the calculated ones being less than 0.5% in general.

2.2.3 Biological evaluation of Au(III)[C^N(R)^C] complexes

For the biological evaluation of complexes **13** - **16**, the respective ligands **5** - **8** were tested first in order to see the cytotoxic potential of the sole ligand and to discuss the influence of the *para* substituent R of the 6-phenyl position without any influence of an Au(III) core. Ligands **5** - **8** were tested for their cytotoxic activity against the cancer cell lines A549 (human lung carcinoma) and SKOV-3 (ovarian carcinoma). Additionally, cisplatin was also tested as reference cytotoxic agent. The reported IC_{50} values are the mean ± standard deviation of at least three evaluations and reported in Table 5.

Table 5. IC_{50} values (µM) of compounds 5-8 and cisplatin against A549 and SKOV-3.

compound	A549	SKOV-3
5	30.0 ± 4.7	28.8 ± 5.5
6	42.3 ± 5.3	44.5 ± 7.9
7	30.8 ± 4.46	59.5 ± 9.7
8	>100	>100
cisplatin	4.5 ± 3.1	1.86 ± 0.7

It can be seen that the sole ligands **5** - **8** display a broad cytotoxic array, with IC_{50} values ranging from a moderately toxic 28.8 µM (ligand **5** for SKOV-3) to minor toxic at 59.5 µM (ligand **7** for SKOV-3) to non-toxic (ligand **8** for both cell lines). All ligands are significantly less toxic than cisplatin which is favourable, as the cytotoxicity of the Au(III) complexes should mainly come from the complete organometallic system and not the organic ligand scaffold alone. The highest cytotoxicity is displayed by ligand **5** for both A549 and SKOV-3 cancer cells with IC_{50} values of 30.0 µM for A549 and 28.8 µM for SKOV-3 cancer cells, respectively. This can possibly be attributed to the fact that within the ligand class, ligand **5** possesses the highest water solubility due to the OH group, which can form hydrogen bonds within the aqueous media, such as the PBS. Ligand **6** displays closely the same cytotoxic activity against A549 and SKOV-3 with IC_{50} values around 40 µM, whereas ligand **7** is nearly 2-fold more cytotoxic towards A549 cells (IC_{50} ca. 30.8 µM) than against SKOV-3

(IC_{50} ca. 59.5 µM). Interestingly, ligand **8** displays neither for A549 cells, nor for SKOV-3 cells any cytotoxic activity. As all other ligands show cytotoxic activity, this has to be most likely contributed to the NO_2 group of the phenyl ring. All herein presented functional groups possess an –I effect, however the NO_2 group is the only group that displays a resonance effect. Therefore, it is most likely that the resonance effect of a ligand in the 6-phenyl position leads to a significant decrease in the cytotoxic activity of the 2,4,6-triaryl pyridine system.

For the biological evaluation of the respective Au(III) complexes **13** - **16** unfortunately precipitation upon dilution in the cell culture medium was detected, which did not allow to assess the exact concentration in solution. Only at relatively high concentrations in DMSO complexes **13** - **16** displayed decent solubility. As already sole DMSO is toxic to cells, cytotoxicity tests could not be conducted for complexes **13** – **16**. The poor solubility is in that case caused by the relatively big, rather non-polar respective C^N^C scaffold. Solubility of complexes **13** - **16** would need to be improved by introducing ancillary ligands that increase the water solubility, as it was conducted for complexes **3** and **4**.

2.3 Au(C^N) coumarin system

2.3.1 Synthesis of the Au(C^N) coumarin system

The (C^N) cyclometalated Au(III) complex **17** of the general formula [Au(py^b-H)Cl$_2$] (py^b-H = C^N cyclometalated 2-benzylpyridine) was chosen as the Au(III) precursor complex for the coupling of the coumarin based ligand **18**. Synthesis of complex **17** was carried out with slight changes to Cinellu *et al.*[86], by refluxing equimolar amounts of $KAuCl_4$ and benzylpyridine in ultrapure water at 100°C for 24 hours.

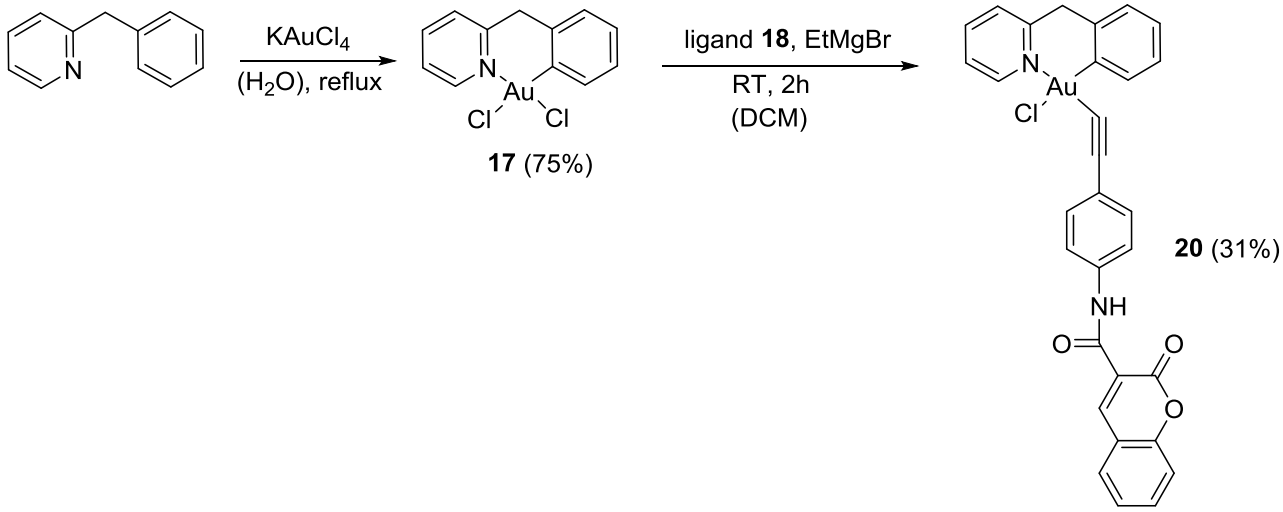

Figure 35. Synthesis of complex 17 and 20.

The coumarin based ligand **18** was prepared according to literature by reacting coumarin-3-carboxylic with 4-ethynylaniline in DCM, utilizing the coupling agent N-(3-dimethylaminopropyl)-N'-ethylcarbodiimmide[132]

At first, conversion of complex **17** into its hydroxide form [Au(py^b-H)OH$_2$] was attempted, as cyclometalated Au(III) complexes with OH groups as ancillary ligands have been reported to be convenient precursors for the coupling of various ligands[133]. Thus, synthesis was at preformed according to previously published procedure for the synthesis of [Au(bipy)(OH)$_2$][PF$_6$] (bipy = bipyridine) by Cinellu *et al.*[133b, 134], utilizing Ag_2O as a base. However, in spite of utilizing different bases, reaction times, reaction temperatures and/or solvent systems (see experimental for a

complete overview of all varied parameters), complex **19** could not be clearly obtained. Instead most approaches, even at long time exposure NMR or in kryo-NMR measurements, displayed an extremely broadened aromatic area between 6 and 8 ppm. A possible explanation could thereby be the formation of a polymeric μ-oxo-bridged Au(III) complex, as has been reported before for other late transition metals, such as iron[135]. Since ^{1}H and ^{13}C NMR spectroscopy did not give conclusive structural hints, crystal structure analysis would surely be the most convenient structural characterization. Crystallisation attempts were conducted by dissolving complex **19** in different solvents (e.g. acetone, DMSO, acetonitrile) and having a second solvent (e.g. diethylether, pentane, hexane) slowly diffuse into the solution. Attempts were conducted at room temperature and at 5°C in the refrigerator, to enable even slower diffusion processes. However, so far crystallisation attempts did not show any success.

Therefore, synthetic efforts were directed to tethering the coumarin based ligand **18** to complex **17**. In that respect, the Grignard reagent EtMgBr proved to be the reagent of choice for the deprotonation of ligand **17**. EtMgBr is a strong base and a convenient reagent for the deprotonation of terminal alkynes[136]. Complex **20** was obtained as a bright neon-yellow solid with a yield of 31%. The ^{1}H NMR spectrum of complex **20** is displayed in Figure 36.

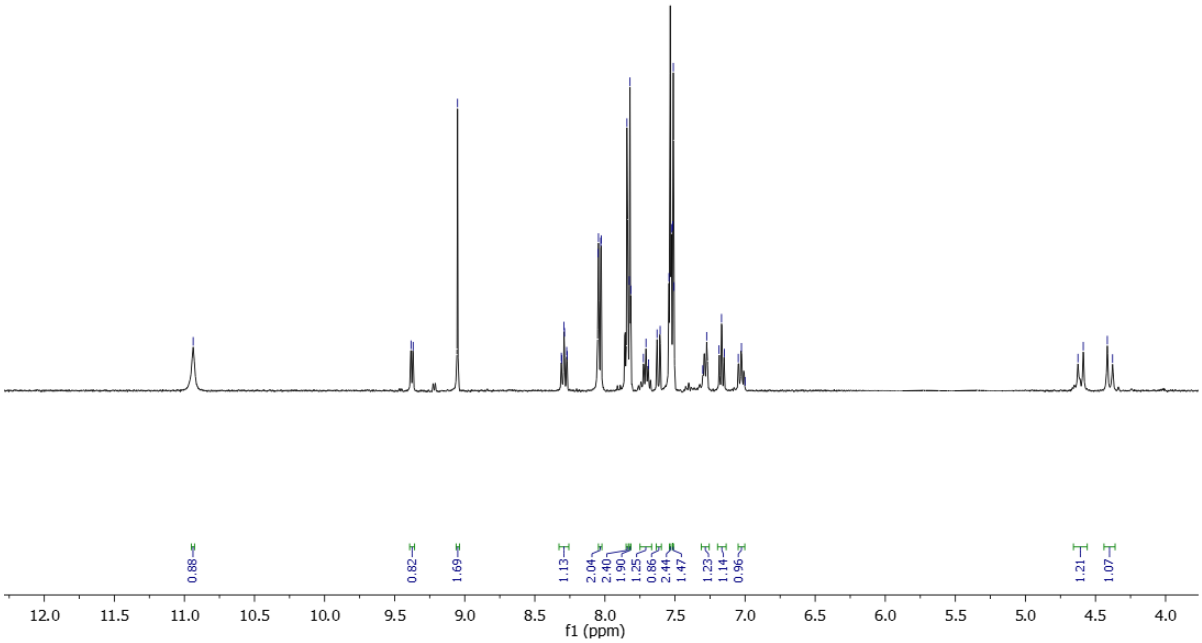

Figure 36. ^{1}H NMR of complex 20.

When comparing the ^{1}H NMR spectrum of complex **20** to the ^{1}H NMR spectra of the gold precursor complex **17** and the sole ligand **18**, complex formation can be observed quite well (Figure 37). The characteristic proton singlet at 3.07 ppm of the alkyne proton has disappeared in the spectrum of complex **20**, confirming a full deprotonation of the applied coumarin ligand **18**. Furthermore, the ^{1}H NMR spectrum of complex **20** displays the typical signals of the coumarin moiety, being the singlet for the NH group at 10,89 ppm and the singlet for the chromene unit at 9.05 ppm. Note that ligand **18** was measured in $CDCl_3$, while complexes **17** and **20** were measured in d-acetone, due to different solubilties. The signals of the C^N scaffold of complex **20** are shifted in general slightly downfield in comparison to complex **17**, which can be attributed to the resonance of ligand **18**.

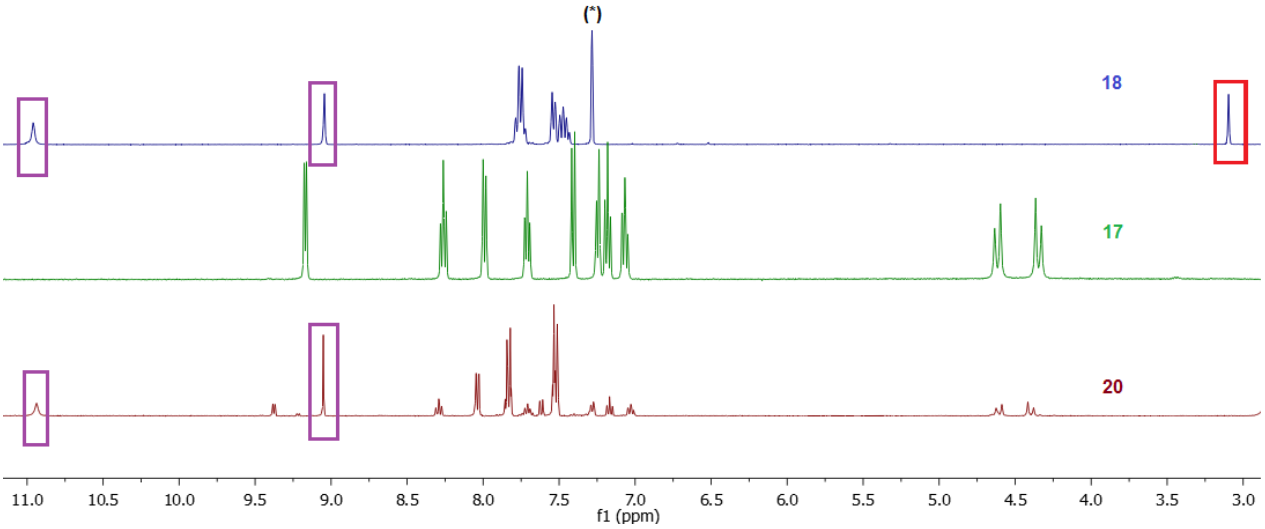

Figure 37. ^{1}H NMRs of complex 17, ligand 18 and complex 20 (* = $CDCl_3$).

ESI-MS was performed for complex **20**. Unfortunately, only fragments of complex **20** could be obtained, even when turning to softer ionization methods such as FAB-MS (fast atom bombardment), CI-MS (chemical ionization) or MALDI-MS (Matrix-assisted laser desorption/ionization). Therefore it can be concluded that complex **20** is particularly labile at high temperatures and/or high voltages, such as those applied during the ionization process. However, further structural verification of complex **20** was provided by means of elemental analysis, with the difference of the measured CHN values to the calculated ones being less than 0.5% in general.

2.3.2 Investigation of photochemical properties

Since several coumarin based ligands are known for their fluorescent properties, ligand **18** and complex **20** were investigated by UV-VIS and fluorescence spectroscopy. The UV-VIS spectra of ligand **18** and complex **20** can be seen in Figure 38 (solution concentrations were chosen to obtain both spectra at absorption values between 0.6 and 0.7, different zoom factors apply due to automated scaling). Measurements were performed in ethanol as its cut-off appears at 240 nm. It can be observed that the UV-VIS spectra of ligand **18** and complex **20** are nearly identical with characteristic absorption maxima at 264 nm, 305 nm and 337 nm (complex **20**) and 338 nm (ligand **18**).

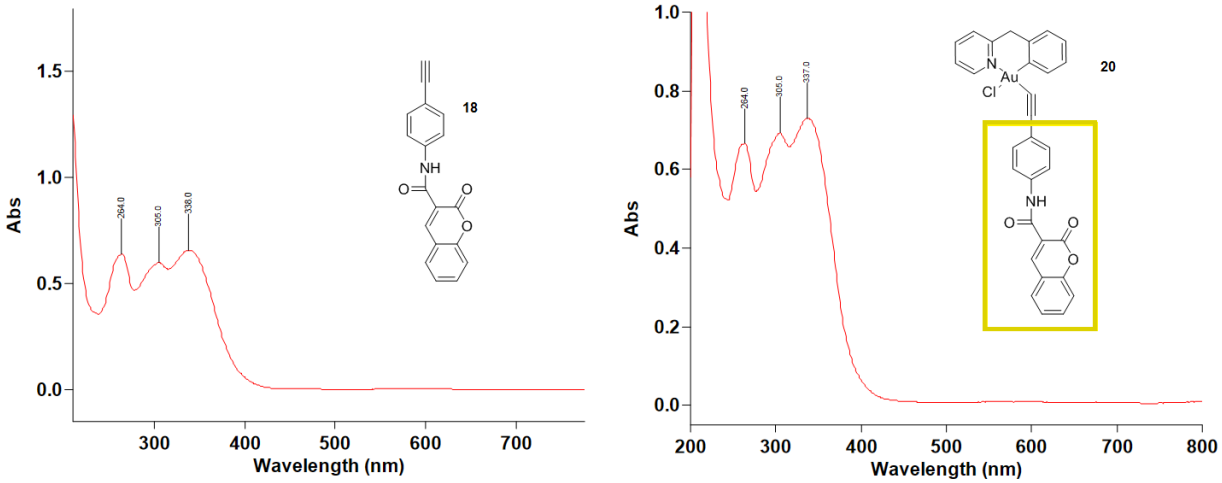

Figure 38. UV-VIS spectra of ligand 18 and complex 20.

As the conjugated chromene part of the coumarin based ligand is most likely responsible for its UV-VIS activity, the nearly identical UV-VIS spectra of ligand **18** and complex **20** are not surprising. This is further being supported by the fact that by the sole complex **17**, no characteristic UV-VIS maxima are displayed. The herein reported maxima for ligand **18** and complex **20** are in good accordance to literature reported coumarin systems[137].

The fluorescence of complex **20** was determined via fluorescence spectroscopy in acetone. The fluorescence maximum was found at 532 nm, as displayed in Figure 39. The quantum yield of complex **20** was automatically detected by the integrated software of the fluorescence spectrometer and is unfortunately quite low with a value of 0.02.

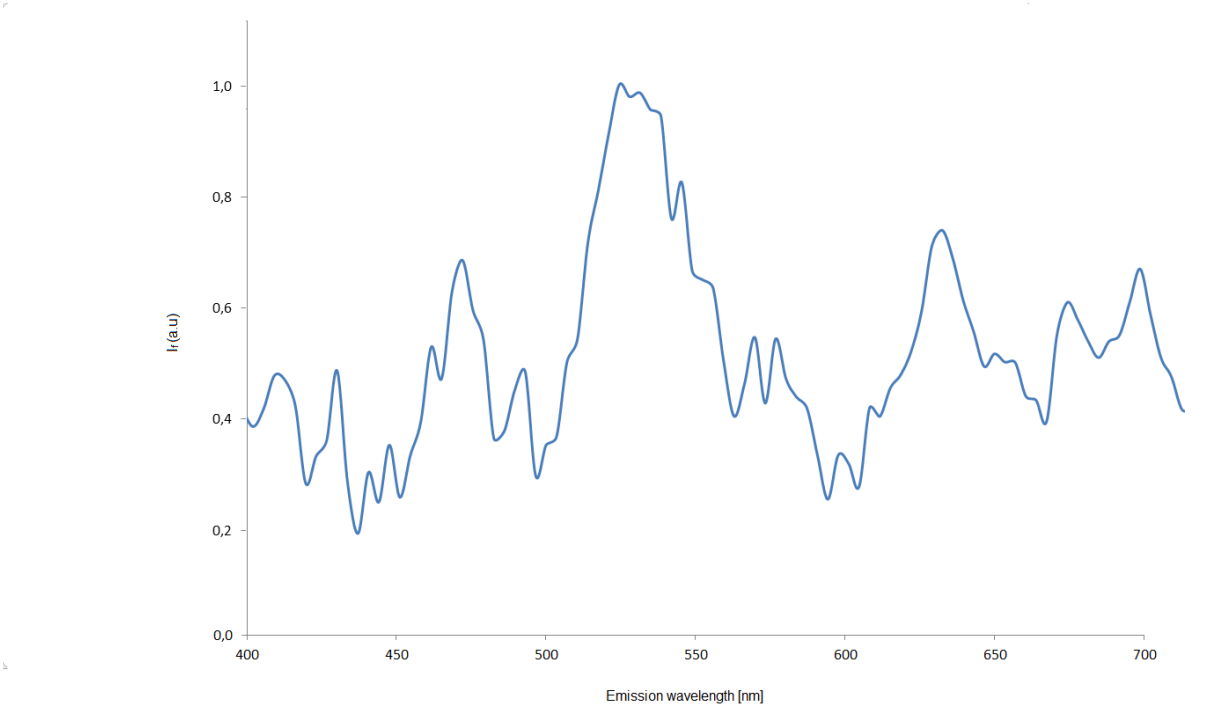

Figure 39. Normalized fluorescence spectrum of complex 20.

The low fluorescence as displayed by complex **20** can probably be attributed to the fact that the conjugation of the aromatic system is broken by the carboxamido moiety of the coumarin based ligand and the methylene bridge of the Au(III) C^N scaffold. As mentioned before, several coumarin based ligand systems with biological properties have been reported. Therefore, complex **20** will be regarded for its biological properties, with setting special focus to its anticancer properties, in further studies.

2.4 Conclusion and outlook

Even though cancer research is a field of high interest, nowadays chemotherapies mostly still involve the use of traditional Pt(II) drugs. These chemotherapeutics display several disadvantages such as a limited spectrum of action, severe side effects in the patients and possible cross-resistance. Therefore, today's research has to focus on developing novel strategies for the synthesis of anticancer drugs.

Au(I) and Au(III) complexes have thereby shown to be able to selectively inhibit target proteins and enzymes. Au(III) complexes present a further challenge, as the Au(III) core is labile to reductions. A convenient way of stabilizing the Au(III) core is in that respect the introduction of a cyclometalated scaffold. Therefore, this thesis focussed on the synthesis and biological evaluation of new cyclometalated Au(III) complexes. As the main scaffolds, C^N^C (= 2,6-diphenylpyridine) and a C^N(R)^C (= 2,4,6-triaryl-pyridine) based ligand system were chosen. All Au(III)[C^N^C] and Au(III)[C^N(R)^C] complexes were obtained via transmetalation of the respective Hg(II) precursor, allowing for synthesis at relatively mild reaction conditions, in contrast to the quite harsh (and often not successful) direct cycloauration.

The C^N^C ligand is a moderately cheap, commercially available ligand, thus the Au(III)[C^N^C] complexes present the benefit of being quite fast to synthesize. This is especially important in clinical drug development, where obtaining large quantities and rapid testing of the drug's effectiveness is demanded. Ligand exchange reactions were performed, transforming the original Au(III)[C^N^C(Cl)] complex to Au(III)[C^N^C(PTA)]PF_6 and Au(III)[C^N^C(GluS)]. Complex formation was proven by ^{1}H NMR and ^{13}C NMR spectroscopy, ESI-MS and elemental analysis. For Au(III)[C^N^C(PTA)]PF_6 crystals suitable for XRD measurements could be obtained. All three complexes showed good cytotoxic activity against ovarian cancer cells. Initial mechanistic studies demonstrate that the compounds are potent inhibitor of the seleno-enzyme thioredoxin reductase. The thioglucose derivative also induces alterations of the overall intracellular redox state, which may be due to additional

interactions with thiol-containing biomolecules. For future synthesis and biological testing, the coupling of PTA analogues like DAPTA (3,7-diacetyl-1,3,7-triaza-5-phosphabicyclo[3.3.1]nonane) to the Au(III)[C^N^C] complex could be very interesting, as these ligands have been reported for Au(I) and Pt(II) systems with promising *in vitro* activities against several cell lines[138]. Furthermore, Au(C^N^C) systems replacing the central pyridine ring with a pyrazine have been reported recently[139]. As they display intense thermally activated delayed fluorescence (TADF), these Au(C^N^C) systems could lead to a convenient way to monitor the uptake of anticancer compounds via fluorescence microscopy over a longer period of time.

For the Au(III)[C^N(R)^C] (R = OH, Cl, Br, NO_2) system, ligand synthesis was optimized by using a microwave synthesis procedure. By elucidating the ideal reaction parameters and the usage of an initiator robot system, a cheap and quick procedure was established in which all [C^N(R)^C] ligands could be obtained at molar scale in less than 24 hours. Especially the prevention of using a metal catalyst makes this synthesis cost efficient and more environment friendly at the same time. The complexes were tested for their biological activity, but already the sole ligands displayed an interesting trend within their cytotoxic activity towards A549 and SKOV-3 cancer cells. The highest cytotoxicity for both A549 and SKOV-3 cancer cells with IC_{50} values around 30.0 µM was displayed for R = OH, which can possibly be attributed to the fact that it possesses the highest water solubility. Interestingly, for R = NO_2 no cytotoxic activity to any of the cells was displayed. It therefore seems that the resonance effect of a ligand in the 6-phenyl position leads to a significant decrease in the cytotoxic activity of the 2,4,6-triaryl pyridine system. Complex formation of all Au(III)[C^N(R)^C] complexes was proven by ^{1}H NMR and ^{13}C NMR spectroscopy, ESI-MS and elemental analysis. The Au(III)[C^N(R)^C] complexes displayed in biological testing only poor solubility within the cell culture medium, which can most likely be contributed to the rather non-polar C^N^C scaffold. For future biological tests it would be interesting to introduce a *para* substituent in the 6-phenyl position with a + I effect, to observe the differences to the herein tested ligands with a - I effect. Furthermore, the polarity of the Au(III) complexes needs to be increased, in order to test their cytotoxic activity. Therein, the coupling of a PTA

moiety in the ancillary position, in accordance with the Au(III)[C^N^C] complexes, could offer a convenient method.

Finally, a coumarin based ligand was coupled to the [Au(py^b-H)$(Cl)_2$] (py^b-H = cyclometalated 2-benzylpyridine) complex. This Au(III) C^N system displays the benefit that no transmetalation step is necessary in order to obtain the complex, making it more easily assessable. At first it was aimed at obtaining the Au(III) hydroxide complex [Au(py^b-H)$(OH)_2$], as cyclometalated Au(III) complexes with OH groups as ancillary ligands have been reported as suitable precursors for the coupling of various ligands. However, synthesis approaches were not successful. Instead, direct coupling of the coumarin based ligand to [Au(py^b-H)$(Cl)_2$] was achieved by utilizing a Grignard reagent. Coumarin based systems often display fluorescent properties, making them suitable for cellular uptake studies. Therefore, the Au(III) coumarin complex was investigated using UV-Vis spectroscopy and fluorescence spectroscopy. While the Au(III) complex featured distinctive absorption peaks in the UV-Vis spectrum, due to the coupled coumarin based ligand, only small quantum yields could be detected. This can probably be attributed to the fact that the conjugation of the aromatic system is broken by the carboxamido moiety of the coumarin based ligand and the methylene bridge of the Au(III) C^N scaffold. Quantum yields were determined in acetone, however future measurements utilizing different solvents and concentrations could be interesting, since some systems display decent fluorescent activity only in specific solvents and/or concentrations[120]. Furthermore, biological testing of this interesting novel Au(III) C^N complex should be performed in the future.

To conclude it can be stated that cyclometalated Au(III) compounds are a fascinating complex class for the use as anticancer agents, as they offer a broad range of variation potential within their cyclometalated scaffold and their ancillary ligand. Thus, specific complex design is made possible to address manifold issues such as physiochemical properties or the introduction of specific targeting moieties.

III Experimental

If necessary, reactions were carried out under purified argon 5.0 (99,99990%, Westfalen AG) using standard Schlenk equipment and techniques. Solvents were dried, degassed by freeze-pump thaw and stored over molecular sieve before use.

All starting materials were used as received from commercial sources without undergoing any further purification.

Chemicals

All utilized chemicals were purchased from VWR International GmbH, Sigma-Aldrich Inc. or Alfa Aesar GmbH & Co KG. Deuterated solvents were purchased from Sigma-Aldrich Inc. and Deutero GmbH.

Analytics

All physico-chemical analytics were performed at the Technische Universität München and the University of Cardiff.

ESI-MS

Electrospray ionization mass spectra (ESI-MS) were obtained on a High Resolution Waters LCT TOF Bruker HR-QTOF maXisPlus operating in positive ionization mode. The samples were dissolved in 1 ml of the appropriate solvent and 10 µl were injected directly in to the mass spectrometer. The mass range was scanned between 100 and 2000 and Leucine Enkephalin was used as an online calibrant.

NMR

NMR spectra were recorded on a Bruker Avance DPX-300, 400 or 500 at 298 K. Chemical shifts are given in δ (ppm) and refer to the residual ^{1}H and $^{13}C(^{1}H)$ signals

of the respective solvent. For ^{199}Hg NMR measurements $Hg(OAc)_2$ was used as an external standard. In allocating the signals the following abbreviations have been used: s - singlet, d - doublet, t - triplet, q - quartet, m - multiplet. Coupling constants J are given in Hz.

Single X-Ray Crystallography

X-ray intensity data were measured on a Bruker D8 Venture Duo IMS system equipped with a Helios optic monochromator and a Mo IMS microsource (λ=0.71073 Å). Data were collected on a single crystal X-ray diffractometer equipped with a CCD detector (APEX II, κ-CCD), a rotating anode FR591 and a Montel mirror optic using the SMART software package. Single crystals were manually picked and coated with perfluorinated ether prior to measurements. The crystals were fixed on the top of a microsampler, transferred to the diffractometer and subsequently frozen under a stream of liquid nitrogen. Initial lattice parameters were defined by matrix measurements. Reflections were merged and corrected for Lorentz and polarization effects, scan speed and background. The frames were integrated with the SAINT software package (Version 7.56a by Bruker AXS Inc.) using a narrow-frame algorithm. Data were corrected for absorption effects using the Multi-Scan method (SADABS) software (Version 2008/1 by Bruker AXS Inc.). Space group assignments were based upon systematic absences, E statistics and successful refinement of the structures. Structures were solved by direct methods with the aid of successive difference Fourier maps and were refined against all data using the APEX 2 software (Version 2014.9-0 by Bruker AXS Inc.) in conjunction with SHELXL-97, SHELXL-2014 or SHELXLE. Hydrogen atoms were placed in calculated positions and refined using a riding model. Non-hydrogen atoms were refined with anisotropic displacement parameters. Full-matrix least-squares refinements were carried with the SHELXL-97 weighting scheme.

Elemental Analysis

Elemental analysis was performed at the Microanalysis Laboratory Munich. For CHNS analytics a Euro EA analyser (HEKAtech GmbH) was utilized.

UV-Vis

UV-VIS spectra were recorded on an Agilent Cary 60 UV-Vis Spectrophotometer in 10 mm cuvettes.

Fluorescence measurements

Fluorescence spectra were recorded on a Hitachi Fluorescence Spectrophotometer F-2710 with an automated detection of quantum yields.

Cytotoxicity tests

All media and supplements were purchased from Invitrogen. The human ovarian cancer cell line SKOV3 and the human alveolar basal epithelial cancer cell line A549 were cultured respectively in DMEM (Dulbecco's Modified Eagle Medium) and RPMI (Roswell Park Memorial Institute medium) containing GlutaMaxI supplement with 10% FBS (fetal bovine serum) and 1% penicillin/streptomycin in an incubator at 37°C with an humidified atmosphere of 95% air and 5% CO_2 (Heraeus, Germany). 2008 ovarian cancer cells were grown in RPMI with 10% and 1% penicillin/streptomycin at the same conditions. For the evaluation of the cellular growth inhibition, cells were grown in 96-well plates (Costar, Integra Biosciences, Cambridge, MA) at a concentration of 10.000-15.000 cells per well and grown for 24 h in complete medium. Solutions of the compounds were prepared by diluting a freshly prepared stock solution (10^{-2}M in DMSO) of the corresponding compound in DMEM. Afterwards, the intermediate dilutions of the compounds were added to the wells (100 µL) to obtain a final concentration ranging from 0 to 150 µM, and the cells were incubated for 72 h. Following 72 h drug exposure, MTT (3-(4,5-dimethylthiazol-

2-yl)-2,5-diphenyltetrazolium bromide) was added to the cells at a final concentration of 0.25 mg ml^{-1} and incubated for 2 h, then the culture medium was removed and the violet formazan (artificial chromogenic precipitate of the reduction of tetrazolium salts by dehydrogenases and reductases) dissolved in DMSO. The optical density of each well (96-well plates) was quantified three times in tetraplicates at 540 nm using a multi-well plate reader, and the percentage of surviving cells was calculated from the ratio of absorbance of treated to untreated cells. The IC50 value was calculated as the concentration reducing the proliferation of the cells by 50% and it is presented as a mean (± SE) of at least three independent experiments.

Enzyme inhibition assays on isolated enzymes.

Highly purified aliquots of cytosolic rat liver thioredoxin reductase[140] and mitochondrial rat liver isoform[141] were utilized to determine their inhibition in the presence of complexes **2 - 4** at different concentrations. Thioredoxin reductases activity was determined by estimating the DTNB reduction in the presence of NADPH. The reaction was started with 1 mM DTNB and followed spectrophotometrically at 412 nm for about 10 min at 25°C. Yeast glutathione reductase activity was measured in 0.2 M Tris–HCl buffer (pH 8.1), 1 mM EDTA, and 0.25 mM NADPH, with the various compounds. The assay was initiated by addition of 1 mM GSSG and followed spectrophotometrically at 340 nm.

Analysis of thioredoxin reductase and glutathione reductase activities in cell lysates

2008 ovarian cancer cells, grown in completed RPMI medium, were treated in the presence of complexes **2 - 4** in various conditions to assess the activities of thioredoxin reductase and, glutathione reductase, the amount of total thiols and total and oxidized glutathione. Briefly, 2008 cells (1×10^6) were incubated with the three compounds for 48 h. After incubation, cells were harvested, washed with PBS and the pellets were lysed with a modified RIPA buffer: 150 mM NaCl, 50 mM Tris-HCl, 1 mM EDTA, 0.1% SDS, 0.5% DOC, 1 mM NaF, and an antiprotease cocktail (“Complete”Roche, Mannheim, Germany) containing 0.1 mM PMSF. After 40 min of incubation at 4 °C, lysates were centrifuged at 14000g for 5 min and aliquots (50µg)

of the supernatants were utilized for enzyme activities as described.

Total thiols estimation in cell lysates

After the treatment with 25 or 50 μM of the gold compounds for 24 h, cells were dissolved with 7.2M guanidine in a buffer containing 0.2M Tris-HCl and 5 mM EDTA. Total thiols were monitored at 412 nm in presence of 3 mM DTNB.

Redox Western Blot Analysis of Trx1 and Trx2.

The redox state of Trx was detected using a modified Western blot analysis[142] utilizing established protocols[143]. Cells incubated with the compounds for 48h, were lysed with 150 μL of urea lysis buffer (100 mM Tris-HCl, pH 8.3) containing 1 mM EDTA, 8 M urea and then treated with 10 mM iodoacetamide (IAM) to derivatize free thiols. Subsequently after the treatment with 3.5 mM DTT to reduce the oxidized thiols, cell lysates were derivatized with iodoacetic acid (IAA) (30 mM final concentration) that gives a negative charge. Proteins were separated by urea-PAGE gel (7% acrylamide/bis(acrylamide) in 8 M urea) in non-reducing conditions and blotted using TurboSystem (Bio-Rad Laboratories, Hercules, CA, USA). Membranes were probed with the primary antibodies respectively for Trx1 (FL 105) and for Trx2 (H75) (Santa Cruz Biotechnology, Santa Cruz, CA, USA).

To determine the redox state of thioredoxin, after 24 h cell treatment with complex **2** (40 μM) and **4** (20 μM), cells were lysed in 150 μL of urea lysis buffer (100 mM Tris-HCl, pH 8.3) containing 1 mM EDTA, 8 M urea, and derivatized in order to alkylate free thiols with IAM/IAA procedure as described before. Proteins were then subjected to Urea-page in non-reducing conditions and to Western blot detection.

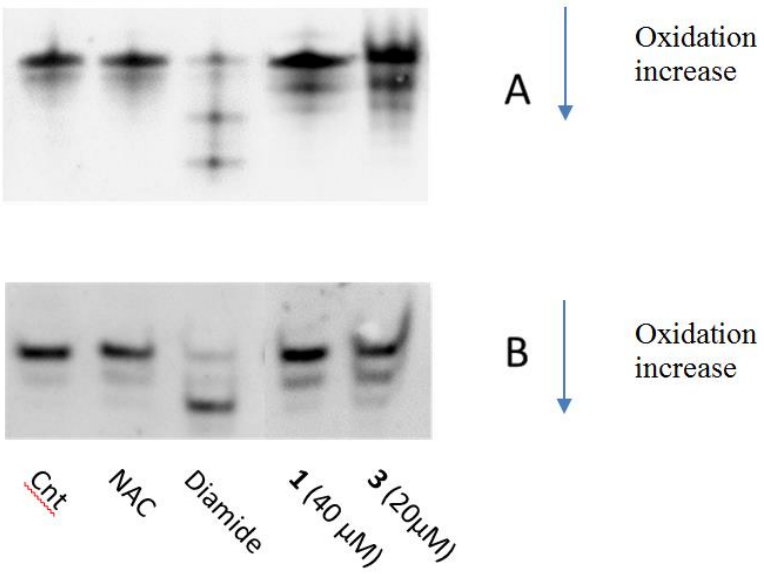

Figure 40. Redox western blot of Trx1 (A) and Trx2 (B) in 2008 cells after incubation with complex 2 and 4. NAC represents the completely reduced status, while diamide is the control for the oxidized status.

Glutathione redox state estimation in cell lysates

5×10^5 2008 cells were incubated for 48 h with 50 µM of complexes **2 - 4**. Then cells, washed twice with cold PBS, were rapidly lysed and deproteinized with 6% meta-phosphoric acid. After 10 min at 4°C, samples were centrifuged and supernatants were neutralized with 15% Na_3PO_4 and assayed for total glutathione[144].

To determine the amount of GSSG, aliquots of the obtained samples were derivatized with 2-vinylpyridine75 in order to block reduced glutathione, and oxidized glutathione was then estimated[145].

Microwave reactions

Microwave reactions were carried out in a CEM Focused Microwave™ Synthesis System or a Biotage® Initiator Robot Eight and Sixty. Vials with a volume of max. 5 mL were fitted with a magnetic stir bar and sealed with plastic caps. Beforehand to the reactions, a pre-stirring period of one minute was applied to ensure an optimal distribution of the educts.

Figure 41. CEM Focused Microwave (left) and Biotage Initiator Robot (right) as applied in the thesis.

4 Synthesis of [Au(III)(C^N^C] complexes

4.1 Hg(II) precursor synthesis

[Hg(C^N^C)Cl], 1

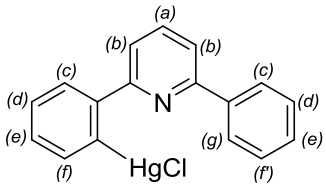

Chemical Formula: $C_{17}H_{12}ClHgN$
Molecular Weight: 466,33 g/mol

Synthesis of the mercury precursor [Hg(C^N^C)Cl] **1** was carried out with slight alterations to the synthesis reported by Constable *et al.*[123]. A mixture of 2,6-diphenylpyridine (2.27 g, 9.81 mmol, 1 eq.) and mercury(II) acetate (3.13 g, 9.81 mmol, 1.0 eq.) in 50 mL absolute ethanol was heated under reflux for 24 hours under argon. Thereafter, a solution of lithium chloride (0.89 g, 21.07 mmol, 2.1 eq.) in 50 mL methanol was added, refluxed for another 30 minutes, and subsequently poured into 100 mL of ice-cold, ultrapure water. The resulting white precipitate was filtered off and washed with ice-cold water and methanol. Extraction of the solid with hot methanol left the bismercurated product as a white solid residue. The methanol extract was concentrated to small volume and stored at low temperature, leading to the precipitation of an off-white solid, which was filtered and washed with ice-cold methanol and pentane. Any remaining solvent was removed under reduced pressure to afford complex **1** as a white solid (1.97 g, 4.22 mmol, 43% yield)

^{1}H NMR (400 MHz, DMSO-d6) δ [ppm] = 8.00 (t, J = 7.2 Hz, 1H, H_a), 7.96 (d, J = 7.3 Hz, 2H, H_c), 7.91 (d, J = 7.8 Hz, 1H, H_f), 7.83 (d, J = 7.8 Hz, 1H, H_g), 7.76 (d, J = 7.7 Hz, 2H, H_b), 7.60 – 7.47 (m, 5H, $H_{d,e,f'}$).

^{13}C NMR (101 MHz, DMSO-d6) δ [ppm] = 163.09 (C-N), 161.70 (C-C), 158.30 (C-HgCl), 138.46 (C-H_a), 137.81(C-H_c), 128.95, 127.97, 127.96, 125.85, 125.12, 123.66, 121.13 (C-H_b).

^{199}Hg NMR ($CDCl_3$, 72 MHz): δ = –1054.73.

Anal. Calc. for $C_{17}H_{12}ClHgN$: C 43.79, H 2.59 N 3.00%. Found: C 43.02, H 2.51, N, 3.00%.

4.2 Synthesis of [Au(III)(C^N^C] complexes

[Au(C^N^C)Cl], 2

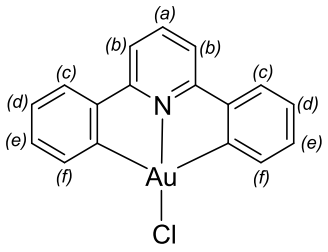

Chemical Formula: $C_{17}H_{11}AuClN$
Molecular Weight: 461,70 g/mol

Preparation was carried out with slight changes to the synthesis by Che *et al.*[95]. Complex **1** (0.51 g, 1.09 mmol, 1eq.) and $K[AuCl_4]$ (0.41 g, 1.09 mmol, 1eq.) were refluxed in 20 mL acetonitrile under argon for 24 h at 80°C upon which a greenish precipitate was formed. The crude solid was filtered, washed with diethyl ether and pentane and dried under reduced pressure to afford complex **2** as an electrostatic, light-yellow solid (0.18 g, 0.39 mmol, 36% yield).

^{13}C NMR spectra have not been reported in the literature so far.

^{1}H NMR (400 MHz, DMSO-d6) δ [ppm] = 8.19 (t, J = 8.0 Hz, 1H, H_a), 7.98 (d, J = 8.1 Hz, 2H,H_f), 7.88(d, J = 7.7 Hz, 2H, H_c), 7.69 (d, J = 7.2 Hz, 2H,H_b), 7.43 (t, J = 7.3 Hz, 2H, H_d), 7.32 (t, J = 7.6 Hz, 2H, H_e).

$^{13}C(^{1}H)$ NMR (101 MHz, DMSO-d6) δ [ppm] = 169.53 (C-N), 164.10 (C-C), 148.43(C-H_a), 142.32(C-Au), 132.95(C-H_c), 131.67(C.H_e), 127.61(C-H_d), 126.14(C-H_f), 118.57(C-H_b).

Positive ESI-MS (acetone): m/z = 462.21 $[M+H]^+$ (calcd for $C_{17}H_{12}AuClN$: 462.03).

Anal. Calc. for $C_{17}H_{11}AuClN$: C, 44.22; H, 2.40; N, 3.03 %. Found: C, 44.16; H, 2.18 ; N, 3.23%.

[Au(C^N^C)(PTA)][PF_6], **3**

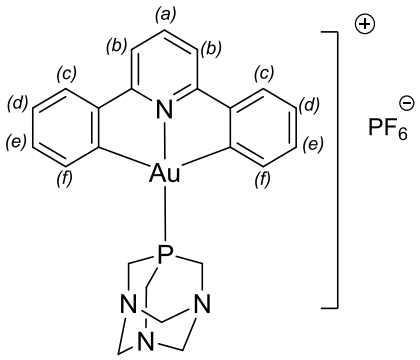

Chemical Formula: $[C_{23}H_{23}AuN_4P]PF_6$
Molecular Weight: 728,37 g/mol

Complex **2** (100 mg, 0.22 mmol, 1 eq.) was added to KPF_6 (202.47 mg, 1.10 mmol, 5 eq.) in 25 mL of acetone under argon. PTA (34.57 mg, 0.22 mmol, 1 eq.) was added to the suspension at room temperature under vigorous stirring, leading to solubilisation of **2**. The reaction was stirred at room temperature for 3 hours. Acetone was subsequently partly removed, DCM was added and the solution was filtered through Celite. The volatiles were removed under reduced pressure and the resulting solid washed with ice-cold acetone, pentane and diethylether. Complex **3** was obtained as a light-yellow solid (114.7 mg, 0.16 mmol, 73% yield).

^{1}H NMR (400 MHz, Acetone-d6) δ [ppm] = 8.28 (t, *J* = 8.0 Hz, 1H, H_a), 8.01 (m, *J* = 8.5 Hz, 6H, $H_{b,c,f}$), 7.56 (t, *J* = 7.5 Hz, 2H, H_d), 7.46 (t, *J* = 7.5 Hz, 2H, H_e), 5.21 (d, *J* = 2.1 Hz, 6H, N-CH_2), 4.99 (d, *J* = 13.1 Hz, 3H, P-CH_aH_b), 4.80 (d, *J* = 13.3 Hz, 3H, P-CH_aH_b).

^{13}C NMR (101 MHz, Acetone-d6) δ [ppm] = 169.48(C-N), 164.69(C-C), 151.39(C-H_a), 146.41(C-Au), 137.61(C-H_c), 133.54(C-H_e), 129.07(C-H_d), 128.01(C-H_f), 119.56(C-H_b), 73.13(N-CH_2), 51.31(P-CH_2).

Positive ESI-MS (acetone): m/z = 583.110 $[M]^+$ (calcd for $C_{23}H_{23}AuN_4P$: 583.126).
Anal. Calc. for $C_{23}H_{23}AuF_6N_4P_2$: C, 37.93; H, 3.18; N, 7.69 %. Found: C, 37.79; H, 3.24; N, 7.38 %.

[Au(C^N^C)(GluS)], **4**

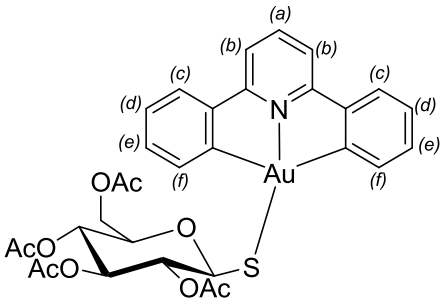

Chemical Formula: $C_{31}H_{30}AuNO_9S$
Molecular Weight: 789,61 g/mol

Complex **2** (50 mg, 0.115 mmol, 1 eq.), was added to thio-β-D-glucose tetraacetate (41.9 mg, 0.115 mmol, 1 eq.) and Na_2CO_3 (61 mg, 0.575 mmol, 5 eq.) in 20 mL DCM under argon. The suspension was stirred for 1.5 hours at room temperature and thereafter filtered through Celite and concentrated under reduced pressure. Upon cooling and subsequent addition of pentane, a precipitate was formed which was filtered, washed with diethylether and pentane and dried under reduced pressure. Complex **4** was obtained as a light-yellow solid (78.96 mg, 0.10 mmol, 87% yield).

^{1}H NMR (500 MHz, Acetone-d6) δ [ppm] = 8.34 –7.69 (m, 5H, $H_{a,b,c}$), 7.61 – 7.14 (m, 6H, $H_{d,e,f}$), 5.20 – 5.10 (m, 2H, 2 CH), 4.98 (m, 1H, CH), 4.89 (t, J = 9.4 Hz, 1H, CH), 4.79 (t, J = 9.7 Hz, 1H, CH), 4.15 (dd, J = 12.3 Hz, 2.1 Hz, 1H, CH_2-sugar), 4.02 (dd, J = 12.3 Hz, 5.6 Hz, 1H, CH_2-sugar), 1.96 (s, 3H, OAc), 1.94 (s, 3H, OAc), 1.86 (s, 3H, OAc), 1.77 (s, 3H, OAc).

Positive ESI-MS (acetone): m/z = 790.1442 $[M+H]^+$ (calcd for $C_{31}H_{31}AuNO_9S$: 790.1385).

Anal. Calc. for $C_{31}H_{30}AuNO_9S$: C, 47.15; H 3.83; N, 1.77; S, 4.06 %. Found: C, 47.01; H, 3.68; N, 1.85; S, 3.75%.

5 Synthesis of Au(III)[C^N(R)^C] complexes

5.1 Synthesis of [C^N(R)^C] ligand system

In the following, the two [C^N(R)^C] ligand system synthesis routes applied in the present thesis are exemplarily shown for the 4-(4'-hydroxyphenyl)-2,6-diphenylpyridine ligand.

General Synthesis Route A

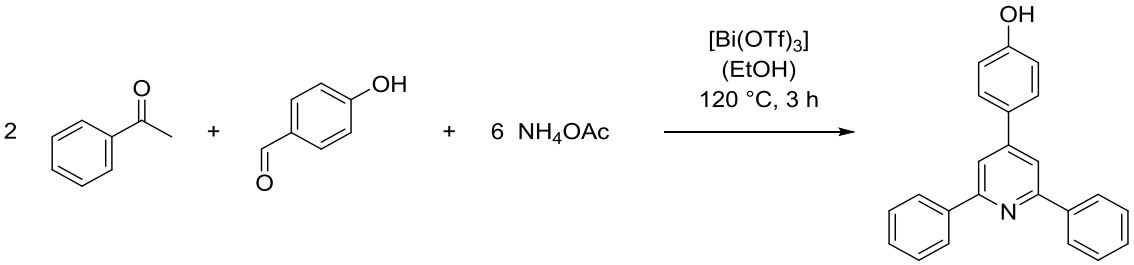

A mixture of acetophenone (1.20 mL, 10.3 mmol, 2.0 eq.), 4-hydroxybenzaldehyde (0.64 g, 5.16 mmol, 1eq.), ammonium acetate (2.38 g, 30.9 mmol, 6 eq.) and bismuth triflate (5 mol%) were heated at 120 °C for 3 h under inert gas atmosphere in 20 mL absolute ethanol. The reaction mass was allowed to cool down to room temperature, extracted with 50 mL aq. ethanol solution (water/ethanol, 7:3) , filtrated and washed with ice-cold water and ice-cold ethanol. In order to obtain a higher yield, the filtrate was concentrated and stored at a low temperature, leading to the precipitation of additional product. The combined crude products were purified by recrystallization in aq. ethanol (water/ethanol, 3:7). 4-(4'-hydroxyphenyl)-2,6-diphenylpyridine was obtained as an off-white crystalline solid with a yield of 20% (0.33 g, 1.02 mmol) after drying.

General Synthesis Route B

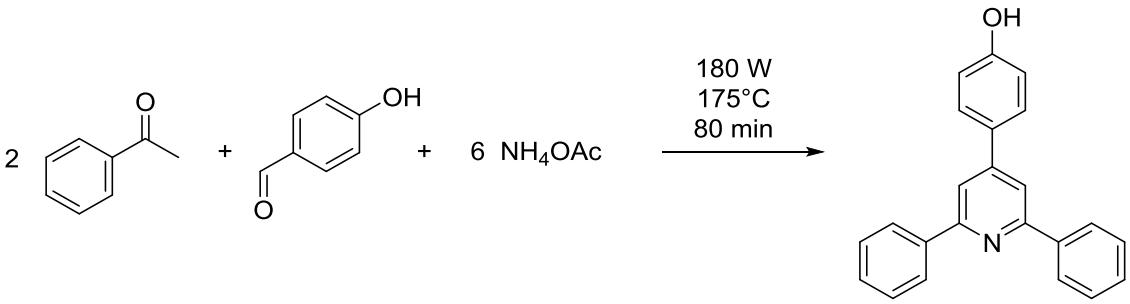

A mixture of acetophenone (0.6 mL, 5.15 mmol, 2.0 eq.), 4-hydroxybenzaldehyde (0.32 g, 2.58 mmol, 1eq.) and ammonium acetate (1.19 g, 15.45 mmol, 6 eq.) were sealed into a microwave tube, pre-stirred for one minute and subsequently exposed to 180 Watt microwave irradiation at 175°C for 80 minutes. The resulting biphasic reaction mixture was then transferred to a separating funnel, treated with equal volumes of ice-water and diethyl ether and shaken well. The aqueous phase containing excess ammonium acetate was extracted three times with diethyl ether. The organic phases were combined and concentrated under reduced pressure to afford the crude product. Recrystallization from ethanol and subsequent drying under reduced pressure delivered 4-(4'-hydroxyphenyl)-2,6-diphenylpyridine as an off-white crystalline solid with a yield of 35% (0.29 g, 0.93 mmol).

Synthesis Route B was optimized concerning applied power, time and temperature of the microwave reaction. Based on the findings, the optimized microwave settings were established to be at 180 W at 175 °C for 80 minutes and were applied for the synthesis of all presented 2,4,6-triaryl pyridine ligands. Column chromatography over silica gel (hexane/ethyl acetate = 1.5/1) can be performed for further ligand purification, if required.

4-(4'-hydroxyphenyl)-2,6-diphenylpyridine C^N(OH)^C, **5**

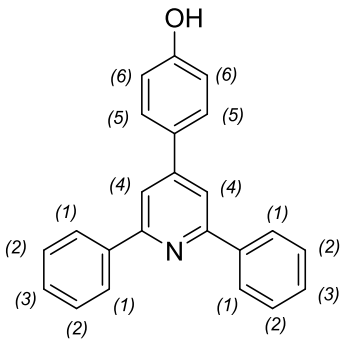

Chemical Formula: $C_{23}H_{17}NO$
Molecular Weight: 323,40 g/mol

A mixture of acetophenone (0.6 mL, 5.15 mmol, 2.0 eq.), 4-hydroxybenzaldehyde (0.32 g, 2.58 mmol, 1eq.) and ammonium acetate (1.19 g, 15.45 mmol, 6 eq.) were sealed into a microwave tube, pre-stirred for one minute and subsequently exposed to 180 Watt microwave irradiation at 175°C for 80 minutes. The resulting biphasic reaction mixture was then transferred to a separating funnel, treated with equal volumes of ice-water and diethyl ether and shaken well. The aqueous phase containing excess ammonium acetate was extracted three times with diethyl ether. The organic phases were combined and concentrated under reduced pressure to afford the crude product. Recrystallization from ethanol and subsequent drying under reduced pressure delivered ligand **5** as an off-white crystalline solid with a yield of 32% (0.29 g, 0.90 mmol).

^{1}H-NMR (400 MHz, DMSO-d6): δ [ppm] = 9.86 (s, 1H, OH), 8.31 (d, J=7.3 Hz, 4H, H_1), 7.85 (s, 2H, H_4), 7.67 (d, J=8.2 Hz, 2H, H_5), 7.51-7.41 (m, 6H, $H_{2,3}$), 6.99 (d, J=8.6 Hz, 2H, H_6).

^{13}C NMR (101 MHz, DMSO-d6) δ [ppm] = 152.09 (2 C-N), 151.20 (C-OH), 148.4 (C_{para}-N), 128.71, 128.66, 128.77, 127.96, 127.28, 127.26, 126.91, 116.81, 114.62, 113.78, 112.21.

Anal. Calc. for $C_{23}H_{17}NO$: C, 85.42; H, 5.30; N, 4.33%. Found: C, 87.11; H, 5.73; N, 4.25%.

4-(4'-fluorophenyl)-2,6-diphenylpyridine C^N(F)^C, **6**

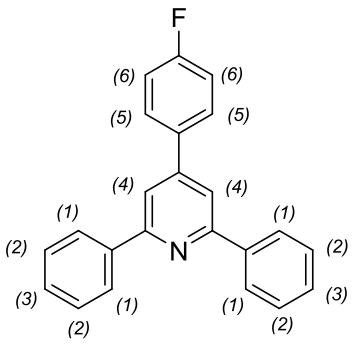

Chemical Formula: $C_{23}H_{16}FN$
Molecular Weight: 325,39 g/mol

A mixture of acetophenone (0.6 mL, 5.15 mmol, 2.0 eq.), 4-fluorobenzaldehyde (0.32 g, 2.58 mmol, 1eq.) and ammonium acetate (1.19 g, 15.45 mmol, 6 eq.) were sealed into a microwave tube, pre-stirred for one minute and subsequently exposed to 180 Watt microwave irradiation at 175°C for 80 minutes. The resulting biphasic reaction mixture was then transferred to a separating funnel, treated with equal volumes of ice-water and diethyl ether and shaken well. The aqueous phase containing excess ammonium acetate was extracted three times with diethyl ether. The organic phases were combined and concentrated under reduced pressure to afford the crude product. Recrystallization from ethanol and subsequent drying under reduced pressure delivered ligand **6** as an off-white crystalline solid with a yield of 33% (0.30 g, 0.92 mmol).

^{1}H-NMR (400 MHz, DMSO-d6): δ [ppm] = 8.20 (d, J=7.8 Hz, 4H, H_1), 7.85 (s, 2H, H_4), 7.75-7.53 (m, 2H, $H_{5,6}$), 7.46 (t, J=7.0 Hz, 2H, H_3), 7.23 (t, J=8.6 Hz, 2H, H_2).

^{13}C NMR (101 MHz, DMSO-d6) δ [ppm] = 188.89 (C-F), 137.23 (2 C-N), 134.94, 133.47 (C_{para}-N), 133.11, 130.47, 128.79, 128.65, 128.41, 122.58.

Anal. Calc. for $C_{23}H_{16}FN$: C, 84.90; H, 4.96; N, 4.30; F, 5.84. Found: C, 83.87; H, 4.36; N, 4.21; F, 5.96.

4-(4'-bromophenyl)-2,6-diphenylpyridine C^N(Br)^C, **7**

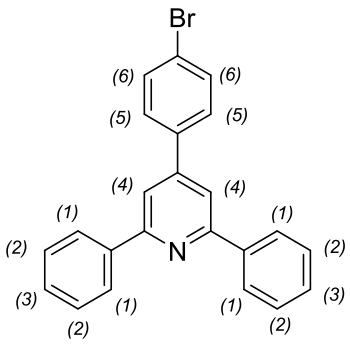

Chemical Formula: $C_{23}H_{16}BrN$
Molecular Weight: 386,29 g/mol

A mixture of acetophenone (0.6 mL, 5.15 mmol, 2.0 eq.), 4-bromobenzaldehyde (0.48 g, 2.58 mmol, 1eq.) and ammonium acetate (1.19 g, 15.45 mmol, 6 eq.) were sealed into a microwave tube, pre-stirred for one minute and subsequently exposed to 180 Watt microwave irradiation at 175°C for 80 minutes. The resulting biphasic reaction mixture was then transferred to a separating funnel, treated with equal volumes of ice-water and diethyl ether and shaken well. The aqueous phase containing excess ammonium acetate was extracted three times with diethyl ether. The organic phases were combined and concentrated under reduced pressure to afford the crude product. Recrystallization from ethanol and subsequent drying under reduced pressure delivered ligand **7** as an off-white crystalline solid with a yield of 39% (0.34 g, 0.88 mmol).

^{1}H-NMR (400 MHz, DMSO-d6): δ [ppm] = 8.20 (d, J=7.7 Hz, 4H, H_1), 7.87 (s, 2H, H_4), 7.70 (d, J=8.5 Hz, 2H, H_5), 7.56-7.40 (m, 6H, $H_{2,3}$), 6.86 (d, J=8.3 Hz, 2H, H_6).

^{13}C NMR (101 MHz, DMSO-d6) δ [ppm] = 156.33 (2 C-N), 149.36 (C_{para}-N), 138.98, 129.13, 128.72, 128.13, 126.91 (C-Br), 115.85, 115.66.

Anal. Calc. for $C_{23}H_{16}BrN$: C, 71.51; H, 4.18; N, 3.63; Br, 20.68. Found: C, 70.93; H, 4.37; N, 3.61; Br, 19.49.

4-(4'-nitrophenyl)-2,6-diphenylpyridine C^N(NO_2)^C, **8**

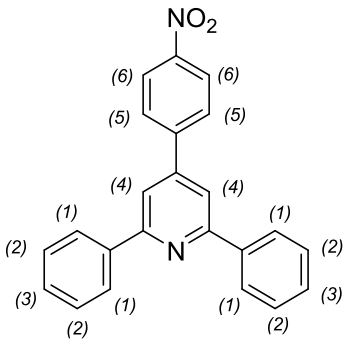

Chemical Formula: $C_{23}H_{16}N_2O_2$
Molecular Weight: 352,39 g/mol

A mixture of acetophenone (0.6 mL, 5.15 mmol, 2.0 eq.), 4-nitrobenzaldehyde (0.39 g, 2.58 mmol, 1eq.) and ammonium acetate (1.19 g, 15.45 mmol, 6 eq.) were sealed into a microwave tube, pre-stirred for one minute and subsequently exposed to 180 Watt microwave irradiation at 175°C for 80 minutes. The resulting biphasic reaction mixture was then transferred to a separating funnel, treated with equal volumes of ice-water and diethyl ether and shaken well. The aqueous phase containing excess ammonium acetate was extracted three times with diethyl ether. The organic phases were combined and concentrated under reduced pressure to afford the crude product. Recrystallization from ethanol and subsequent drying under reduced pressure delivered ligand **8** as an off-white crystalline solid with a yield of 35% (0.33 g, 0.93 mmol).

^{1}H NMR (400 MHz, DMSO-d6) δ [ppm] = 8.34 (d, J = 8.6 Hz, 4H. H_1), 8.08 (m, 4H, $H_{4,5}$), 7.90 – 7.84 (d, J = 8.5 Hz, 2H, H_6), 7.55 (t, J = 7.5 Hz, 2H, H_3), 7.44 (t, J = 7.7 Hz, 2H, H_2).

^{13}C NMR (101 MHz, DMSO-d6) δ [ppm] = 156.78 (2 C-N), 147.89 (C-NO_2), 147.35 (C_{para}-N), 144.13, 138.50, 129.47, 128.91, 128.81, 128.19, 124.04, 117.01.

Anal. Calc. for $C_{23}H_{16}N_2O_2$: C, 78.39; H, 4.58; N, 7.95. Found: C, 79.37; H, 4.37; N, 7.91.

5.2 Synthesis of [Hg(II)[C^N(R)^C]Cl] complexes

4-(4'-hydroxophenyl)-2,6-diphenylpyridinylmercury(II) chloride [Hg(C^N(OH)^C)Cl], **9**

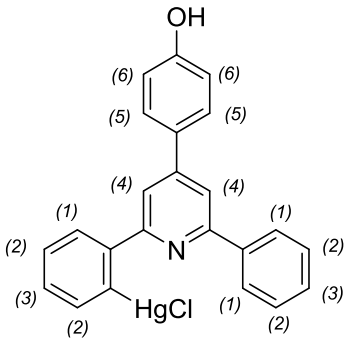

Chemical Formula: $C_{23}H_{16}ClHgNO$
Molecular Weight: 558,43 g/mol

Ligand **5** (1.90 g, 5.87 mmol, 1.0 eq.) and mercury(II) acetate (1.70 g, 5.34 mmol, 0.9 eq.) were heated in 50 mL absolute ethanol under reflux for 24 h under argon. Thereafter, a solution of lithium chloride (0.50 g, 11.74 mmol, 2.0 eq.) in 20 mL absolute methanol was added, refluxed for another 15 minutes, and subsequently given into 100 mL ice-cold, ultrapure water. The formed precipitate was filtered off and washed with ice-cold water and methanol. The solid was extracted with hot methanol to leave the bismercurated product as a solid residue. Upon cooling the formation of a precipitate could be observed, which was filtered and washed with ice-cold methanol. Any remaining solvent was removed under reduced pressure to afford complex **9** as a white, fine crystalline solid with a yield of 23% (0.75 g, 1.35 mmol).

^{1}H-NMR (400 MHz, DMSO-d6): δ [ppm] = 8.12 (d, J = 7.5 Hz, 3H, H_1), 7.98 (s, 2H, H_4), 7.83 (d, J = 8.4 Hz, 2H, H_6), 7.71 – 7.60 (m, 6H, $H_{2,2',3}$), 7.54 (d, J = 8.3 Hz, 2H, H_5).

^{13}C-NMR (101 MHz, DMSO-d6): δ [ppm] = 157.7 (2 C-N), 156.7(2 C-OH), 149.8 (C_{para}-N), 139.8 (C-HgCl), 131.6, 129.7, 129.5, 129.2, 128.9, 128.8, 128.7, 128.3, 128.0, 127.3, 116.8, 116.2.

^{199}Hg-NMR (72 MHz, DMSO-d6): δ [ppm] = -1054.22.

4-(4'-fluorophenyl)-2,6-diphenylpyridinylmercury(II) chloride [Hg(C^N(F)^C)Cl], **10**

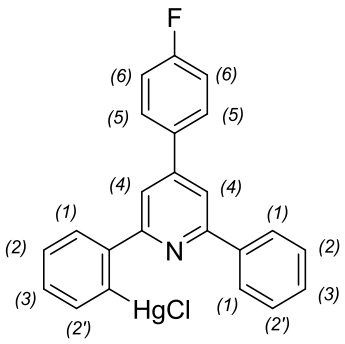

Chemical Formula: $C_{23}H_{15}ClFHgN$
Molecular Weight: 560,42 g/mol

Ligand **6** (1.91 g, 5.87 mmol, 1.0 eq.) and mercury(II) acetate (1.70 g, 5.34 mmol, 0.9 eq.) were heated in 50 mL absolute ethanol under reflux for 24 h under argon. Thereafter, a solution of lithium chloride (0.50 g, 11.74 mmol, 2.0 eq.) in 20 mL absolute methanol was added, refluxed for another 15 minutes, and subsequently given into 100 mL ice-cold, ultrapure water. The formed precipitate was filtered off and washed with ice-cold water and methanol. The solid was extracted with hot methanol to leave the bismercurated product as a solid residue. Upon cooling the formation of a precipitate could be observed, which was filtered and washed with ice-cold methanol. Any remaining solvent was removed under reduced pressure to afford complex **10** as a white solid with a yield of 25% (0.82 g, 1.45 mmol).

^{1}H-NMR (400 MHz, DMSO-d6): δ [ppm] = 8.33 (d, J=7.4 Hz, 3H, H_1), 8.18 (s, 2H, H_4), 8.15-8.08 (m, 2H, H_5), 7.55 (t, J=7.4 Hz, 4H, $H_{2,3}$), 7.48 (m, 2H, $H_{2'}$), 7.40 (d, J=8.7 Hz, 2H, H_6).

^{13}C-NMR (101 MHz, DMSO-d6): δ [ppm] = 189.09 (C-F), 142.58 (C-HgCl), 137.43(2 C-N), 135.14, 133.67(C_{para}-N), 133.31, 130.66, 128.99, 128.85, 128.61, 122.78, 119.12, 109.60.

^{199}Hg-NMR (72 MHz, DMSO-d6): δ [ppm] = -1054.93.

4-(4'-bromophenyl)-2,6-diphenylpyridinylmercury(II) chloride [Hg(C^N(Br)^C)Cl], **11**

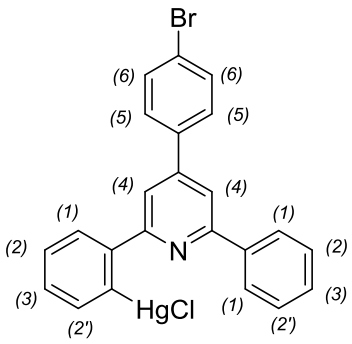

Chemical Formula: $C_{23}H_{15}BrClHgN$
Molecular Weight: 621,32 g/mol

Ligand **7** (2.27 g, 5.87 mmol, 1.0 eq.) and mercury(II) acetate (1.70 g, 5.34 mmol, 0.9 eq.) were heated in 50 mL absolute ethanol under reflux for 24 h under argon. Thereafter a solution of lithium chloride (0.89 g, 21.07 mmol, 2.0 eq.) in 20 mL absolute methanol was added, refluxed for another 15 minutes, and subsequently given into 100 mL ice-cold, ultrapure water. The formed precipitate was filtered off and washed with ice-cold water and methanol. The solid was extracted with hot methanol to leave the bismercurated product as a solid residue. Upon cooling the formation of a precipitate could be observed, which was filtered and washed with ice-cold methanol. Any remaining solvent was removed under reduced pressure to afford complex **11** as a white, fine crystalline solid with a yield of 27% (0.98 g, 1.58 mmol).

^{1}H NMR (400 MHz, DMSO-d6) δ [ppm] = 8.31 (d, J = 6.7 Hz, 3H, H_1), 8.12 (s, 2H, H_4), 7.94 (d, J = 8.2 Hz, 2H, H_5), 7.60 (t, J = 6.7 Hz, 4H, $H_{2,3}$), 7.49 (m, 2H, $H_{2'}$), 6.86 (d, J = 8.3 Hz, 2H, H_6).

^{13}C-NMR (101 MHz, DMSO-d6): δ [ppm] = 156.90 (2 C-N), 156.24 (C_{para}-N), 143.91(C-HgCl), 138.66, 134.03, 128.80, 128.02, 127.32 (C-Br), 123.34, 118.41, 116.22, 113.25, 109.15.

^{199}Hg-NMR (72 MHz, DMSO-d6): δ [ppm] = -1055.12

4-(4'-nitrophenyl)-2,6-diphenylpyridinylmercury(II) chloride [Hg(C^N(NO_2)^C)Cl], **12**

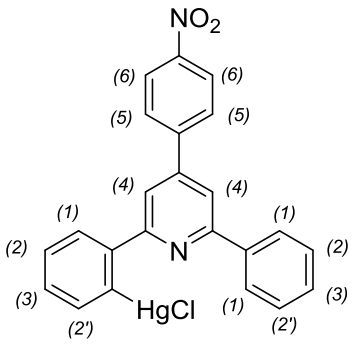

Chemical Formula: $C_{23}H_{15}ClHgN_2O_2$
Molecular Weight: 587,43 g/mol

Ligand **8** (2.07 g, 5.87 mmol, 1.0 eq.) and mercury(II) acetate (1.70 g, 5.34 mmol, 0.9 eq.) were heated in 50 mL absolute ethanol under reflux for 24 h under argon. Thereafter a solution of lithium chloride (0.89 g, 21.07 mmol, 2.0 eq.) in 20 mL absolute methanol was added, refluxed for another 15 minutes, and subsequently given into 100 mL ice-cold, ultrapure water. The formed precipitate was filtered off and washed with ice-cold water and methanol. The solid was extracted with hot methanol to leave the bismercurated product as a solid residue. Upon cooling the formation of a precipitate could be observed, which was filtered and washed with ice-cold methanol. Any remaining solvent was removed under reduced pressure to afford complex **12** as a white, fine crystalline solid with a yield of 25% (0.86 g, 1.47 mmol).

^{1}H NMR (400 MHz, DMSO-d6) δ [ppm] = 8.33 (d, J = 7.3 Hz, 3H, H_1), 8.20 (s, 2H, H_4), 8.10 (d, J = 8.5 Hz, 2H, H_5), 7.62 (d, J = 8.5 Hz, 2H, H_6), 7.55 (t, J = 7.4 Hz, 4H, $H_{2,3}$), 7.52 – 7.45 (m, 2H, $H_{2'}$).

^{13}C NMR (101 MHz, DMSO-d6): δ [ppm] =163.21 (2 C-N), 156.37(C_{para}-N), 149.55 (C-HgCl), 138.99 (C-NO_2), 138.03, 136.14, 129.22, 128.80, 126.76, 115.44, 115.17.

^{199}Hg-NMR (72 MHz, DMSO-d6): δ [ppm] = - 1054.37.

5.3 Synthesis of [Au(III)[C^N(R)^C]Cl] complexes

4-(4'-hydroxophenyl)-2,6-diphenylpyridinylgold(III) chloride [Au(C^N(OH)^C)Cl], **13**

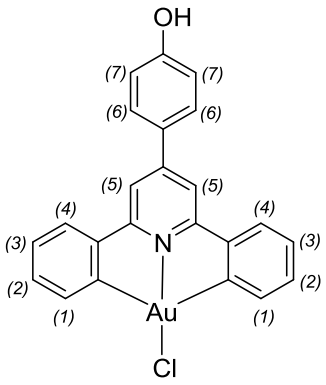

Chemical Formula: $C_{23}H_{15}AuClNO$
Molecular Weight: 553,80 g/mol

$K[AuCl_4]$ (37.8 mg, 0.1 mmol, 1eq.) was added to a suspension of complex **9** (55.8 mg, 0.1 mmol, 1eq.) in 20 mL dry and degassed acetonitrile under vigorous stirring. The suspension was refluxed under argon at 100°C for 48 h upon which solubilisation of the educts occurred. The solution was then allowed to cool down, leading to the precipitation of a solid. The crude product was filtrated *via* a Whatman filter and washed with ice-cold diethyl ether and pentane. Any remaining solvent was removed under reduced pressure to afford complex **13** as a light-yellow solid with a yield of 70% (38,77 mg, 70 µmol).

^{1}H NMR (400 MHz, DMSO-d6) δ [ppm] = 9.76 (s, 1H, OH), 8.27 (d, J = 6.8 Hz, 4H, $H_{1,4}$), 8.06 (d, J = 13.7 Hz, 4H,$H_{6,7}$), 7.60 – 7.53 (m, 4H, $H_{2,3}$), 7.51 – 7.46 (m, 2H,H_5).

^{13}C NMR (101 MHz, DMSO-d6) δ [ppm] = 157.47(2 C-N), 151.21 (C-OH), 150.02 (C_{para}-N), 140.14 (C-Au), 128.95, 128.87, 128.77, 127.96, 127.28, 127.26, 126.18, 116.81, 116.17, 112.64.

Positive ESI-MS (acetone/water): m/z = 571.0382 $[M+H_2O]^+$ (calcd for $C_{23}H_{17}AuClNO_2$: 571.0613).

Anal. Calc. for $C_{23}H_{15}AuClNO$: C, 49.88; H, 2.73; N, 2.53;%. Found: C, 49.63; H, 2.55; N, 2.57;%.

4-(4'-fluorophenyl)-2,6-diphenylpyridinylgold(III) chloride [Au(C^N(F)^C)Cl], **14**

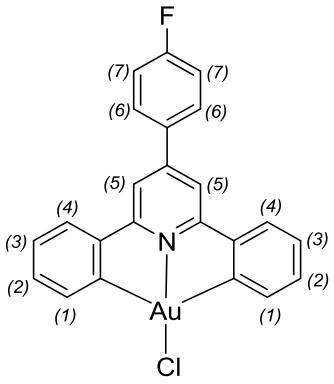

Chemical Formula: $C_{23}H_{14}AuClFN$
Molecular Weight: 555,79 g/mol

$K[AuCl_4]$ (37.8 mg, 0.1 mmol, 1eq.) was added to a suspension of complex **10** (62.1 mg, 0.1 mmol, 1eq.) in 20 mL dry and degassed acetonitrile under vigorous stirring. The suspension was refluxed under argon at 100°C for 48 h upon which solubilisation of the educts occurred. The solution was then allowed to cool down, leading to the precipitation of a solid. The crude product was filtrated *via* a Whatman filter and washed with ice-cold diethyl ether and pentane. Any remaining solvent was removed under reduced pressure to afford complex **14** as a light-yellow solid with a yield of 63 % (35.01 mg, 63 µmol).

^{1}H NMR (300 MHz, DMSO-d6) δ [ppm] = 8.32 (s, 2H, H_5), 8.25 (m, 2H, H_7), 8.12 (d, *J* = 7.7 Hz, 2H, H_4), 7.70 (d, *J* = 7.2 Hz, 2H, H_1), 7.54 – 7.41 (m, 4H, $H_{2,3}$), 7.34 (m, 2H, H_6).

^{13}C NMR (101 MHz, DMSO-d6) δ [ppm] = 189.11 (C-F), 142.69 (C-Au), 137.42 (2 C-N), 133.99 (C_{para}-N), 133.34, 131.93, 131.27, 130.88, 128.87, 128.62, 128.13, 124.06, 122.83.

Positive ESI-MS (acetone): m/z = 555.0463 $[M]^+$ (calcd for $C_{23}H_{17}AuClNO_2$: 555.0464).

Anal. Calc. for $C_{23}H_{14}AuClFN$: C, 47.15; H 3.83; N, 1.77 %. Found: C, 47.04; H 3.68;N, 1.79 %.

4-(4'-bromophenyl)-2,6-diphenylpyridinylgold(III) chloride [Au(C^N(Br)^C)Cl], **15**

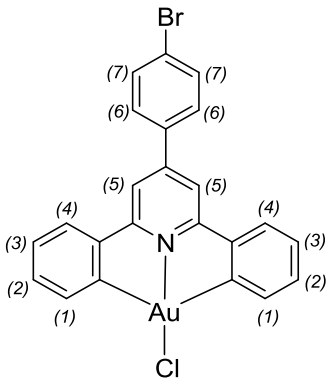

Chemical Formula: $C_{23}H_{14}AuBrClN$
Molecular Weight: 616,69 g/mol

$K[AuCl_4]$ (37.8 mg, 0.1 mmol, 1eq.) was added to a suspension of complex **11** (56.4 mg, 0.1 mmol, 1eq.) in 20 mL dry and degassed acetonitrile under vigorous stirring. The suspension was refluxed under argon at 100°C for 48 h upon which solubilisation of the educts occurred. The solution was then allowed to cool down, leading to the precipitation of a solid. The crude product was filtrated *via* a Whatman filter and washed with ice-cold diethyl ether and pentane. Any remaining solvent was removed under reduced pressure to afford complex **15** as a light-yellow solid with a yield of 65 % (40.08 mg, 65 µmol).

^{1}H NMR (300 MHz, DMSO-d6) δ [ppm] = 8.32 (s, 2H, H_5), 8.12 (m, 4H, $H_{4,1}$), 7.85 (d, J = 6.0 Hz, 2H, H_7), 7.71 (d, J = 8.0 Hz, 2H, H_6), 7.50 – 7.41 (m, 2H, H_2), 7.40 – 7.29 (m, 2H, H_3).

^{13}C NMR (75 MHz, DMSO-d6) δ [ppm] = 157.05 (2 C-N), 148.76 (C_{para}-N), 139.11 (C-Au), 137.30, 132.42, 129.99, 129.79, 129.22, 127.44 (C-Br), 124.39, 116.90.

Positive ESI-MS (acetone): m/z = 616.9659 $[M]^+$ (calcd for $C_{23}H_{17}AuClNO_2$: 614.9664).

Anal. Calc. for $C_{23}H_{14}AuBrClN$: C, 44.80; H, 2.29; N, 2.27 %. Found: C, 44.61; H, 2.24; N, 2.36 %.

4-(4'-nitrophenyl)-2,6-diphenylpyridinylgold(III) chloride [Au(C^N(NO_2)^C)Cl], **16**

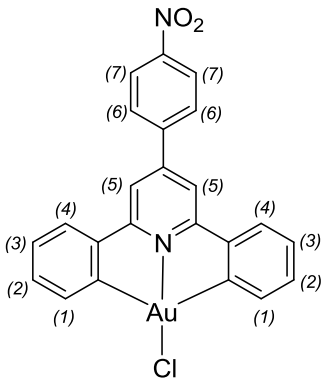

Chemical Formula: $C_{23}H_{14}AuClN_2O_2$
Molecular Weight: 582,79 g/mol

$K[AuCl_4]$ (37.8 mg, 0.1 mmol, 1eq.) was added to a suspension of complex **12** (58.7 mg, 0.1 mmol, 1eq.) in 20 mL dry and degassed acetonitrile under vigorous stirring. The suspension was refluxed under argon at 100°C for 48 h upon which solubilisation of the educts occurred. The solution was then allowed to cool down, leading to the precipitation of a solid. The crude product was filtrated *via* a Whatman filter and washed with ice-cold diethyl ether and pentane. Any remaining solvent was removed under reduced pressure to afford complex **16** as a light-yellow solid with a yield of 61 % (35.55 mg, 61 µmol).

^{1}H NMR (400 MHz, DMSO-d6) δ [ppm] = 8.44 (s, 2H, H_5), 8.32 (d, J = 8.6 Hz, 2H, H_7), 8.23 (d, J = 8.7 Hz, 2H, H_6), 7.87 – 7.74 (m, 4H, $H_{1,4}$), 7.58 – 7.51 (m, 2H, H_3), 7.50 – 7.40 (m, 2H, H_2).

^{13}C NMR (75 MHz, DMSO-d6) δ [ppm] = 157.20 (2 C-N), 148.29 (C-NO_2), 147.77 (C_{para}-N), 144.55, 144.10, 138.91 (C-Au), 129.96, 129.90, 129.33, 129.25, 127.48, 124.49, 117.42.

Positive ESI-MS (acetone): m/z = 582.0400 $[M]^+$ (calcd for $C_{23}H_{17}AuClNO_2$: 582.0409).

Anal. Calc. for $C_{23}H_{14}AuClN_2O_2$: C, 47.40; H, 2.42; N, 4.81 %. Found: C, 47.34; H, 2.37; N, 4.83 %.

6 Synthesis of C^N Au(III) complexes

Benzylpyridinylgold(III) dichloride [Au(pyb-H)Cl_2], 17

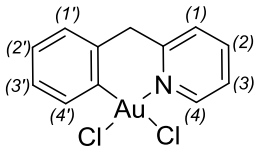

Chemical Formula: $C_{12}H_{10}AuCl_2N$
Molecular Weight: 436,09 g/mol

(py^b-H = C^N cyclometalated 2-benzylpyridine)

Synthesis was carried out with slight changes according to Cinellu *et al.*[86] $KAuCl_4$ (1.00 g, 2.65 mmol, 1 eq.) and benzylpyridine (0.43 mL, 2.65 mmol, 1 eq.) were dissolved in 50 mL ultrapure water and refluxed at 100°C for 24 hours. A white precipitate was formed which filtered off and washed with methanol, diethylether and pentane. Any remaining solvent was removed under reduced pressure to afford complex **17** as a white solid with a yield of 75 % (0.87 g, 1.99 mmol).

^{1}H NMR (400 MHz, DMSO-d6) δ [ppm] = 9.17 (d, J = 5.6 Hz, 1H, H_4), 8.26 (t, J = 8.1 Hz, 1H, H_2), 7.99 (d, J = 7.6 Hz, 1H, H_1), 7.71 (t, J = 6.7 Hz, 1H, H_3), 7.41 (d, J = 8.0 Hz, 1H, $H_{4'}$), 7.25 (d, J = 6.6 Hz, 1H, $H_{1'}$), 7.18 (t, J = 7.2 Hz, 1H, $H_{3'}$), 7.07 (t, J = 8.2 Hz, 1H, $H_{2'}$), 4.62 (d, J = 15.2 Hz, 1H, CH_aH_b), 4.35 (d, J = 15.1 Hz, 1H, CH_aH_b). Assignments based on 2D-COSY spectra.

^{13}C NMR (101 MHz, DMSO-d6) δ [ppm] = 155.66 (C-N), 152.05 (C_4-N), 143.25 (C-Au), 141.05, 132.68, 131.93, 128.60, 127.93, 126.90, 126.38, 124.47, 46.05 (CH_2).

Anal. Calc. for $C_{12}H_{10}AuCl_2N$: C, 33.05; H, 2.31; N, 3.21 %. Found: C, 32.45; H, 2.43; N, 3.86 %.

N-(4-ethynylphenyl)-2-oxo-2H-chromene-3-carboxamide, **18**

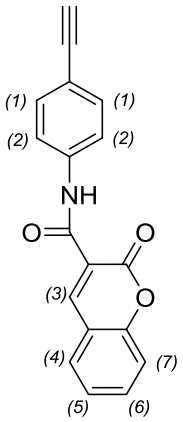

Chemical Formula: $C_{18}H_{11}NO_3$
Molecular Weight: 289,29 g/mol

To a solution of coumarin-3-carboxylic acid (1.00 g, 5.26 mmol, 1.05 eq.) in 50 mL DCM, N-(3-dimethylaminopropyl)-N'-ethylcarbodiimmide (0.89 mL 5.01 mmol, 1eq.) was added dropwise under vigorous stirring. Subsequently, a solution of 4-ethynylaniline (0.59 g, 5.01 mmol, 1.05 eq.) in 50 mL DCM was added. The reaction was stirred at 0°C for 24h upon which a formation of a yellow solid was observed. The solid was filtered and washed with distilled water, ethanol, and diethyl ether. Any remaining solvent was removed under reduced pressure to afford ligand **18** as a yellow solid with a yield of 61% (0.88 g, 3.06 mmol).

^{1}H NMR (400 MHz, $CDCl_3$) δ [ppm] = 10.93 (s, 1H, N-H), 9.02 (s, 1H, H_3), 7.73 (m, 4H, H_{4-7}), 7.51 (d, J = 8.6 Hz, 2H, H_2), 7.48 – 7.39 (m, 2H, H_1), 3.07 (s, 1H, C≡ CH).

^{13}C NMR (101 MHz, $CDCl_3$) δ [ppm] = 161.98 (C=O), 159.50 (O-C=O), 154.68 (O-C=C), 149.33(C_3), 138.26 (C-C≡ CH), 134.70 (C_6), 133.16 (C_1), 130.16 (C_4), 125.72 (C_5), 120.33 (C_2), 118.82, 118.55, 118.37, 116.93 (C_7), 83.57 (C≡ CH), 77.36 (C≡ CH).

Anal. Calc. for $C_{18}H_{11}NO_3$: C, 74.73; H, 3.83; N, 4.84 %. Found C, 75.61; H, 3.73; N, 4.25 %.

Benzylpyridinylgold(III) hydroxide [Au(pyb-H)OH_2], **19**

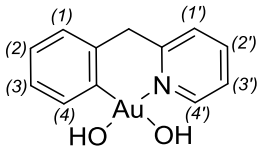

Chemical Formula: $C_{12}H_{12}AuNO_2$
Molecular Weight: 399,20 g/mol

(py^b-H = C^N cyclometalated 2-benzylpyridine)

Route A

Synthesis was carried out analogously to a previously reported procedure for the synthesis of [Au(bipy)$(OH)_2$][PF_6] (bipy=bipyridine) by Cinellu *et al.*[133b, 134].

An aqueous suspension of Ag_2O (0.054 g, 0.23 mmol, 2eq.) was added to a solution of complex **17** (0.05 g, 0.115 mmol, 1 eq.) in acetone. The suspension was stirred for 24 hours at room temperature. Subsequently, AgCl was removed by filtration and the solution evaporated to dryness under reduced pressure. The residue was extracted with acetonitrile and filtered over Celite to afford a pale-yellow solution. The solution was concentrated to a small volume, and pentane was added to afford a white precipitate.

Variation of the applied temperature, solvent and reaction time has been conducted as can be seen in Table 6.

Table 6. Varied reaction conditions for complex 19.

temperature [°C]	time [h]	solvent
RT	24	acetone/water
RT	12	acetone/water
RT	1.5	acetone/water
60	24	acetone/water
100 (reflux)	24	acetone/water
RT	24	DCM/water
60	24	DCM/water
100 (reflux)	24	DCM/water
RT	24	MeCN/DCM
60	24	DCM/ DCM
100 (reflux)	24	DCM/ DCM

Route B

An aqueous solution of KOH (33 mg, 0.59 mmol, 2 eq.) was added to an aqueous suspension of complex **17** (179 mg, 0.27 mmol). The mixture was refluxed at 100°C for 1 h under vigorous stirring. Subsequent filtration over Celite gave a colourless filtrate. The filtrate was concentrated under reduced pressure and stored at 0°C upon which crystallization of white crystals occurred. The white solid was filtrated and any remaining solvent removed under reduced pressure.

Route C

An aqueous solution of CsOH (88 mg, 0.59 mmol, 2 eq.) was added to an aqueous suspension of complex **17** (179 mg, 0.27 mmol). The mixture was refluxed at 100°C for 1 h under vigorous stirring. Subsequent filtration over Celite gave a colourless filtrate. The filtrate was concentrated under reduced pressure and stored at 0°C upon which crystallization of white crystals occurred. The white solid was filtrated and any remaining solvent removed under reduced pressure.

All routes didn't lead to an isolation of the target complex **19**.

N-(4-ethynylphenyl)-2-oxo-2H-chromene-3-carboxamido-benzylpyridinylgold(III) chloride, **20**

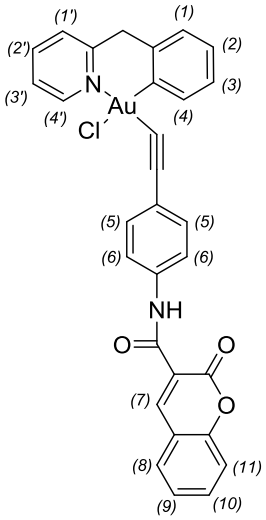

Chemical Formula: $C_{30}H_{20}AuClN_2O_3$
Molecular Weight: 688,92 g/mol

Complex **17** (0.20 g, 0.5 mmol, 1eq.) and ligand **18** (0.15 g, 0.55 mmol, 1.1eq.) were dissolved in 20 mL DCM and cooled to 0°C. Under vigorous stirring a 3M in Et_2O solution of ethylmagnesiumbromide (0.17mL, 0.55 mmol, 1.1 eq.) was added dropwise upon which the yellow solution turned brown. The solution was stirred at room temperature for two hours and afterwards filtered over Celite, giving a bright yellow solution. The solution was reduced to a small volume and pentane was added, leading to the precipitation of yellow solid and dark yellow oil, which was removed by fractionated filtering at 0°C. The solid was washed with ice-cold diethylether and pentane. Any remaining solvent was removed under reduced pressure to afford complex **20** as a neon-yellow solid with a yield of 31% (0.11 g, 0.15 mmol).

^{1}H NMR (400 MHz, Acetone-d6) δ [ppm] =10.94 (s, 1H, N-H), 9.38 (d, J = 6.1 Hz, 1H, H_4), 9.05 (s, 1H, H_7), 8.29 (t, J = 7.7, 1H, H_2), 8.04 (d, J = 7.9, 2H, $H_{8,11}$), 7.85 (m, 2H, H_5), 7.83 (m, 2H, H_6), 7.71 (t, J = 7.4 Hz, 1H, H_3), 7.62 (d, J = 8.8 Hz, 1H, H_1), 7.53 (t, *J* = 7.0 Hz, 2H, $H_{9,10}$), 7.51 (t, *J* = 7.9 Hz, 1H, $H_{3'}$), 7.29 (d, J = 11.1 Hz, 1H, $H_{4'}$), 7.17 (t, J = 7.7 Hz, 1H, $H_{2'}$), 7.04 (d, J = 9.1 Hz, 1H, $H_{1'}$), 4.61 (d, J = 15.1 Hz, 1H, CH_aH_b), 4.40 (d, J = 15.0 Hz, 1H, CH_aH_b). Assignments based on 2D-COSY spectra.

Anal. Calc. for $C_{30}H_{20}AuClN_2O_3$: C, 52.30; H, 2.93; N, 4.07; %. Found C, 52.81; H, 2.68; N, 4.31; %.

Appendix

Crystalstructur report for [Au(C^N^C)(PTA)][PF_6]

Single X-Ray Crystallography was performed for the obtained crystals of complex **3**. Table 7 gives an overview of the physical data collection details of complex **3**.

Table 7. Physical data collection details for complex 3.

Axis	dx/mm	2θ/°	ω/°	φ/°	χ/°	Width/°	Frames	Time/s	T/K
Phi	34.024	1.38	2.64	0.00	-23.00	0.50	720	1.00	100.00
Omega	34.025	1.38	5.84	270.00	-44.94	0.50	187	1.00	99.99
Omega	34.025	55.60	324.89	244.83	68.07	0.50	187	1.00	100.01
Omega	34.024	1.38	5.84	90.00	-44.94	0.50	187	1.00	100.00
Omega	34.026	55.99	322.60	61.46	66.20	0.50	192	1.00	99.99
Phi	34.026	1.37	272.05	360.00	23.00	0.50	720	1.00	99.99
Omega	34.026	1.37	5.84	180.00	-44.94	0.50	103	1.00	100.04

(U= 50 kV, I= 1.0 mA, λ= 0.71073 Å)

A total of 2296 frames were collected. The total exposure time was 0.64 hours. The integration of the data using a triclinic unit cell yielded a total of 42875 reflections to a maximum θ angle of 25.35° (0.83 Å resolution), of which 4235 were independent (average redundancy 10.124, completeness = 100.0%, Rint = 5.26%, Rsig = 2.31%) and 4125 (97.40%) were greater than 2σ(F2). The final cell constants of a = 9.0119(2) Å, b = 9.6107(2) Å, c = 14.7237(4) Å, α = 93.2060(10)°, β = 97.9400(10)°, γ = 112.8820(10)°, volume = 1155.19(5) Å3, are based upon the refinement of the XYZ-centroids of 156 reflections above 20 σ(I) with 17.74° < 2θ < 56.77°. The ratio of minimum to maximum apparent transmission was 0.466. The calculated minimum and maximum transmission coefficients (based on crystal size) are 0.1210 and 0.2920. The final anisotropic full-matrix least-squares refinement on F2 with 405 variables converged at R1 = 1.33%, for the observed data and wR2 = 3.63% for all data. The goodness-of-fit was 1.215. The largest peak in the final difference electron density synthesis was 0.315 e-/Å3 and the largest hole was -0.786 e-/Å3 with an RMS deviation of 0.106 e-/Å3. On the basis of the final model, the calculated density

was 2.146 g/cm3 and F(000), 724 e^-.

Table 8 gives an overview of the determined crystal data of complex **3**.

Table 8. Sample and crystal data for complex 3.

Chemical formula	$C_{23}H_{25}AuCl_0F_6N_4OP_2$	
Formula weight	746.38 g/mol	
Temperature	100(2) K	
Wavelength	0.71073 Å	
Crystal size	0.248 x 0.348 x 0.554 mm	
Crystal habit	clear yellow fragment	
Crystal system	triclinic	
Space group	P -1	
Unit cell dimensions	a = 9.0119(2) Å	α = 93.2060(10)°
	b = 9.6107(2) Å	β = 97.9400(10)°
	c = 14.7237(4) Å	γ = 112.8820(10)°
Volume	1155.19(5) $Å^3$	
Z	2	
Density (calculated)	2.146 g/cm^3	
Absorption coefficient	6.582 mm^{-1}	
F(000)	724	

Structure refinement was performed for complex **3** as presented in Table 9.

Table 9. Data collection and structure refinement for complex 3.

Diffractometer	Bruker D8 Venture Duo IMS
Radiation source	IMS microsource, Mo
Theta range for data collection	2.32 to 25.35°
Index ranges	-10<=h<=10, -11<=k<=11, -17<=l<=17
Reflections collected	42875
Independent reflections	4235 [R(int) = 0.0526]
Coverage of independent reflections	100.0%
Absorption correction	Multi-Scan
Max. and min. transmission	0.2920 and 0.1210
Refinement method	Full-matrix least-squares on F^2
Refinement program	SHELXL-2014/7 (Sheldrick, 2014)
Function minimized	$\Sigma\, w(F_o^2 - F_c^2)^2$
Data / restraints / parameters	4235 / 275 / 405

Goodness-of-fit on F^2	1.215
Δ/σ_{max}	0.024
Final R indices	4125 data; I>2σ(I) R1 = 0.0133, wR2 = 0.0361 all data R1 = 0.0142, wR2 = 0.0363
Weighting scheme	$w=1/[\sigma^2(F_o^2)+(0.0120P)^2+0.3302P]$ where $P=(F_o^2+2F_c^2)/3$
Largest diff. peak and hole	0.315 and -0.786 eÅ^{-3}
R.M.S. deviation from mean	0.106 eÅ^{-3}

Images of the crystal structures were generated with the crystallographic software PLATON and represent Ortep drawings with 50% ellipsoids. The $[PF_6]^-$ counterion could be detected, as well as a co-crystalized H_2O molecule as displayed in Figure 42.

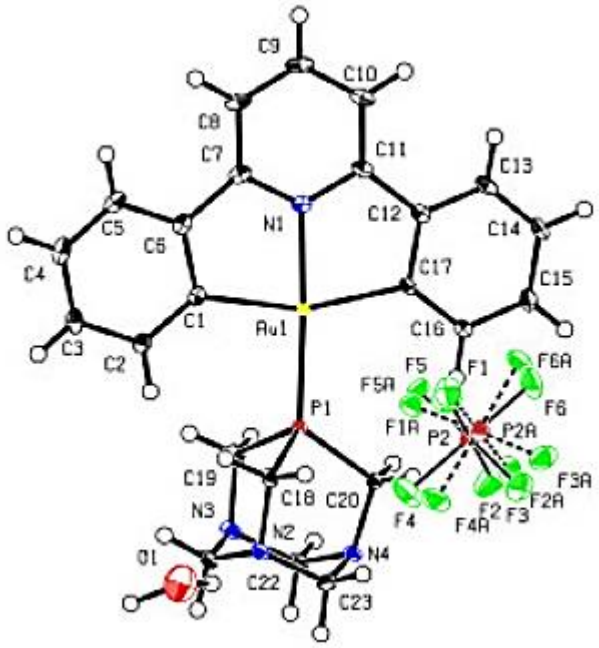

Figure 42 . Complete crystal structure with Ortep drawings complex 3.

The determined bond lengths, angles and torsion angles of complex **3** are given in Table 10,

Table 11 and Table 12, respectively.

Table 10. Bond lengths(Å) of complex 3.

bond	length (Å)	bond	length (Å)
Au1-N1	2.025(2)	Au1-C17	2.091(2)
Au1-C1	2.106(2)	Au1-P1	2.2706(6)
P1-C18	1.840(3)	P1-C19	1.843(2)
P1-C20	1.848(3)	N1-C7	1.353(3)
N1-C11	1.353(3)	N2-C18	1.470(3)
N2-C23	1.471(3)	N2-C21	1.483(3)
N3-C22	1.465(3)	N3-C19	1.473(3)
N3-C21	1.474(3)	N4-C22	1.465(3)
N4-C23	1.470(3)	N4-C20	1.476(3)
C1-C2	1.394(4)	C1-C6	1.417(4)
C2-C3	1.400(4)	C2-H2	0.95
C3-C4	1.384(4)	C3-H3	0.95
C4-C5	1.380(4)	C4-H4	0.95
C5-C6	1.397(4)	C5-H5	0.95
C6-C7	1.461(4)	C7-C8	1.395(4)
C8-C9	1.381(4)	C8-H8	0.95
C9-C10	1.384(4)	C9-H9	0.95
C10-C11	1.385(4)	C10-H10	0.95
C11-C12	1.465(4)	C12-C13	1.396(4)
C12-C17	1.415(4)	C13-C14	1.383(4)
C13-H13	0.95	C14-C15	1.386(4)
C14-H14	0.95	C15-C16	1.396(4)
C15-H15	0.95	C16-C17	1.394(4)
C16-H16	0.95	C18-H18A	0.99
C18-H18B	0.99	C19-H19A	0.99
C19-H19B	0.99	C20-H20A	0.99
C20-H20B	0.99	C21-H21A	0.99
C21-H21B	0.99	C22-H22A	0.99
C22-H22B	0.99	C23-H23A	0.99
C23-H23B	0.99	O1-H1A	0.9599(11)
O1-H1B	0.9599(11)	P2-F2	1.590(2)
P2-F6	1.593(3)	P2-F1	1.601(2)
P2-F4	1.602(3)	P2-F3	1.605(2)
P2-F5	1.605(2)	P2A-F2A	1.587(4)
P2A-F6A	1.596(4)	P2A-F4A	1.601(4)
P2A-F1A	1.603(4)	P2A-F5A	1.605(4)
P2A-F3A	1.606(4)		

Table 11. Bond angles(°) for complex 3.

bond	angle(°)	bond	angle(°)
N1-Au1-C17	80.44(9)	N1-Au1-C1	80.32(9)
C17-Au1-C1	160.75(10)	N1-Au1-P1	177.26(6)
C17-Au1-P1	102.11(7)	C1-Au1-P1	97.13(7)
C18-P1-C19	101.25(11)	C18-P1-C20	99.60(12)
C19-P1-C20	99.20(12)	C18-P1-Au1	114.64(8)
C19-P1-Au1	113.82(9)	C20-P1-Au1	124.76(8)
C7-N1-C11	124.3(2)	C7-N1-Au1	117.88(17)
C11-N1-Au1	117.84(17)	C18-N2-C23	110.69(19)
C18-N2-C21	111.5(2)	C23-N2-C21	108.9(2)
C22-N3-C19	111.0(2)	C22-N3-C21	108.8(2)
C19-N3-C21	112.09(19)	C22-N4-C23	109.4(2)
C22-N4-C20	111.7(2)	C23-N4-C20	111.8(2)
C2-C1-C6	117.5(2)	C2-C1-Au1	132.17(19)
C6-C1-Au1	110.35(18)	C1-C2-C3	121.3(2)
C1-C2-H2	119.3	C3-C2-H2	119.3
C4-C3-C2	120.1(3)	C4-C3-H3	119.9
C2-C3-H3	119.9	C5-C4-C3	120.0(2)
C5-C4-H4	120.0	C3-C4-H4	120.0
C4-C5-C6	120.3(2)	C4-C5-H5	119.8
C6-C5-H5	119.8	C5-C6-C1	120.8(2)
C5-C6-C7	121.3(2)	C1-C6-C7	117.9(2)
N1-C7-C8	117.9(2)	N1-C7-C6	113.6(2)
C8-C7-C6	128.5(2)	C9-C8-C7	119.2(2)
C9-C8-H8	120.4	C7-C8-H8	120.4
C8-C9-C10	120.9(2)	C8-C9-H9	119.5
C10-C9-H9	119.5	C9-C10-C11	119.2(2)
C9-C10-H10	120.4	C11-C10-H10	120.4
N1-C11-C10	118.3(2)	N1-C11-C12	113.2(2)
C10-C11-C12	128.5(2)	C13-C12-C17	120.6(2)
C13-C12-C11	121.6(2)	C17-C12-C11	117.8(2)
C14-C13-C12	120.4(2)	C14-C13-H13	119.8
C12-C13-H13	119.8	C13-C14-C15	119.7(2)
C13-C14-H14	120.1	C15-C14-H14	120.1
C14-C15-C16	120.3(3)	C14-C15-H15	119.8
C16-C15-H15	119.8	C17-C16-C15	121.1(2)
C17-C16-H16	119.5	C15-C16-H16	119.5
C16-C17-C12	117.9(2)	C16-C17-Au1	131.30(19)
C12-C17-Au1	110.71(18)	N2-C18-P1	110.30(16)
N2-C18-H18A	109.6	P1-C18-H18A	109.6
N2-C18-H18B	109.6	P1-C18-H18B	109.6
H18A-C18-H18B	108.1	N3-C19-P1	109.69(17)
N3-C19-H19A	109.7	P1-C19-H19A	109.7
N3-C19-H19B	109.7	P1-C19-H19B	109.7
H19A-C19-H19B	108.2	N4-C20-P1	109.08(17)
N4-C20-H20A	109.9	P1-C20-H20A	109.9
N4-C20-H20B	109.9	P1-C20-H20B	109.9
H20A-C20-H20B	108.3	N3-C21-N2	114.0(2)

N3-C21-H21A	108.7	N2-C21-H21A	108.7
N3-C21-H21B	108.7	N2-C21-H21B	108.7
H21A-C21-H21B	107.6	N3-C22-N4	113.9(2)
N3-C22-H22A	108.8	N4-C22-H22A	108.8
N3-C22-H22B	108.8	N4-C22-H22B	108.8
H22A-C22-H22B	107.7	N4-C23-N2	113.7(2)
N4-C23-H23A	108.8	N2-C23-H23A	108.8
N4-C23-H23B	108.8	N2-C23-H23B	108.8
H23A-C23-H23B	107.7	H1A-O1-H1B	98.(3)
F2-P2-F6	90.42(18)	F2-P2-F1	179.9(2)
F6-P2-F1	89.48(17)	F2-P2-F4	90.32(18)
F6-P2-F4	179.22(19)	F1-P2-F4	89.77(18)
F2-P2-F3	90.72(16)	F6-P2-F3	91.18(18)
F1-P2-F3	89.29(17)	F4-P2-F3	89.04(17)
F2-P2-F5	89.81(16)	F6-P2-F5	90.68(17)
F1-P2-F5	90.18(16)	F4-P2-F5	89.09(17)
F3-P2-F5	178.1(2)	F2A-P2A-F6A	90.8(4)
F2A-P2A-F4A	90.7(4)	F6A-P2A-F4A	178.4(5)
F2A-P2A-F1A	179.6(5)	F6A-P2A-F1A	88.9(4)
F4A-P2A-F1A	89.6(4)	F2A-P2A-F5A	90.1(4)
F6A-P2A-F5A	90.3(4)	F4A-P2A-F5A	89.1(4)
F1A-P2A-F5A	90.2(4)	F2A-P2A-F3A	90.4(4)
F6A-P2A-F3A	91.3(4)	F4A-P2A-F3A	89.3(4)
F1A-P2A-F3A	89.3(4)	F5A-P2A-F3A	178.3(5)

Table 12. Torsion angles (°) for complex 3.

bond	torsion angle(°)	bond	torsion angle(°)
C6-C1-C2-C3	0.3(4)	Au1-C1-C2-C3	178.69(19)
C1-C2-C3-C4	-0.2(4)	C2-C3-C4-C5	-0.1(4)
C3-C4-C5-C6	0.2(4)	C4-C5-C6-C1	-0.1(4)
C4-C5-C6-C7	-179.0(2)	C2-C1-C6-C5	-0.1(3)
Au1-C1-C6-C5	-178.88(18)	C2-C1-C6-C7	178.8(2)
Au1-C1-C6-C7	0.1(3)	C11-N1-C7-C8	0.8(3)
Au1-N1-C7-C8	-178.90(17)	C11-N1-C7-C6	-179.1(2)
Au1-N1-C7-C6	1.2(3)	C5-C6-C7-N1	178.1(2)
C1-C6-C7-N1	-0.8(3)	C5-C6-C7-C8	-1.7(4)
C1-C6-C7-C8	179.3(2)	N1-C7-C8-C9	-2.9(3)
C6-C7-C8-C9	176.9(2)	C7-C8-C9-C10	2.3(4)
C8-C9-C10-C11	0.5(4)	C7-N1-C11-C10	2.0(4)
Au1-N1-C11-C10	-178.32(17)	C7-N1-C11-C12	-177.5(2)
Au1-N1-C11-C12	2.2(3)	C9-C10-C11-N1	-2.6(4)
C9-C10-C11-C12	176.8(2)	N1-C11-C12-C13	174.8(2)
C10-C11-C12-C13	-4.7(4)	N1-C11-C12-C17	-2.4(3)
C10-C11-C12-C17	178.1(2)	C17-C12-C13-C14	0.6(4)
C11-C12-C13-C14	-176.5(2)	C12-C13-C14-C15	-0.7(4)
C13-C14-C15-C16	-0.5(4)	C14-C15-C16-C17	1.9(4)
C15-C16-C17-C12	-2.0(4)	C15-C16-C17-Au1	173.56(19)

C13-C12-C17-C16	0.8(4)	C11-C12-C17-C16	178.0(2)
C13-C12-C17-Au1	-175.69(18)	C11-C12-C17-Au1	1.5(3)
C23-N2-C18-P1	61.8(2)	C21-N2-C18-P1	-59.6(2)
C19-P1-C18-N2	49.49(19)	C20-P1-C18-N2	-52.00(19)
Au1-P1-C18-N2	172.46(13)	C22-N3-C19-P1	-62.2(2)
C21-N3-C19-P1	59.7(2)	C18-P1-C19-N3	-49.12(19)
C20-P1-C19-N3	52.69(19)	Au1-P1-C19-N3	-172.65(13)
C22-N4-C20-P1	61.7(2)	C23-N4-C20-P1	-61.4(2)
C18-P1-C20-N4	51.10(19)	C19-P1-C20-N4	-52.07(19)
Au1-P1-C20-N4	-179.70(13)	C22-N3-C21-N2	54.6(3)
C19-N3-C21-N2	-68.5(3)	C18-N2-C21-N3	68.1(3)
C23-N2-C21-N3	-54.3(3)	C19-N3-C22-N4	68.6(3)
C21-N3-C22-N4	-55.1(3)	C23-N4-C22-N3	55.6(3)
C20-N4-C22-N3	-68.8(3)	C22-N4-C23-N2	-55.1(3)
C20-N4-C23-N2	69.2(3)	C18-N2-C23-N4	-68.7(3)
C21-N2-C23-N4	54.2(3)		

Bibliography

[1] *World Cancer Report 2014*, International Agency for Research on Cancer, Lyon, **2014**.

[2] P. Anand, A. B. Kunnumakara, C. Sundaram, K. B. Harikumar, S. T. Tharakan, O. S. Lai, B. Sung, B. B. Aggarwal, *Pharmaceutical research* **2008**, *25*, 2097-2116.

[3] M. S. Pednekar, P. C. Gupta, B. B. Yeole, J. R. Hébert, *Cancer Causes & Control* **2011**, *22*, 859-868.

[4] J. H. Hoeijmakers, *New England Journal of Medicine* **2009**, *361*, 1475-1485.

[5] C. J. Lord, A. Ashworth, *Nature* **2012**, *481*, 287-294.

[6] aM. E. Moynahan, M. Jasin, *Nature reviews Molecular cell biology* **2010**, *11*, 196-207; bM. R. Lieber, *Nature structural & molecular biology* **2010**, *17*, 393-395.

[7] aE. B. C. T. C. Group, *The Lancet* **2006**, *366*, 2087-2106; bW. Catalona, D. Smith, *The Journal of urology* **1994**, *152*, 1837-1842.

[8] W. D. Travis, E. Brambilla, G. J. Riely, *Journal of Clinical Oncology* **2013**, *31*, 992-1001.

[9] B. Rosenberg, L. Van Camp, T. Krigas, *Nature* **1965**, *205*, 698-699.

[10] aM. G. Apps, E. H. Y. Choi, N. J. Wheate, *Endocrine-Related Cancer* **2015**, *22*, R219-R233; bN. J. Wheate, S. Walker, G. E. Craig, R. Oun, *Dalton Transactions* **2010**, *39*, 8113-8127.

[11] D. Wang, S. J. Lippard, *Nature reviews Drug discovery* **2005**, *4*, 307-320.

[12] aI. Ott, *Coordination Chemistry Reviews* **2009**, *253*, 1670-1681; bS. Nobili, E. Mini, I. Landini, C. Gabbiani, A. Casini, L. Messori, *Medicinal Research Reviews* **2010**, *30*, 550-580.

[13] C. Bombardier, J. Ware, I. J. Russell, M. Larson, A. Chalmers, J. L. Read, W. Arnold, R. Bennett, J. Caldwell, P. K. Hench, *The American journal of medicine* **1986**, *81*, 565-578.

[14] M. J. McKeage, L. Maharaj, S. J. Berners-Price, *Coordination Chemistry Reviews* **2002**, *232*, 127-135.

[15] J. M. McKeage, J. S. Berners-Price, P. Galettis, J. R. Bowen, W. Brouwer, L. Ding, L. Zhuang, C. B. Baguley, *Cancer Chemotherapy and Pharmacology* **2000**, *46*, 343-350.

[16] A. Bindoli, M. P. Rigobello, G. Scutari, C. Gabbiani, A. Casini, L. Messori, *Coordination Chemistry Reviews* **2009**, *253*, 1692-1707.

[17] aT. Zou, C. T. Lum, C.-N. Lok, J.-J. Zhang, C.-M. Che, *Chemical Society Reviews* **2015**, *44*, 8786-8801; bP. I. da Silva Maia, V. M. Deflon, U. Abram, *Future medicinal chemistry* **2014**, *6*, 1515-1536.

[18] L. Messori, F. Abbate, G. Marcon, P. Orioli, M. Fontani, E. Mini, T. Mazzei, S. Carotti, T. O'Connell, P. Zanello, *Journal of Medicinal Chemistry* **2000**, *43*, 3541-3548.

[19] A. de Almeida, G. Soveral, A. Casini, *MedChemComm* **2014**, *5*, 1444-1453.

[20] A. Serna, A. Galan-Cobo, C. Rodrigues, I. Sanchez-Gomar, J. J. Toledo-Aral, T. F. Moura, A. Casini, G. Soveral, M. Echevarria, *Journal of cellular physiology* **2014**, *229*, 1787-1801.

[21] aF. Mendes, M. Groessl, A. A. Nazarov, Y. O. Tsybin, G. Sava, I. Santos, P. J. Dyson, A. Casini, *Journal of medicinal chemistry* **2011**, *54*, 2196-2206; bM. Serratrice, F. Edafe, F. Mendes, R. Scopelliti, S. M. Zakeeruddin, M. Grätzel, I. Santos, M. A. Cinellu, A. Casini, *Dalton Transactions* **2012**, *41*, 3287-3293.
[22] A. Citta, V. Scalcon, P. Gobel, B. Bertrand, M. Wenzel, A. Folda, M. P. Rigobello, E. Meggers, A. Casini, *RSC Advances* **2016**, *6*, 79147-79152.
[23] S. M. Schmitt, M. Frezza, Q. P. Dou, *Frontiers in bioscience (Scholar edition)* **2012**, *4*, 375.
[24] C. Nardon, S. M. Schmitt, H. Yang, J. Zuo, D. Fregona, Q. P. Dou, *PloS one* **2014**, *9*, e84248.
[25] G. Gasser, I. Ott, N. Metzler-Nolte, *Journal of medicinal chemistry* **2010**, *54*, 3-25.
[26] P. J. Dyson, *CHIMIA International Journal for Chemistry* **2007**, *61*, 698-703.
[27] G. Gasser, I. Ott, N. Metzler-Nolte, *Journal of Medicinal Chemistry* **2011**, *54*, 3-25.
[28] aW. A. Herrmann, *Angewandte Chemie International Edition* **2002**, *41*, 1290-1309; bW. A. Herrmann, B. Cornils, *Angewandte Chemie International Edition in English* **1997**, *36*, 1048-1067.
[29] D. Schlawe, A. Majdalani, J. Velcicky, E. Heßler, T. Wieder, A. Prokop, H.-G. Schmalz, *Angewandte Chemie International Edition* **2004**, *43*, 1731-1734.
[30] V. D. Reddy, *Journal of Organometallic Chemistry* **2006**, *691*, 27-34.
[31] C. Nagel, S. McLean, R. K. Poole, H. Braunschweig, T. Kramer, U. Schatzschneider, *Dalton Transactions* **2014**, *43*, 9986-9997.
[32] aI. Ott, T. Koch, H. Shorafa, Z. Bai, D. Poeckel, D. Steinhilber, R. Gust, *Organic & Biomolecular Chemistry* **2005**, *3*, 2282-2286; bC. D. Sergeant, I. Ott, A. Sniady, S. Meneni, R. Gust, A. L. Rheingold, R. Dembinski, *Organic & Biomolecular Chemistry* **2008**, *6*, 73-80.
[33] I. Ott, B. Kircher, C. P. Bagowski, D. H. Vlecken, E. B. Ott, J. Will, K. Bensdorf, W. S. Sheldrick, R. Gust, *Angewandte Chemie International Edition* **2009**, *48*, 1160-1163.
[34] E. Meggers, *Chemical Communications* **2009**, 1001-1010.
[35] K. S. M. Smalley, R. Contractor, N. K. Haass, A. N. Kulp, G. E. Atilla-Gokcumen, D. S. Williams, H. Bregman, K. T. Flaherty, M. S. Soengas, E. Meggers, M. Herlyn, *Cancer Research* **2007**, *67*, 209-217.
[36] J. C. Franke, M. Plötz, A. Prokop, C. C. Geilen, H.-G. Schmalz, J. Eberle, *Biochemical Pharmacology* **2010**, *79*, 575-586.
[37] aM.-L. Teyssot, A.-S. Jarrousse, M. Manin, A. Chevry, S. Roche, F. Norre, C. Beaudoin, L. Morel, D. Boyer, R. Mahiou, A. Gautier, *Dalton Transactions* **2009**, 6894-6902; bL. Oehninger, R. Rubbiani, I. Ott, *Dalton Transactions* **2013**, *42*, 3269-3284.
[38] B. Cetinkaya, E. Çetinkaya, H. Kuecuekbay, R. Durmaz, *ARZNEIMITTEL FORSCHUNG* **1996**, *46*, 821-823.
[39] J. L. Hickey, R. A. Ruhayel, P. J. Barnard, M. V. Baker, S. J. Berners-Price, A. Filipovska, *Journal of the American Chemical Society* **2008**, *130*, 12570-12571.
[40] M. Cinellu, I. Ott, A. Casini, in *Bioorganometallic Chemistry: Applications in Drug Discovery, Biocatalysis, and Imaging*, First Edition ed. (Ed.: M. S. Gérad Jaouen), Wiley-VCH Verlag GmbH & Co. KGaA, **2015**, pp. 117-139.

[41] T. V. Serebryanskaya, A. A. Zolotarev, I. Ott, *MedChemComm* **2015**, *6*, 1186-1189.
[42] D. J. Nelson, S. P. Nolan, *Chemical Society Reviews* **2013**, *42*, 6723-6753.
[43] B. Bertrand, L. Stefan, M. Pirrotta, D. Monchaud, E. Bodio, P. Richard, P. Le Gendre, E. Warmerdam, M. H. de Jager, G. M. M. Groothuis, M. Picquet, A. Casini, *Inorganic chemistry* **2014**, *53*, 2296-2303.
[44] J. W. Daly, *Cell. Mol. Life Sci.* **2007**, *64*, 2153.
[45] C. Bazzicalupi, M. Ferraroni, F. Papi, L. Massai, B. Bertrand, L. Messori, P. Gratteri, A. Casini, *Angewandte Chemie International Edition* **2016**.
[46] aD. P. Gonçalves, R. Rodriguez, S. Balasubramanian, J. K. Sanders, *Chemical communications* **2006**, 4685-4687; bM. Düchler, *Journal of drug targeting* **2012**, *20*, 389-400.
[47] J. K. Muenzner, T. Rehm, B. Biersack, A. Casini, I. A. de Graaf, P. Worawutputtapong, A. Noor, R. Kempe, V. Brabec, J. Kasparkova, R. Schobert, *Journal of medicinal chemistry* **2015**, *58*, 6283-6292.
[48] aG. Lummen, H. Sperling, H. Luboldt, T. Otto, H. Rubben, *Cancer Chemother. Pharmacol.* **1998**, *42*, 415-417; bP. Köpf-Maier, *Anticancer Res* **1999**, *19*, 493-504.
[49] G. Mokdsi, M. M. Harding, *Journal of Organometallic Chemistry* **1998**, *565*, 29-35.
[50] aS. Top, E. B. Kaloun, A. Vessières, I. Laïos, G. Leclercq, G. Jaouen, *Journal of Organometallic Chemistry* **2002**, *643–644*, 350-356; bK. Mross, P. Robben-Bathe, L. Edler, J. Baumgart, W. E. Berdel, H. Fiebig, C. Unger, *Onkologie* **2000**, *23*, 576-579.
[51] O. Allen, L. Croll, A. Gott, R. Knox, P. McGowan, *Organometallics* **2004**, *23*, 288-292.
[52] M. Tacke, L. T. Allen, L. Cuffe, W. M. Gallagher, Y. Lou, O. Mendoza, H. Müller-Bunz, F.-J. K. Rehmann, N. Sweeney, *Journal of Organometallic Chemistry* **2004**, *689*, 2242-2249.
[53] aW. H. Ang, A. Casini, G. Sava, P. J. Dyson, *Journal of Organometallic Chemistry* **2011**, *696*, 989-998; bP. Nowak-Sliwinska, J. R. van Beijnum, A. Casini, A. A. Nazarov, G. Wagnieres, H. van den Bergh, P. J. Dyson, A. W. Griffioen, *Journal of medicinal chemistry* **2011**, *54*, 3895-3902.
[54] aW. H. Ang, E. Daldini, C. Scolaro, R. Scopelliti, L. Juillerat-Jeannerat, P. J. Dyson, *Inorganic chemistry* **2006**, *45*, 9006-9013; bC. A. Vock, A. K. Renfrew, R. Scopelliti, L. Juillerat-Jeanneret, P. J. Dyson, *European Journal of Inorganic Chemistry* **2008**, *2008*, 1661-1671.
[55] C. Scolaro, A. Bergamo, L. Brescacin, R. Delfino, M. Cocchietto, G. Laurenczy, T. J. Geldbach, G. Sava, P. J. Dyson, *Journal of Medicinal Chemistry* **2005**, *48*, 4161-4171.
[56] A. Bergamo, A. Masi, P. J. Dyson, G. Sava, *Int. J. Oncol* **2008**, 1281.
[57] S. Chatterjee, S. Kundu, A. Bhattacharyya, C. G. Hartinger, P. J. Dyson, *JBIC Journal of Biological Inorganic Chemistry* **2008**, *13*, 1149-1155.
[58] I. Romero-Canelón, A. M. Pizarro, A. Habtemariam, P. J. Sadler, *Metallomics* **2012**, *4*, 1271-1279.
[59] aF. Dubar, C. Biot, in *Bioorganometallic Chemistry*, Wiley-VCH Verlag GmbH & Co. KGaA, **2014**, pp. 141-164; bM. Patra, G. Gasser, N. Metzler-Nolte, *Dalton transactions* **2012**, *41*, 6350-6358.

[60] E. A. Hillard, A. Vessières, G. Jaouen, in *Medicinal Organometallic Chemistry* (Eds.: G. Jaouen, N. Metzler-Nolte), Springer Berlin Heidelberg, Berlin, Heidelberg, **2010**, pp. 81-117.
[61] G. Jaouen, A. Vessières, S. Top, *Chemical Society Reviews* **2015**, *44*, 8802-8817.
[62] E. Ekengard, L. Glans, I. Cassells, T. Fogeron, P. Govender, T. Stringer, P. Chellan, G. C. Lisensky, W. H. Hersh, I. Doverbratt, S. Lidin, C. de Kock, P. J. Smith, G. S. Smith, E. Nordlander, *Dalton Transactions* **2015**, *44*, 19314-19329.
[63] W. A. Wani, E. Jameel, U. Baig, S. Mumtazuddin, L. T. Hun, *European Journal of Medicinal Chemistry* **2015**, *101*, 534-551.
[64] aF. Dubar, T. J. Egan, B. Pradines, D. Kuter, K. K. Ncokazi, D. Forge, J.-F. Paul, C. Pierrot, H. Kalamou, J. Khalife, E. Buisine, C. Rogier, H. Vezin, I. Forfar, C. Slomianny, X. Trivelli, S. Kapishnikov, L. Leiserowitz, D. Dive, C. Biot, *ACS Chemical Biology* **2011**, *6*, 275-287; bG. Jaouen, A. Vessieres, S. Top, *Chemical Society Reviews* **2015**, *44*, 8802-8817.
[65] aM. P. Donzello, E. Viola, C. Ercolani, Z. Fu, D. Futur, K. M. Kadish, *Inorganic chemistry* **2012**, *51*, 12548-12559; bJ. F. González-Pantoja, M. Stern, A. A. Jarzecki, E. Royo, E. Robles-Escajeda, A. Varela-Ramírez, R. J. Aguilera, M. Contel, *Inorganic chemistry* **2011**, *50*, 11099-11110.
[66] M. Auzias, B. Therrien, G. Süss-Fink, P. Štěpnička, W. H. Ang, P. J. Dyson, *Inorganic chemistry* **2008**, *47*, 578-583.
[67] N. Lease, V. Vasilevski, M. Carreira, A. de Almeida, M. Sanaú, P. Hirva, A. Casini, M. Contel, *Journal of medicinal chemistry* **2013**, *56*, 5806-5818.
[68] M. Wenzel, B. Bertrand, M. J. Eymin, V. Comte, J. A. Harvey, P. Richard, M. Groessl, O. Zava, H. Amrouche, P. D. Harvey, P. Le Gendre, M. Picquet, A. Casini, *Inorg Chem* **2011**, *50*, 9472-9480.
[69] F. Pelletier, V. Comte, A. Massard, M. Wenzel, S. Toulot, P. Richard, M. Picquet, P. Le Gendre, O. Zava, F. Edafe, *Journal of medicinal chemistry* **2010**, *53*, 6923-6933.
[70] J. Fernández-Gallardo, B. T. Elie, T. Sadhukha, S. Prabha, M. Sanaú, S. A. Rotenberg, J. W. Ramos, M. Contel, *Chemical Science* **2015**, *6*, 5269-5283.
[71] I. Omae, *Current Organic Chemistry* **2014**, *18*, 2776-2795.
[72] G. Wilke, H. Müller, *Justus Liebigs Annalen der Chemie* **1960**, *629*, 222-240.
[73] M. Albrecht, *Chemical reviews* **2009**, *110*, 576-623.
[74] A. Casini, L. Messori, *Current topics in medicinal chemistry* **2011**, *11*, 2647-2660.
[75] L. Messori, F. Abbate, G. Marcon, P. Orioli, M. Fontani, E. Mini, T. Mazzei, S. Carotti, T. O'Connell, P. Zanello, *Journal of Medicinal Chemistry* **2000**, *43*, 3541-3548.
[76] S. P. Pricker, *Gold bulletin* **1996**, *29*, 53-60.
[77] R. G. Buckley, A. M. Elsome, S. P. Fricker, G. R. Henderson, B. R. Theobald, R. V. Parish, B. P. Howe, L. R. Kelland, *Journal of medicinal chemistry* **1996**, *39*, 5208-5214.
[78] S. P. Fricker, R. M. Mosi, B. R. Cameron, I. Baird, Y. Zhu, V. Anastassov, J. Cox, P. S. Doyle, E. Hansell, G. Lau, J. Langille, M. Olsen, L. Qin, R. Skerlj, R. S. Y. Wong, Z. Santucci, J. H. McKerrow, *Journal of Inorganic Biochemistry* **2008**, *102*, 1839-1845.

[79] L. Engmann, M. McNaughton, M. Gajewska, S. Kumar, A. Birmingham, G.Powis, *Anticancer drugs* **2006**, *17*, 539.
[80] M. Coronnello, E. Mini, B. Caciagli, M. A. Cinellu, A. Bindoli, C. Gabbiani, L. Messori, *Journal of Medicinal Chemistry* **2005**, *48*, 6761-6765.
[81] T. Gamberi, L. Massai, F. Magherini, I. Landini, T. Fiaschi, F. Scaletti, C. Gabbiani, L. Bianchi, L. Bini, S. Nobili, G. Perrone, E. Mini, L. Messori, A. Modesti, *Journal of Proteomics* **2014**, *103*, 103-120.
[82] J.-J. Zhang, R. W.-Y. Sun, C.-M. Che, *Chemical Communications* **2012**, *48*, 3388-3390.
[83] H. Urra, C. Hetz, *Cell Death Differ* **2012**, *19*, 1893-1895.
[84] C.-M. Che, R. W.-Y. Sun, *Chemical Communications* **2011**, *47*, 9554-9560.
[85] N. Shaik, A. Martínez, I. Augustin, H. Giovinazzo, A. Varela-Ramírez, M. Sanaú, R. J. Aguilera, M. Contel, *Inorganic Chemistry* **2009**, *48*, 1577-1587.
[86] M. A. Cinellu, A. Zucca, S. Stoccoro, G. Minghetti, M. Manassero, M. Sansoni, *Journal of the Chemical Society, Dalton Transactions* **1996**, 4217-4225.
[87] B. Bertrand, S. Spreckelmeyer, E. Bodio, F. Cocco, M. Picquet, P. Richard, P. Le Gendre, C. Orvig, M. A. Cinellu, A. Casini, *Dalton Transactions* **2015**, *44*, 11911-11918.
[88] aF. Mendes, M. Groessl, A. A. Nazarov, Y. O. Tsybin, G. Sava, I. Santos, P. J. Dyson, A. Casini, *Journal of Medicinal Chemistry* **2011**, *54*, 2196-2206; bY. Zhu, B. R. Cameron, R. Mosi, V. Anastassov, J. Cox, L. Qin, Z. Santucci, M. Metz, R. T. Skerlj, S. P. Fricker, *Journal of Inorganic Biochemistry* **2011**, *105*, 754-762.
[89] S. P. Jackson, J. Bartek, *Nature* **2009**, *461*, 1071-1078.
[90] C. Gabbiani, A. Casini, G. Kelter, F. Cocco, M. A. Cinellu, H. H. Fiebig, L. Messori, *Metallomics* **2011**, *3*, 1318-1323.
[91] aP. Kandagal, S. Ashoka, J. Seetharamappa, S. Shaikh, Y. Jadegoud, O. Ijare, *Journal of pharmaceutical and biomedical analysis* **2006**, *41*, 393-399; bW. H. Ang, E. Daldini, L. Juillerat-Jeanneret, P. J. Dyson, *Inorganic chemistry* **2007**, *46*, 9048-9050; cA. Divsalar, M. J. Bagheri, A. A. Saboury, H. Mansoori-Torshizi, M. Amani, *The Journal of Physical Chemistry B* **2009**, *113*, 14035-14042.
[92] aM. E. Sitar, S. Aydin, U. Cakatay, *Clin Lab* **2013**, *59*, 945-952; bM. Anraku, V. T. G. Chuang, T. Maruyama, M. Otagiri, *Biochimica et Biophysica Acta (BBA)-General Subjects* **2013**, *1830*, 5465-5472.
[93] A. Casini, G. Kelter, C. Gabbiani, M. A. Cinellu, G. Minghetti, D. Fregona, H.-H. Fiebig, L. Messori, *JBIC Journal of Biological Inorganic Chemistry* **2009**, *14*, 1139-1149.
[94] A. Casini, M. A. Cinellu, G. Minghetti, C. Gabbiani, M. Coronnello, E. Mini, L. Messori, *Journal of Medicinal Chemistry* **2006**, *49*, 5524-5531.
[95] K.-H. Wong, K.-K. Cheung, M. C.-W. Chan, C.-M. Che, *Organometallics* **1998**, *17*, 3505-3511.
[96] C. K. L. Li, R. W. Y. Sun, S. C. F. Kui, N. Zhu, C. M. Che, *Chemistry–A European Journal* **2006**, *12*, 5253-5266.
[97] S. Berners-Price, P. Sadler, *Chemistry in Britain* **1987**, *23*, 541-544.
[98] S. Castelli, O. Vassallo, P. Katkar, C.-M. Che, R. W.-Y. Sun, A. Desideri, *Archives of biochemistry and biophysics* **2011**, *516*, 108-112.

[99] J. J. Yan, A. L.-F. Chow, C.-H. Leung, R. W.-Y. Sun, D.-L. Ma, C.-M. Che, *Chemical Communications* **2010**, *46*, 3893-3895.
[100] R. Wai-Yin Sun, D.-L. Ma, E. L.-M. Wong, C.-M. Che, *Dalton Transactions* **2007**, 4884-4892.
[101] J. J. Zhang, W. Lu, R. W. Y. Sun, C. M. Che, *Angewandte Chemie International Edition* **2012**, *51*, 4882-4886.
[102] aR. Parish, J. P. Wright, R. G. Pritchard, *Journal of Organometallic Chemistry* **2000**, *596*, 165-176; bY. Shi, S. A. Blum, *Organometallics* **2011**, *30*, 1776-1779; cA. Herbst, C. Bronner, P. Dechambenoit, O. S. Wenger, *Organometallics* **2013**, *32*, 1807-1814.
[103] A. S. K. Hashmi, J. P. Weyrauch, M. Rudolph, E. Kurpejović, *Angewandte Chemie International Edition* **2004**, *43*, 6545-6547.
[104] aC. R. Wilson, A. M. Fagenson, W. Ruangpradit, M. T. Muller, O. Q. Munro, *Inorganic chemistry* **2013**, *52*, 7889-7906; bL. Maiore, M. C. Aragoni, C. Deiana, M. A. Cinellu, F. Isaia, V. Lippolis, A. Pintus, M. Serratrice, M. Arca, *Inorganic chemistry* **2014**, *53*, 4068-4080.
[105] A. Amoedo, M. Graña, J. Martínez, T. Pereira, M. López-Torres, A. Fernández, J. J. Fernández, J. M. Vila, *European Journal of Inorganic Chemistry* **2002**, *2002*, 613-620.
[106] aD. Pandiarajan, R. Ramesh, *Inorganic Chemistry Communications* **2011**, *14*, 686-689; bP. G. Bomben, K. C. Robson, P. A. Sedach, C. P. Berlinguette, *Inorganic chemistry* **2009**, *48*, 9631-9643.
[107] U. Abram, K. Ortner, R. Gust, K. Sommer, *Journal of the Chemical Society, Dalton Transactions* **2000**, 735-744.
[108] M. W. Johnson, A. G. DiPasquale, R. G. Bergman, F. D. Toste, *Organometallics* **2014**, *33*, 4169-4172.
[109] J. Hoult, M. Paya, *General Pharmacology: The Vascular System* **1996**, *27*, 713-722.
[110] G. Jones, W. R. Jackson, C. Y. Choi, W. R. Bergmark, *The Journal of Physical Chemistry* **1985**, *89*, 294-300.
[111] aM. Grazul, E. Budzisz, *Coordination Chemistry Reviews* **2009**, *253*, 2588-2598; bT. Okamoto, T. Kobayashi, S. Yoshida, *Current Medicinal Chemistry-Anti-Cancer Agents* **2005**, *5*, 47-51.
[112] M. Gellert, M. H. O'Dea, T. Itoh, J.-I. Tomizawa, *Proceedings of the National Academy of Sciences* **1976**, *73*, 4474-4478.
[113] aE. Arathoon, J. Hamilton, C. Hench, D. Stevens, *Antimicrobial agents and chemotherapy* **1990**, *34*, 1655-1659; bT. Walsh, H. Standiford, A. Reboli, J. John, M. Mulligan, B. Ribner, J. Montgomerie, M. Goetz, C. Mayhall, D. Rimland, *Antimicrobial agents and chemotherapy* **1993**, *37*, 1334-1342.
[114] L. Pari, N. Rajarajeswari, *Chemico-biological interactions* **2009**, *181*, 292-296.
[115] B. S. Creaven, E. Czegledi, M. Devereux, E. A. Enyedy, A. Foltyn-Arfa Kia, D. Karcz, A. Kellett, S. McClean, N. V. Nagy, A. Noble, A. Rockenbauer, T. Szabo-Planka, M. Walsh, *Dalton Transactions* **2010**, *39*, 10854-10865.
[116] X.-M. Peng, G. LV Damu, H. Zhou, *Current pharmaceutical design* **2013**, *19*, 3884-3930.
[117] G. J. Finn, B. S. Creaven, D. A. Egan, *European journal of pharmaceutical sciences* **2005**, *26*, 16-25.
[118] X.-M. Peng, G. L.V. Damu, C. He Zhou, *Current Pharmaceutical Design* **2013**,

19, 3884-3930.
[119] E. Budzisz, B. K. Keppler, G. Giester, M. Wozniczka, A. Kufelnicki, B. Nawrot, *European Journal of Inorganic Chemistry* **2004**, *2004*, 4412-4419.
[120] J. S. Casas, E. E. Castellano, M. D. Couce, O. Crespo, J. Ellena, A. Laguna, A. Sánchez, J. Sordo, C. Taboada, *Inorganic Chemistry* **2007**, *46*, 6236-6238.
[121] R. G. Kalkhambkar, G. M. Kulkarni, C. M. Kamanavalli, N. Premkumar, S. Asdaq, C. M. Sun, *European journal of medicinal chemistry* **2008**, *43*, 2178-2188.
[122] E. C. Constable, T. A. Leese, *Journal of Organometallic Chemistry* **1989**, *363*, 419-424.
[123] E. C. Constable, T. A. Leese, *Journal of organometallic chemistry* **1987**, *335*, 293-299.
[124] aM. Albrecht, G. van Koten, *Angewandte Chemie International Edition* **2001**, *40*, 3750-3781; bS. D. Brown, W. Henderson, K. J. Kilpin, B. K. Nicholson, *Inorganica chimica acta* **2007**, *360*, 1310-1315.
[125] M. AgostinaáCinellu, *Journal of the Chemical Society, Dalton Transactions* **1996**, 4217-4225.
[126] V. K.-M. Au, D. P.-K. Tsang, K. M.-C. Wong, M.-Y. Chan, N. Zhu, V. W.-W. Yam, *Inorganic chemistry* **2013**, *52*, 12713-12725.
[127] Y. Fuchita, H. Ieda, Y. Tsunemune, J. Kinoshita-Nagaoka, H. Kawano, *Journal of the Chemical Society, Dalton Transactions* **1998**, 791-796.
[128] P. V. Shinde, V. B. Labade, J. B. Gujar, B. B. Shingate, M. S. Shingare, *Tetrahedron Letters* **2012**, *53*, 1523-1527.
[129] K. Olofsson, M. Larhed, in *Microwave Assisted Organic Synthesis*, Blackwell Publishing Ltd., **2009**, pp. 23-43.
[130] G. Yin, Q. Liu, J. Ma, N. She, *Green Chemistry* **2012**, *14*, 1796-1798.
[131] W.-P. To, K. T. Chan, G. S. M. Tong, C. Ma, W.-M. Kwok, X. Guan, K.-H. Low, C.-M. Che, *Angewandte Chemie International Edition* **2013**, *52*, 6648-6652.
[132] aS. Carboni, Master Thesis thesis, Universita degli studi di sassari (Sassari), **2014**; bM. Maldonado-Domínguez, R. Arcos-Ramos, M. Romero, B. Flores-Pérez, N. Farfán, R. Santillan, P. G. Lacroix, I. Malfant, *New Journal of Chemistry* **2014**, *38*, 260-268.
[133] aD.-A. Rosca, D. A. Smith, M. Bochmann, *Chemical Communications* **2012**, *48*, 7247-7249; bM. A. Cinellu, G. Minghetti, M. V. Pinna, S. Stoccoro, A. Zucca, M. Manassero, *Journal of the Chemical Society, Dalton Transactions* **2000**, 1261-1265.
[134] G. Marcon, S. Carotti, M. Coronnello, L. Messori, E. Mini, P. Orioli, T. Mazzei, M. A. Cinellu, G. Minghetti, *Journal of Medicinal Chemistry* **2002**, *45*, 1672-1677.
[135] W. Hiller, J. Straehle, A. Datz, M. Hanack, W. E. Hatfield, L. W. Ter Haar, P. Guetlich, *Journal of the American Chemical Society* **1984**, *106*, 329-335.
[136] E. Ashby, A. Goel, *Journal of the American Chemical Society* **1981**, *103*, 4983-4985.
[137] aH. Ammar, S. Fery-Forgues, R. El Gharbi, *Dyes and pigments* **2003**, *57*, 259-265; bX. Liu, J. M. Cole, K. S. Low, *The Journal of Physical Chemistry C* **2013**, *117*, 14731-14741; cV. Barone, A. Polimeno, *Chemical Society Reviews* **2007**, *36*, 1724-1731.
[138] aE. Vergara, S. Miranda, F. Mohr, E. Cerrada, E. R. Tiekink, P. Romero, A.

Mendía, M. Laguna, *European journal of inorganic chemistry* **2007**, *2007*, 2926-2933; bS. Miranda, E. Vergara, F. Mohr, D. de Vos, E. Cerrada, A. Mendía, M. Laguna, *Inorganic chemistry* **2008**, *47*, 5641-5648; cE. García-Moreno, A. Tomás, E. Atrián-Blasco, S. Gascón, E. Romanos, M. J. Rodriguez-Yoldi, E. Cerrada, M. Laguna, *Dalton Transactions* **2016**, *45*, 2462-2475.

[139] J. Fernandez-Cestau, B. Bertrand, M. Blaya, G. A. Jones, T. J. Penfold, M. Bochmann, *Chemical Communications* **2015**, *51*, 16629-16632.

[140] M. Luthman, A. Holmgren, *Biochemistry* **1982**, *21*, 6628-6633.

[141] M. P. Rigobello, M. T. Callegaro, E. Barzon, M. Benetti, A. Bindoli, *Free Radical Biology and Medicine* **1998**, *24*, 370-376.

[142] Y. Du, H. Zhang, X. Zhang, J. Lu, A. Holmgren, *Journal of Biological Chemistry* **2013**, *288*, 32241-32247.

[143] A. Folda, A. Citta, V. Scalcon, T. Calì, F. Zonta, G. Scutari, A. Bindoli, M. P. Rigobello, *Scientific reports* **2016**, *6*.

[144] A. Citta, E. Schuh, F. Mohr, A. Folda, M. L. Massimino, A. Bindoli, A. Casini, M. P. Rigobello, *Metallomics* **2013**, *5*, 1006-1015.

[145] M. E. Anderson, *Methods in enzymology* **1985**, *113*, 548-555.

Curriculum Vitae

Kontaktdaten
Sophie Jürgens
Preziosastraße 41
sophie.juergens@mytum.de
persönliche Daten
geb. 23.06.1988 in Rostock, Deutschland

Bildungsweg

2013-2016: Promotionsstudium, Technische Universität München, Lehrstuhl für Anorganische Chemie und University of Cardiff, School of Chemistry Abschlussziel: Dr. rer. nat
2010-2012: Chemiestudium, Technische Universität München, Abschluss: Master of Science
2007-2010: Chemiestudium, Technische Universität München, Abschluss: Bachelor of Science
2005-2007: Schule Schloss Salem, Salem, Abschluss: Abitur
1999-2004: Werkgymnasium, Heidenheim a. d. Brenz
1998-1999: St. Ansgar Gymnasium, Hamburg

Sprachkenntnisse

Deutsch
Englisch
Französisch
Latein

Publikationsliste

- Lilian R. Graser, Sophie Jürgens, Michael E. Wilhelm, Mirza Cokoja, Wolfgang A. Herrmann, Fritz E. Kühn, *Epoxidation of olefins catalyzed by polyoxomolybdates formed in-situ in liquid*, Z. Naturforsch., **2013**, DOI: 10.5560/ZNB.2013-3139
- Sophie Jürgens, Wolfgang A. Herrmann, Fritz E. Kühn, *Rhenium and Technetium Based Radiopharmaceuticals: Development and Recent Advances*, J. Organomet. Chem., **2014**; DOI: 10.1002/chin.201423285
- Sophie Jürgens, Fritz E. Kühn, Angela Casini, *Cyclometalated complexes of platinum and gold with biological properties: state-of-the-art and future perspectives*, J. Med. Chem., **2016** (akzeptiert)
- Sophie Jürgens, Angela Casini, *Mechanistic insights into gold organometallic compounds and their biomedical applications*, CHEMIA, **2017** (akzeptiert)
- Sophie Jürgens, Valeria Scalcon, Natalia Estrada-Ortiz, Alessandra Folda, Federica Tonolo, Christian Jandl, Duncan Browne, Maria Pia Rigobello, Fritz E. Kühn, Angela Casini: *Exploring the C^N^C theme: synthesis and biological properties of tridentate cyclometalated gold(III) complexes* (in Vorbereitung)